Incorporation of polysaccharide nanowhiskers into a poly(ethylene-co-vinyl alcohol) matrix

by

Madeleine Leonore du Toit

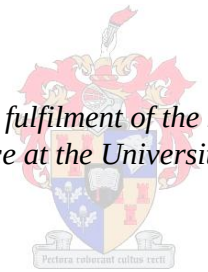

Thesis presented in partial fulfilment of the requirements for the degree Master of Science at the University of Stellenbosch

Supervisor: Dr M Lutz
Co-supervisor: Prof Albert J. van Reenen

Faculty of Science
Department of Chemistry and Polymer Science

March 2013

Declaration

By submitting this thesis/dissertation electronically, I declare that the entirety of the work contained therein is my own, original work, that I am the sole author thereof (save to the extent explicitly otherwise stated), that reproduction and publication thereof by Stellenbosch University will not infringe any third party rights and that I have not previously in its entirety or in part submitted it for obtaining any qualification.

March 2013

Abstract

The main aim of this study was to use poly (ethylene-co-vinyl alcohol) (EVOH) as vehicle to incorporate nanofillers into low density polyethylene (LDPE). For this purpose, chitin and cellulose nanowhiskers were prepared through a process of acid hydrolysis and then incorporated into different EVOH copolymers with varying ethylene contents by means of two different experimental methods, namely solution casting and electrospinning. The extremely small dimensions of nanowhiskers make it difficult to observe the degree of dispersion in the electrospun fibers using methods such as transmission electron microscopy (TEM) and scanning electron microscopy (SEM). Fluorescence microscopy was therefore investigated as an alternative characterization technique to obtain better results with regard to tracking the filler dispersion. TEM analysis proved to be the most successful method for observing the dispersion of nanowhiskers for solution cast EVOH nanocomposites as well as electrospun EVOH nanocomposites. Clear differences between EVOH composites with low nanowhisker and high nanowhisker loading were observed in TEM images for these nanocomposites. Thermal analysis of solution cast as well as electrospun fibers were carried out using techniques such as differential scanning calorimetry (DSC) and thermogravimetric analysis (TGA). These results revealed changes in crystallization behaviour as well as changes in thermal stability of the EVOH nanocomposites compared to the pure polymer matrix. The incorporation of cellulose and chitin nanowhiskers indicated a general increase in percentage crystallization which probably resulted from the nanowhiskers acting as nucleating agents and therefore increasing the crystallization of most EVOH nanocomposites. The thermal stability is observed to increase as the cellulose nanowhisker loading is increased. This increase in thermal stability proved to be partly attributed to the presence of sulphuric acid which were not completely removed during dialysis of cellulose nanowhiskers. Neutralisation of cellulose nanowhiskers and the treatment with a strong base was therefore further investigated to improve degradation within the EVOH nanocomposites during thermal treatment. The last step in this study involved the incorporation of electrospun EVOH nanofibers containing cellulose nanowhiskers into LDPE in order to improve the mechanical properties. The tensile strength and Young's modulus of these LDPE nanocomposites were seen to improve quite significantly while a decrease in elongation at break was observed.

Opsomming

Die hoofdoel van hierdie studie was om poliëtileen (ko-viniel alkohol) (EVOH) as voertuig te gebruik om nanofillers in lae digtheid poliëtileen (LDPE) te inkorporeer. Kitien en sellulose nanokristalle is vir hierdie doel geproduseer deur middel van ’n suurhidrolise proses en daarna in verskillende EVOH-kopolimere met verskillende etileeninhoude geïnkorporeer met behulp van twee verskillende eksperimentele metodes, naamlik ’n drogings- en elektrospinproses. Die uiters klein dimensies van die nanokristalle maak dit uitdagend om die mate van verspreiding van die nanokristalle binne in die elekrogespinde vesels waar te neem m.b.v. metodes soos transmissie-elektronmikroskopie (TEM) en skandeerelektronmikroskopie (SEM). Fluoressensie is dus as ’n moontlike alternatiewe karakteriserings tegniek bestudeer om beter resultate rakende die verspreiding van die nanokristalle te kan waarneem. In hierdie studie is gevind dat TEM-analise die suksesvolste metode was om die verspreiding van nanokristalle te bestudeer en dit geld vir beide die gedroogte en gespinde EVOH-nanosamestellings. Duidelike verskille is waargeneem vir monsters wat hoër en laer nanokristalinhoude gehad het. Saambondeling van die nanokristalle kom duideliker voor by dié wat ’n hoër inhoud van nanokristalle bevat. Termiese analises van gedroogte EVOH-nanosamestellings en ook die gespinde nanosaamgestelde vesels is uitgevoer d.m.v. tegnieke soos differensieëlskandeerkalorometrie (DSC) en termiese-gravimetriese analise (TGA). Die resultate wat verkry is vanaf die bogenoemde tegnieke het bewys dat daar verandering in die kristallisasie, sowel as die degradasie temperatuur, van die EVOH-nanosamestelling is. Die byvoeging van sellulose en kitien nanokristalle het ’n algemene verhoging in die persentasie kristallisasie van die EVOH-nanosamestelling te wee gebring. Die byvoeging van nanokristalle tree waarskynlik gedeeltelik op as kernvormings agent vir die EVOH-molekules. TGA analises toon dat die termiese stabiliteit van die EVOH-nanosamestelling verhoog met die byvoeging van nanokristalle. Die teenwoordigheid van die sulfaatgroepe wat nie heeltemal verwyder is tydens die wasproses nie, is bewys om gedeeltelik verantwoordelik te wees vir die verhoging in termiese stabiliteit van die EVOH-nanosamestellings. Die neutralisasie en behandeling van die nanokristalle met ’n sterk basis is dus verder ondersoek om die degradasie van die EVOH-nanosamestellings tydens verhitting te verbeter. Die laaste stap in hierdie studie het behels dat elektrogespinde EVOH vesels wat verskillende hoeveelhede sellulose nanokristalle bevat, geïnkorporeer is in LDPE ten einde die meganiese eienskappe te verbeter. Die treksterkte en die Young’s modulus het met ’n beduidendende hoeveelheid verbeter terwyl die verlenging by breekpunt verlaag het.

-This thesis is dedicated to my Mother and Father-

Acknowledgements

Dr M Lutz my supervisor, for her guidance, support and motivation.

Prof AJ van Reenen my co supervisor, for guidance, advice and financial support.

Polymer science group for all the assistance and support especially the **polyolefins** group.

Dr Margaretha Brand ('Maggie') for her IT support, advice and endless patience.

My friends and family for their endless support and advice.

Freda-Jean Meltz for her advice, support and laughter.

I want to thank the following people for assisting in sample analysis:

Francious Cummings at University of Cape Town for TEM analysis.

Miranda Waldron at University of Cape Town for FESEM analysis.

Illana Bergh at Roediger agencies for the TGA analysis.

Madelaine Frazenburg at Stellenbosch University for SEM analysis.

Lize Engelbrecht at Stellenbosch University for fluorescence microscopy imaging.

I also want to thank the **National Research Foundation (NRF)** for the financial support, providing me with the opportunity to attain my MSc.degree.

Table of Contents

List of Figures

List of Tables

List of Abbreviations

EVOH	Poly(ethylene vinyl alcohol)
EVA	Ethylene vinyl acetate copolymers
PEO	Poly(ethylene oxide)
PS	Polystyrene
PVA	Poly(vinyl alcohol)
PCL	Poly(caprolactone)
PLA	Poly lactic acid
PMMA	Poly(methyl methacrylate)
PAA	Poly(acrylic acid)
PP	Poly propylene
PEG	Poly(ethylene glycol)
LDPE	Linear low density polyethylene
PE-g-MA	Polyethylene-graft-(maleic anhydride)
TEM	Transmission electron microscopy
AFM	Atomic force microscopy
SEM	Scanning electron microscopy
FE-SEM	Field emission scanning microscopy
FTIR	Fourier transform infrared
XRD	X-ray diffraction
DMTA	Dynamic mechanical thermal analysis
NMR	Nuclear magnetic resonance
POL	Polarized optical light microscopy
MCC	Micro crystalline cellulose
cnw	Cellulose nanowhiskers
chnw	Chitin nanowhiskers
BC	Bacterial cellulose
BCNW	Bacterial cellulose nanowhiskers

cnp	Cellulose nano particles
Rd-B	Rhodamine B
FITC	5(6)-Fluorescein isothiocyanate mixed isomer
EVOH27	EVOH with 27 mole % ethylene content
EVOH44	EVOH with 44 mole % ethylene content
EVOH/cnw	EVOH nanocomposite containing cellulose nano whiskers
EVOH/chnw	EVOH nanocomposite containing chitin nano whiskers
LDPE/EVOH	LDPE composite incorporated with EVOH electrospun fibers
LDPE/EVOH/cnw	LDPE composite incorporated with EVOH cellulose nanocomposite
fd	freeze dried
sus	suspension

Chapter 1:
Introduction and Objectives

1.1 Introduction

Polysaccharide nanocomposites have received increased interest during the past few years due to various advantages polysaccharides have. These include biodegradability, abundance, low weight and high modulus[1]. Water suspensions of polysaccharide nanocrystals can be prepared by acid hydrolysis[2-4] and these nanocrystals have previously been incorporated into a variety of polymers such as poly(ethylene oxide), poly(vinyl alcohol), polypropylene and polystyrene[5-16]. Many researchers refer to these materials as nanowhiskers due to their rodlike structure as observed with characterization techniques such as transmission electron microscopy (TEM) and atomic force microscopy (AFM)[3,17]. Homogeneous dispersion of the nanowhiskers is a big challenge when these highly hydrophilic nanopolysaccharides are incorporated into a hydrophobic polymer matrix[3]. Ethylene-co-vinyl alcohol copolymers (EVOH) have a hydrophilic nature and therefore provide a method to produce a homogeneous dispersion of cellulose nanowhiskers when EVOH is used as the matrix in a nanocomposite. Nanowhisker reinforced nanocomposites with uniformly distributed nanofillers throughout the polymer matrix is, therefore, possible to achieve without any chemical modification. This has been shown by Martinez-Sanz et al. who incorporated bacterial cellulose nanowhiskers (BCNW) into EVOH, obtaining EVOH/BCNW fibers by means of the electrospinning technique[18]. Additionally, it was shown that the relative degree of incorporation as well as the T_g of the composite is higher when incorporating BCNW as a partially hydrated precipitate[18]. In a subsequent study, electrospun EVOH fibers containing up to 40 wt% cellulose nanowhiskers were used as a method of dispersing the cellulose nanowhiskers into an EVOH matrix by way of melt compounding[12].

In this study, cellulose and chitin nanowhiskers were isolated through acid hydrolysis[2,3] and incorporated into different EVOH copolymers with varying ethylene contents. Addition of nanowhiskers as a suspension therefore, motivated the choice of an aqueous blend as electrospinning solvent. Experimental techniques such as electrospinning and solution casting were used to process the EVOH nanocomposites, and were proven to be a viable route to incorporate and disperse nanowhiskers into a highly hydrophobic low density polyethylene (LDPE) matrix. Electrospinning is a unique process that enables the production of fibers from the micrometer range, which is typical of conventional fibers, down to nanometer range fibers. Outstanding properties such as a very large surface area to volume ratio, flexibility in surface functionalities, and superior mechanical performance make the polymer nanofibers to be most favourable candidates for many important applications such as in filtration, in electronic and

biomedical applications as well as in nanocomposite materials[19]. The extremely small dimensions of nanowhiskers, however, make it difficult to observe the degree of dispersion in the electrospun fibers using methods such as transmission electron microscopy (TEM) and scanning electron microscopy (SEM). Fluorescence was therefore investigated as an alternative characterization technique to obtain better results with regard to tracking the filler dispersion. Fluorescence has previously proven to be a possible technique in observing poor dispersion and agglomeration of nanoparticles[20].

LDPE and EVOH both contain polyethylene segments which results in miscible blends during melt blending when used in conjunction with a polyethylene–graft–(maleic anhydride) (PE-g-MA) compatibilizer[21]. Electrospun nanocomposite fibers containing different nanowhisker loadings were therefore sandwiched between LDPE/PE-g-MA films in order to study the change in mechanical properties of these LDPE multilayer composites.

1.2 Objectives

The main objective of this study was to incorporate biodegradable nanocrystals known as nanowhiskers, owing to their morphological structure, into an EVOH matrix to achieve a well dispersed nanofiller medium. These EVOH/nanowhisker nanocomposites were then to serve as a possible route for incorporation of the nanowhiskers into a polyethylene matrix.

The project was divided into three stages. The first stage involved the preparation and characterization of cellulose and chitin nanowhiskers. The second stage comprised of incorporation of the nanowhiskers into an EVOH matrix was studied by using simple solution casting and electrospinning. Characterization techniques were refined to study the extent of incorporation as well as effectiveness of the dispersion achieved.

And the third stage concerned the dispersion of the nanowhiskers into a polyethylene matrix by making use of the EVOH/nanowhisker electrospun fiber nanocomposites produced in stage 2.

1.3 Thesis outline

1. Chapter 1 presents an introduction, objective and short overview of the study.
2. Chapter 2 provides a brief history and literature review on the composite materials, characterization and processing methods used in this study.
3. Chapter 3 describes the experimental procedures followed in the study.
4. Chapter 4 discusses the isolation and characterization of cellulose and chitin nanowhiskers.
5. Chapter 5 describes the production of EVOH nanocomposites as solution cast materials as well as the chemical and thermal analysis thereof.

6. Chapter 6 discusses the morphology of electrospun nanocomposites containing different filler loadings as well as the chemical and thermal analysis of these electrospun fibers.
7. Chapter 7 deals with the production and mechanical analysis of LDPE multilayer composites. The production of the composites includes introduction of the EVOH electrospun fibers into LDPE films through a process of sandwiching followed by hot pressing.
8. Chapter 8 presents the conclusions and recommendations for future work.

1.4 References

(1) Azizi Samir MAS, Alloin F, Dufresne A. Review of recent research into cellulosic whiskers, their properties and their application in nanocomposite field. *Biomacromolecules* 2005;6(2):**612-626.**

(2) Bondeson D, Mathew A, Oksman K. Optimization of the isolation of nanocrystals from microcrystalline cellulose. *Cellulose* 2006;13(2):**171-180**.

(3) Dufresne A. Processing of polymer nanocomposites reinforced with polysaccharide nanocrystals. *Molecules* 2010;15(6):**4111-4128**.

(4) Goodrich JD, Winter WT. α-Chitin Nanocrystals Prepared from Shrimp Shells and Their Specific Surface Area Measurement. *Biomacromolecules* 2007;8(1):**252-257**.

(5) Azizi Samir MAS, Alloin F, Sanchez J-Y, Dufresne A. Cellulose nanocrystals reinforced poly(oxyethylene). *Polymer* 2004;45(12):**4149-4157**.

(6) Bondeson D, Oksman K. Polylactic acid/cellulose whisker nanocomposites modified by polyvinyl alcohol. *Composites Part A: Applied Science and Manufacturing* 2007;38(12):**2486-2492**.

(7) Brown EE, Laborie MG. Bioengineering Bacterial Cellulose/Poly(ethylene oxide) Nanocomposites. *Biomacromolecules* 2007;8(10):**3074-3081**.

(8) Capadona JR, Shanmuganathan K, Trittschuh S, Seidel S, Rowan SJ, Weder C. Polymer Nanocomposites with Nanowhiskers Isolated from Microcrystalline Cellulose. *Biomacromolecules* 2009;10(4):**712-716**.

(9) Cheng Q, Wang S, Rials TG. Poly(vinyl alcohol) nanocomposites reinforced with cellulose fibrils isolated by high intensity ultrasonication. *Composites Part A: Applied Science and Manufacturing* 2009;40(2):**218-224**.

(10) Favier V, Chanzy H, Cavaille JY. Polymer Nanocomposites Reinforced by Cellulose Whiskers. *Macromolecules* 1995;28(18):**6365-6367**.

(11) Liu H, Liu D, Yao F, Wu Q. Fabrication and properties of transparent polymethylmethacrylate/cellulose nanocrystals composites. Bioresource *Technology* 2010;101(14):**5685-5692**.

(12) Martinez-Sanz M, Olsson RT, Lopez-Rubio A, Lagaron JM. Development of bacterial cellulose nanowhiskers reinforced EVOH composites by electrospinning. *Journal of Applied Polymer Science* 2012;124(2):**1398-1408**.

(13) Nair KG, Dufresne A. Crab shell chitin whisker reinforced natural rubber nanocomposites. 1. Processing and swelling behavior. *Biomacromolecules* 2003;4(3):**657-665**.

(14) Nair KG, Dufresne A. Crab shell chitin whisker reinforced natural rubber nanocomposites. 2. Mechanical behavior. *Biomacromolecules* 2003;4(3):**666-674**.

(15) Morin A, Dufresne A. Nanocomposites of chitin whiskers from Riftia tubes and poly(caprolactone). *Macromolecules* 2002;35(6):**2190-2199**.

(16) Sriupayo J, Supaphol P, Blackwell J, Rujiravanit R. Preparation and characterization of α-chitin whisker-reinforced chitosan nanocomposite films with or without heat treatment. *Carbohydrate Polymers* 2005;62(2):**130-136**.

(17) Eichhorn S, Dufresne A, Aranguren M, Marcovich N, Capadona J, Rowan S, et al. Review: current international research into cellulose nanofibres and nanocomposites. *Journal of Material Science* 2010;45(1):**1-33**.

(18) Martínez-Sanz M, Olsson R, Lopez-Rubio A, Lagaron J. Development of electrospun EVOH fibres reinforced with bacterial cellulose nanowhiskers. Part I: Characterization and method optimization. *Cellulose* 2011;18(2):**335-347**.

(19) Huang Z, Zhang Y-Z, Kotaki M, Ramakrishna S. A review on polymer nanofibers by electrospinning and their applications in nanocomposites. *Composites Science and Technology* 2003;63(15):**2223-2253**.

(20) Langat J, Bellayer S, Hudrlik P, Hudrlik A, Maupin PH, Gilman Sr. JW, et al. Synthesis of imidazolium salts and their application in epoxy montmorillonite nanocomposites. *Polymer* 2006;47(19):**6698-6709**.

(21) Huang C, Wu J, Huang C, Lin L. Morphological, Thermal, Barrier and Mechanical Properties of LDPE/EVOH Blends in Extruded Blown Films. *Journal of Polymer Research* 2004;11(1):**75-83**.

2 Chapter 2:
Literature Review

2.1 Poly(ethylene-co-vinyl alcohol) (EVOH)

Ethylene vinyl copolymers are some of the most widely used packaging materials. These semi crystalline copolymers were discovered in the United States and developed commercially in Japan. EVOH is a random combination of hydrophobic ethylene and hydrophilic vinyl alcohol segments which is produced by a hydrolysis reaction of a parent ethylene-co-vinyl acetate copolymer (EVA) where the acetoxy groups are converted to a secondary alcohol[1]. This is illustrated by Figure 2.1.

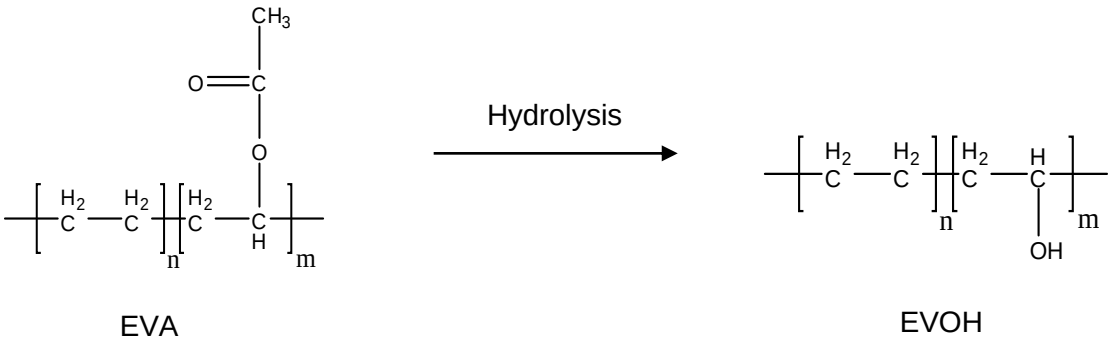

Figure 2.1: Conversion of EVA into EVOH through hydrolysis.

EVOH is, therefore, an amphoteric polymer composed of hydrophilic and hydrophobic segments which differ widely in properties depending on the copolymer composition. The end applications are determined by these properties that again depend on the differing ethylene contents. Two modifications of EVOH exist: The first is an EVOH copolymer with an ethylene content of 82-90 mole % which is used as an adhesive. The second one is an EVOH copolymer which is fully hydrolysed from EVA containing 60-75 mole % vinyl alcohol and mainly used as a barrier material. The vinyl alcohol content is responsible for the outstanding barrier properties (superior to other polymers) of the material under dry conditions while ethylene offers good moisture resistance as well as good mechanical and thermal properties[2]. EVOH also have many additional properties such as chemical and biological resistance as well as the ability to be easily sterilized[3], which makes it superior to similar semicrystalline materials. Strong intra- and inter-hydrogen bonding exists between alcohol groups which form a barrier for oxygen, other gasses and organic solvents. However, these hydrogen bonds can get intercepted by water molecules which weaken the bonds, increase the free volume and make EVOH a moisture sensitive

polymer[1,4]. The decrease in glass transition temperature (T_g), which is known as the plasticization effect, is a disadvantage when using EVOH as a food packaging material under humid conditions[5]. The presence of small amounts of water does not only negatively affect the oxygen permeability but also cause a decrease in mechanical[6] and thermal properties[7]. It is for that reason that EVOH need to be associated with hydrophobic materials such as polypropylene and polyethylene in multilayer structures in order to reduce water uptake[6,8]. It was also proposed by some authors that introduction of nanofillers such as clay platelets into a polyvinyl alcohol (PVA) matrix system might decrease water permeability by preventing easy access of water between polymer chains[9].

The main application for EVOH is currently as a barrier layer in the food packaging sector in order to increase the shelf life[5]. Other properties such as high transparency, biocompatibility, thermal resistance and high crystallization kinetics, contribute to the popularity of EVOH as a packaging material as well as its uses in the construction and biomedical field.

Progress is increasingly made towards the tailoring of materials which have potential use in the biomedical sector where they are applied in tissue engineering, wound healing or drug delivery systems[10,11]. A previous study proved the biocompatibility of EVOH by culturing neuronal cells[12], myoblast cells[13] and the formation of a uniform bonelike apatite layer using EVOH membranes as the substrate[11]. EVOH is a non-biodegradable but proven to be biocompatible polymer which is easily electrospun into nanofibers and it has been reported to be a suitable fiber substrate in supporting the culturing of smooth muscle cells and fibroblasts[10]. The blood compatibility of EVOH also resulted in positive outcomes during an investigation of hemodialyzers consisting of EVOH hollow-fiber membranes[14,15]. EVOH was furthermore seen to improve the permeability of 5-aminosalicyclic acid where an EVOH pH sensitive membrane was synthesized by covalent bonding of glycine in order to act as a colon specific drug delivery system[16].

One of the most attractive properties of EVOH results from the availability of the hydroxyl groups on the molecular chain. These hydroxyl groups make surface functionalization attractive and allow for specific interactions with other chemical species. This is an important property for blending with other polymeric materials, compatibilization with possible fillers and future biomedical applications[11,17,18].

2.2 Polyethylene (PE): an overview

Polyethylene(PE) is part of a semicrystalline group of polymers which consist of ethylene monomer segments in the backbone. The formula for PE is $-(CH_2)_n-$ and is the simplest polyolefin structure. PE can have many different properties depending on the amount and type of branching existing in the main chain. Branching depends on the polymerization process conditions which have been developed over the years. Commercial production of PE started in 1939 in the UK after ICL laboratories discovered the polymerization of ethylene in the presence of benzaldehyde at very

high pressure by accident. This was the introduction of low density poly(ethylene) (LDPE) manufacturing[19,20].

PE can be tailored in order to produce a variety PE based products by way of catalytic polymerization. This can be done by controlling the molecular weight, density molecular weight distribution or crosslinking. The three most popular types of PE are LDPE, linear low density polyethylene (LLDPE) and high density polyethylene(HDPE). These polymers differ mainly in density which routes from the branching in the main chain. Branching can either be extremely scarce on the main chain resulting in linear chain molecules known as HDPE or branching can be quite prominent in the form of long chain branching or short chain branching[19,20]. The rough sketches in Figure 2.2 provide good representations of how the three types of PE differ in molecular structure.

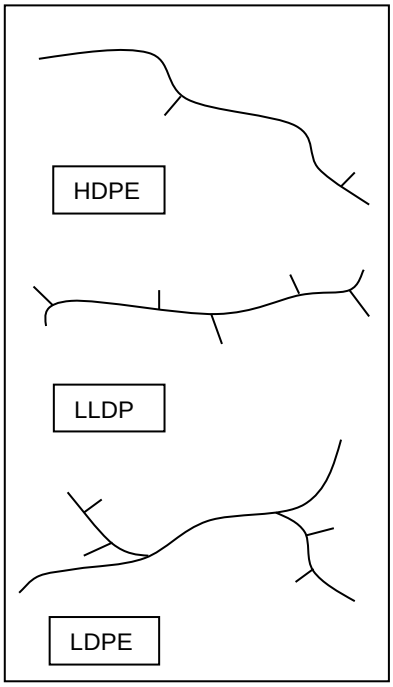

Figure 2.2: A rough representation of the different molecular structures of polyethylene.

2.2.1 LDPE

LDPE is produced via a free radical polymerization reaction under very high pressure processes. LDPE has a very wide molecular weight distribution and can range from a waxy appearance to a very tough material with high molecular weight. An advantage of LDPE to the other PE products is the ability to incorporate polar molecules or monomers along the chain. The mechanical characteristics of LDPE is totally dependent on the three different properties namely molecular weight, molecular weight distribution and the extent of long and short chain branching. Depending on the properties named above, LDPE can either be a quite rigid material or an extremely flexible material. The crystallinity of LDPE is directly proportional to the amount of short chain branching on the polymer chain. Density is directly proportional to the polymer crystallinity.

Long chain branching is responsible for the molecular weight distribution of LDPE. The melt viscosity is directly proportional to the average molecular weight. Other properties such as resistance to creep, tensile strength, abrasion resistance, low temperature resistance to brittleness, shrinkage, warpage and impact strength are also seen to increase with an increase in molecular weight. Yield strength, tensile strength and elongation are crucial properties due to the popularity of LDPE as a commercial material[19-21]. LDPE has excellent barrier properties and is highly impermeable to moisture. It is, therefore, a highly attractive material in packaging applications for chemicals and foods. Unfortunately polyolefins do not have high barrier properties for hydrocarbons. It is for that reason that LDPE often get processed in multilayer films with materials which have good barrier properties against organic solvents. EVOH is a copolymer which is often sandwiched between these polyolefin layers due to the excellent resistance to permeability for oxygen and hydrocarbons[18,22-24].

2.3 Cellulose

Anselme Payen, a French scientist, was the first to isolate and identify cellulose from plants and determined the chemical formula in 1838 as $(C_6H_{10}O_5)_n$[25]. Cellulose is a natural polymer made up of sugar monomers and is therefore known as a polysaccharide. It consists of a linear chain with thousands of β (1→4) linked D-glucose units, known as cellobiose. Cellulose was chemically modified and the first thermoplastic polymer produced in 1870 by Hyatt Manufacturing Company, called Celluloid[25,26]. The structure was determined in 1920 by Herman Staudinger and in 1992, Kobayashi and Shoda were the first to chemically synthesize cellulose[25,27-29]. Figure 2.3 illustrates the molecular structure of cellulose.

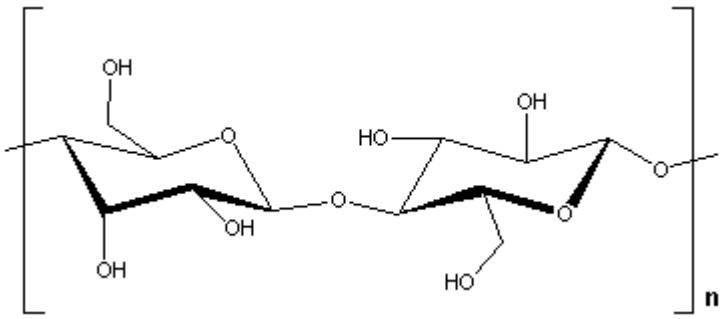

Figure 2.3: The molecular structure of cellulose.

Each of the glucose repeat units contains three hydroxyl groups which are arranged in such a way to form extensive hydrogen bonding between the molecules and cause the chains to form highly ordered crystalline regions. The extent to which molecular bonding occurs therefore, determines the physical characteristics of cellulose[30,31]. The amount of water taken up by cellulose

can be a measure of the degree of crystallinity as it was previously shown that the amorphous (unordered) regions are likely to absorb more water than the crystalline regions[32]. The cellulose crystal exists as two allomorphs namely alpha cellulose which has a parallel configuration and beta cellulose with an antiparallel configuration. Cellulose does not easily dissolve in aqueous solvents and degrades before it melts at high temperatures due to the strong hydrogen-bonding network[33]. Cellulose is the most abundant biological polymer on the planet and found in the cell wall of green plants, algae and bacteria. The fibers are arranged in such a way to provide structure and support[28,33]. Bacteria belonging to certain genera like acetobacterxylinum produce bacterial cellulose (BC) by extracellular secretion forming biofilms. BC is chemically exactly the same as plant cellulose but differs in terms of higher crystallinity, mechanical properties and purity. These properties have shown great potential in biomedical applications[28,34]. The abundance of cellulose as well as its renewability, biodegradability and strength, makes it an extremely attractive material for industrial use.

Wood is the cellulose resource which is probably used mostly in the commercial field. Wood pulp is a natural composite of cellulose fibers, hemicellulose and lignin. Wood pulp needs to undergo an extraction and bleaching process before obtaining pure cellulose[35]. Cellulose chains pack together, repeatedly to form microfibrils in the cell walls. These microfibrils aggregate together forming larger fibers. The microfibrils have diameters of approximately 3.5 x 10 nm and indeterminate lengths[29,36]. The macro sized fiber structures which consist of crystalline and amorphous regions often get broken down to produce nano sized fibers where both length and width are in nanometer range. These nanocrystals are highly crystalline and it has been proven in several studies to act as excellent reinforcement fillers in nanocomposite materials[37-41]. Strong hydrogen bonding between the individual cellulose nanocrystals results in larger aggregates also known as microcrystalline cellulose (MCC). MCC is a commercially available material produced mainly from a spray drying process and generally used in the pharmaceutical industry[36,42]. When MCC is used as the source for producing cellulose nanowhiskers, the isolation steps are significantly reduced in terms of extraction and hydrolysis in comparison to other sources such as wood pulp, ramie fibers and sugarcane[43].

2.3.1 Cellulose nanowhiskers

Cellulose nanocrystals are the monocrystalline domains which form the elementary fibrils which in turn aggregate to form native cellulose fibers. These nanocrystals are often referred to as nanowhiskers due to the rodlike crystalline structure which narrows down towards the ends exactly like a cat's whiskers. Acid hydrolysis of cellulose is probably the most widely used process in order to obtain these nano structures[25,44-47]. It is based on the principle that the acid first degrades the unordered amorphous regions by easy access and cleavage of the glycosides bonds[32]. Ranby was the first to report a sulphuric acid hydrolysis process of cellulose[49]. Further studies that was carried

out on nanowhiskers in suspension reported on the ability of the nanowhiskers to self- order in a helicoidally manner as well as the formation of birefringent gels[45,50].

Nanowhisker diameters of 3-30 nm and lengths between 30nm and several microns have been reported[33,51]. Techniques such as Transmission electron microscopy (TEM), wide angle X- ray diffraction (WAXD) and atomic force microscopy (AFM) was used by Elazzouzie-Hafraoui et al in order to determine dimensions of nanowhiskers produced from different cellulose sources[51]. It was found that the polydispersity differ for plant and animal cellulose sources and is related to the elementary crystals (fibrils). Plant cellulose nanowhiskers were found to have a lower average aspect ratio where aspect ratio is the ratio of length to width of an individual crystal.

The optimum hydrolysis conditions of cellulose nanowhiskers results in a highly organized crystalline structure which has excellent mechanical properties[44]. It has also been shown that by using sulphuric acid instead of hydrochloric acid (HCl), a more stable aqueous suspension of nanowhiskers can be prepared due to the presence of negatively charged ester sulphate groups. These negative ester sulphate groups create double layer electric repulsion between particles. Hydrolysis with HCl on the other hand results in nanowhiskers with a higher thermal stability[52].

Due to a near perfect crystalline arrangement, cellulose nanowhiskers have a high modulus. A value of 138 GPa for the crystal modulus was reported using X-ray diffraction[28] and since then many publications followed with values between 100 and 160 GPa using molecular dynamic methods[53-56].

In a review article by Eichhorn et al., Favier was the first to report on nanocomposites using cellulose nanowhiskers as the reinforcing phase[28]. Following his report, extensive studies have been done on the use of cellulose nanowhiskers in nanocomposites due to the attractive properties of these nanofillers: high mechanical strength and modulus, biodegradability, light weight, renewability and non-toxicity[42,44,57,58,59]. The high surface area of several hundred m^2/g [60] gives these nano structures high reinforcement potential even at low filler values. Important factors which play a big role in the development of reinforced nanocomposites are the nanowhisker aspect ratio, thermal stability of the nanoparticles, nanofiller-matrix compatibility and the dispersion of the nanowhiskers in the matrix. The source of cellulose nanowhiskers determines the aspect ratio, shape and certain physical properties of the nanowhiskers which influence the effectiveness of the processed nanocomposites. Figure 2.4 displays TEM images of different types of cellulose nanowhiskers taken from literature[28].

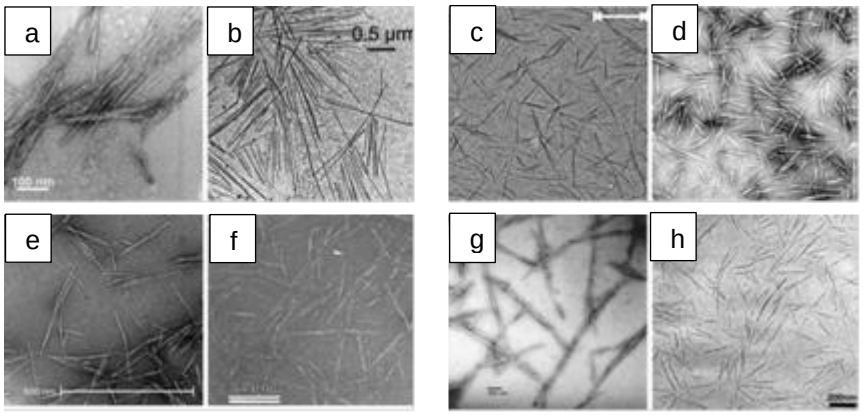

Figure 2.4: Transmission electron microscopy images of cellulose whiskers obtained from acid hydrolysis of[28] (a) MCC, (b) tunicate, (c) cotton, (d) ramie, (e) sisal, (f) straw, (g) bacterial cellulose and (h) sugar beet.

2.4 Chitin

Chitin is chemically almost identical to the structure of cellulose where the hydroxyl on the second carbon is replaced with an acetamido group as illustrated by Figure 2.5.

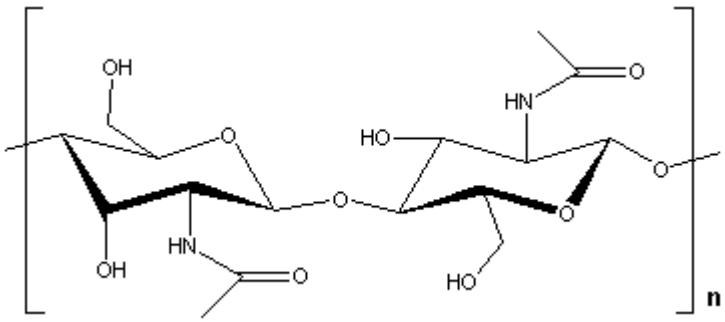

Figure 2.5: Molecular structure of chitin.

Chitin is the second most abundant polysaccharide and is found mainly in the shells of crabs and shrimps[61]. Other sources of chitin which have also been explored in several reports are squid pens[62] and tubes of Riftia pachyptila tube worms[63]. Chitin was for the first time identified in 1884 and is a long linear polymer known as poly(β(1→4)-N-acetyl-D-glucosamine)[64,65]. The isolation of chitin is very similar to that of cellulose and depends on the source. The first step is pretreatment of the chitin with acid in order to dissolve the calcium carbonate. Thereafter an alkaline extraction results in deproteination. A final bleaching step is carried out to remove all the pigments[64]. The chitin chains form highly crystalline regions of closely packed microfibrils which act as the structural component in the exoskeleton of arthropods as well as in the cell walls of fungi and yeast[64,66,67]. The high mechanical reinforcement and strength of these crystalline structures are attributed to strong intra and inter chain hydrogen bonding[68] (Figure 2.6).

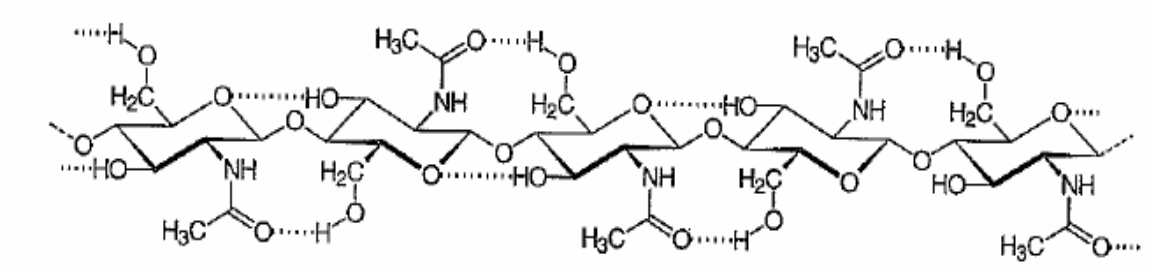

Figure 2.6: Chemical structure of chitin: the intramolecular hydrogen bonds are represented by the dotted lines.

Chitin exists as two allomorphs, depending on the source, and differs slightly in terms of crystal morphology[64]. Inter-sheet hydrogen bonding is only found in alpha chitin, therefore, and makes beta chitin chains therefore much more prone to the penetration of polar organic molecules. Alpha chitin is most abundant in crab shells and is insoluble in water and most organic solvents[64]. This property of chitin is disadvantageous in the processing step when used. These crystal structures have been characterized using crystallography[69,70] and FTIR[64,71,72,73] and it is seen in Figure 2.7 that the C=O stretching region of the amide moiety between 1600 cm^{-1} and 1500 cm^{-1} differs for the two crystal structures. The Amide I band for alpha chitin is split at 1656 cm^{-1} and 1621 cm^{-1} and Amide II is unique at 1556cm^{-1} [64].

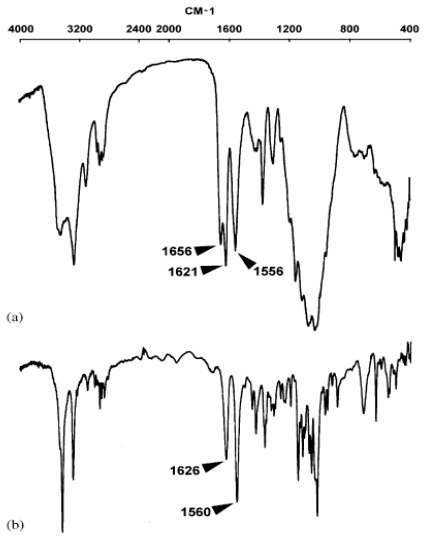

Figure 2.7: FTIR spectra of (a) α-chitin and (b) β-chitin.

Chitin has received plenty of attention lately due to the attractive chemical and physical properties. Chitin is a biodegradable polymer with low toxicity and has antibacterial properties with physiological inertness. It is hydrophobic and can be used in moisture controlling applications[64,74]. Chitin is, therefore, especially popular in the biomedical field where it has been proved to be successful in wound healing[75,76] and drug release applications[76,77]. Its affinity for proteins makes it an excellent substrate for the immobilization of enzymes and whole cells[78]. The food industry takes advantage of the antimicrobial property and it is also used in the treatment of wastewater due to

the metal chelating property and insolubility[79]. Another very important application of chitin, which has been studied and reported on a few times, is the use of chitin nanocrystals as reinforcing nanofillers in polymer composites in order to improve mechanical strength[61,67,74,80,81-84].

2.4.1 Chitin nanowhiskers

The extraction method for chitin nanowhiskers is nearly the same as previously described for cellulose. Morin and Dufresne describe a deproteination process where after the sample gets bleached[63]. The purified sample is then treated with hydrochloric acid (3 N) in order to hydrolyse the polysaccharide by cleavage of the glucose bonds. Suspensions are centrifuged and transferred to dialysis bags where it is dialyzed for several days until it reaches a neutral pH.

Usually the pH is then adjusted to 3.5 by the addition of HCl which results in protonation of the amino groups. The positively charged groups on the whisker surface result in a stable suspension which displays colodial behaviour[85]. Dimensions similar to those of cellulose crystals have been reported for several different chitin sources[66,67,86,87]. Chitin nanowhiskers are attractive nano reinforcements due to many excellent properties such as high aspect ratio, high surface area, mechanical strength and stiffness, light weight, ease of chemical modification, biodegradability and abundance[67,88]. Chitin nanowhiskers have been used as reinforcement in many different synthetic as well as natural polymer matrixes as already mentioned in the section above. Improvement in mechanical properties has been shown as well as a decrease in the water sensitivity of soy protein nanocomposites[89].

Similar to cellulose nanowhiskers, several strategies have been investigated in order to improve the dispersion of chitin nanowhiskers in different polymer matrixes. A thermoformable polymer-grafted nanocrystal has been reported where chitin whisker-graft polycaprolactone (PCL) has been synthesized by initiating the ring-opening polymerization of caprolactone monomer onto the chitin nanowhisker surface under microwave radiation[88].

As mentioned previously, chitin nanowhiskers have been produced from several different sources which were characterized using TEM analysis as illustrated in Figure 2.8: TEM images of isolated chitin nanowhiskers[62,63,80,84,87] from (a) squid pen and (b) crab shells[62,63,80,84,87]. It is clear from these TEM images that the crystal dimensions differ depending on the source of chitin.

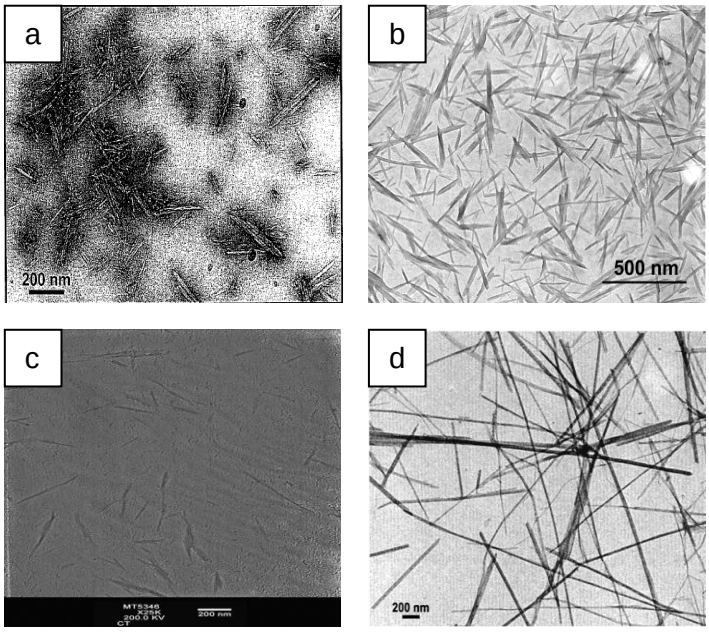

Figure 2.8: TEM images of isolated chitin nanowhiskers[62,63,80,84,87] from (a) squid pen and (b) crab shells.

2.5 Nanocomposites

Composite materials are made up of at least two individual constituents. One is usually the matrix and the other the reinforcing phase. The matrix surrounds the reinforcing particles, keeping them in place while the reinforcing particles provide the composite with specific chemical or physical properties. Composite materials can be natural occurring or synthetic and very often using polymers as the matrix material. Wood is one of the oldest and still is one of the most widely used natural composites. Bakelite, which is a fiber reinforced thermoset polymer, was one of the first polymer composites synthesized by man in 1907. Even in earlier years, carbon black nanoparticles were already incorporated into vulcanized rubber in order to strengthen automobile tires[90].

In order for a composite material to be called a nanocomposite, the reinforcing particle should have at least one dimension less than 100 nm[91]. The superiority of nano sized particles to macro sized particles lie in the reduced amount of voids and imperfections which leads to better composite properties[92]. The surface area of nano particles is much larger and, therefore, a better option for possible interaction with the matrix compared to macro particles. Nanocomposites are also unique in the sense that they can display optical clarity. The incorporated nanoparticles usually do not scatter light because they have wavelengths shorter than that of light[28,42].

Unlike macro composites, nano reinforcements do not produce large stress concentrations which reduce the ductility of the material[93]. Nano reinforcements exist as different shapes and sizes and can be natural or synthetically made. Particles can be in the form of sheets for example silica plates, tubes and whiskers or they can be spherical[57]. Incorporation of these geometrical shapes into the matrix phase result respectively in a one, two or three dimensional nanocomposite[31]. The potential and application of nanocomposites in various areas of research,

engineering and the medical sector is increasingly attracting attention. The function of different nanoparticles within the polymer nanocomposite may differ depending on the geometrical shape or source of nanoparticles. The main purpose of nanocomposite production is most often for reinforcement or biomedical applications.

The incorporation of these nanoparticles may enhance or reduce certain characteristics of the polymer depending on the end application. Improvement in reinforced nanocomposite can only be achieved increasing three important factors namely: i) thermal stability of the nanoparticles, ii) surface interaction between nanoparticle and polymer matrix, iii) dispersion of nanoparticles in the matrix.

2.6 Nanopolysaccharide composites

Nanowhiskers have unique structural and physical aspects which give them superior tensile, optical, electrical and chemical properties compared to macrofibers used as reinforcing fillers within a polymer matrix[91]. Utilizing specifically natural polymers for the production of nanowhiskers is gaining wide interest due the high abundance, biodegradable nature, renewability and off course the previously mentioned superior physical properties. The effective transfer of stress in a reinforced nanocomposite can only be achieved during proper adhesion between matrix and nanofiller. Proper adhesion results from uniform dispersion of fillers in the matrix as well as compatibility between matrix and filler. Uniform dispersion of cellulose nanowhiskers in thermoplastics is challenging and difficult to achieve during incorporation. The cellulose fibers are highly hydrophilic and due to strong inter fiber hydrogen bonding, fibers tend to agglomerate resulting in poor dispersion. This is especially true for nonpolar polymer solutions[36]. Hydrophilic polymer matrices is expected to associate better with the hydrophilic nanofiller, which contain a large amount of hydroxyl groups on the backbone, and therefore obtaining better dispersion. The negative charges induced on the surface of nanowhiskers from sulphuric acid hydrolysis of MCC, result in stable dispersed aqueous suspensions of whiskers[38,52,91,94] as previously reported. Hydro soluble polymers such as polyethylene oxide (PEO)[38], polyvinyl alcohol PVA[95], hydroxypropyl cellulose (HPC)[96], soy protein islolate (SPI)[97] and carboxymethyl cellulose (CMC)[28] are therefore effectively mixed with these stable nanofiller dispersions obtaining nanocomposites with improved characteristics[97]. The objective is, therefore, to decrease the surface tension by using various processing aids, treatment of cellulose and coupling agents to facilitate in more effective dispersion of cellulose nanowhiskers in solutions with lower polarity.

2.7 Methods of nanowhisker dispersion

2.7.1 Polymer latexes

The use of polymer latexes as a method of dispersion and processing, allows researchers to produce nanocomposites by using a water medium to dissolve the matrix and then suspend the nanofiller as a water suspension. The blending of the matrix and filler, therefore, preserves the homogeneous dispersion of the nanowhiskers. A latex obtained from poly(styrene-*co*-butyl acrylate), was used to prepare the cellulose nanocomposite using different sources of cellulose nanowhiskers and Riftia tube chitin whiskers as reinforcements[63,98,99]. Polyvinyl(acetate)[100] poly(vinyl chloride)[41] and natural rubber[39,61] are only a few mentioned of various polymer matrices used to prepare latexes for the processing of nanocomposites. It has also been reported that the addition of a reactive silane as a stabilizer during a mini emulsion polymerization reaction, resulted in a stable water composite dispersion of poly(styrene-co-(hexyl-acrylate) and cellulose nanowhiskers[101]. One of the techniques used for processing these aqueous dispersions, is solution casting, leaving the water to evaporate at a temperatures above the glass transition temperature (T_g). Freeze drying followed by hot pressing or followed by extrusion and then hot pressing was shown to be another but more effective method in obtaining homogeneously dispersed nanocomposite films[102,103].

2.7.2 Grafting

Grafting of polysaccharide nanoparticles, known as long chain surface chemical modification, has been done in a number of studies in order to create a homogeneous nanocomposite with strong interfacial interactions. Grafting agents consist of a reactive end group and a long compatibilizing tail which generally increase the hydrophobicity of the nanowhiskers and improve the bonding between nanowhisker and polymer matrix. Two routes can be followed in order to achieve grafting reactions namely grafting onto or grafting from the surface[91]. Chemical grafting may potentially alter the physical and mechanical properties. Grafting of the poly(caprolactone) (PCL) phase directly onto/from the cellulose nanowhiskers using coupling agents and ring opening polymerization respectively has been previously reported[104]. A similar microwave assisted ring opening polymerization of PCL from chitin nanowhiskers has also been shown to successfully enhance mechanical properties[88]. The formation of a covalent bond between filler and matrix cause the stress transfer at the interphase to significantly increase. In order to achieve well dispersed cellulose nanowhiskers in a highly hydrophobic LDPE matrix, different lengths of organic acid chlorides were grafted onto cellulose nanowhiskers by an esterification reaction. The surface modified nanowhiskers with different lengths of aliphatic chains showed increased hydrophobicity and consequently better compatibility with the LDPE matrix. The LDPE and modified cellulose nanowhiskers were co extruded and hot pressed forming solid nanocomposite films[105]. Very few

studies regarding the extrusion of polysaccharide nanowhisker reinforced nanocomposites have been reported.

2.7.3 Chemical surface modification

Suitable organic solvents are necessary for dissolving a nonpolar polymer matrix. An alternative way is, therefore, necessary to effectively disperse polysaccharide nanowhiskers in the organic medium in order to form homogeneous nanocomposites.

One way to improve compatibility between the non-aqueous medium and hydrophilic cellulose nanowhiskers is to reduce the surface energy by chemically modifying the surface of either nanofiller or polymer matrix. Cellulose contains hydroxyl functionalities which make it attractive nano reinforcements for surface modification. Treatment of fibers with hydrophobic molecules containing reactive groups capable of covalent bonding to the matrix polymer for example silation[106,107].Such methods have been shown in previous studies to impart hydrophobicity to the surface of cellulose[108] and chitin[61,80] nanowhiskers followed by improved dispersion in non-aqueous solvents[107]. The polymer matrix can also be chemically modified in order to enhance compatibility and eventually lead to better dispersion of the filler. Maleated polypropylene (PP) is an example of a chemically modified hydrophobic polymer[109] where it is proposed that the acid groups from maleic anhydride form strong bonding with the hydroxyl groups of cellulose nanowhiskers.

2.7.4 Adsorption

The use of surfactants is another way of reducing the surface tension in order to increase filler/matrix interfacial adhesion. A phosphoric ester, consisting of a hydrophilic head and hydrophobic tail, was added as the surfactant to coat tunicin and cotton cellulose whiskers which led to stable suspensions in different organic solvents[43,52]. Solvent cast reinforced composite films were obtained using coated tunican whiskers dispersed in toluene mixed with solutions of poly(ethylene-co-vinyl acetate)[110], atactic PP[109] and isotactic PP[111] as matrices. Treatment of cellulosic surfaces with cationic polyelectrolytes results in irreversible adsorption[112] and strategies based on the adsorption of polyelectrolytes were shown to be another way of improving adhesion and distribution of cellulose-reinforced composites.

The building up of multilayers on cellulosic surfaces by the careful application of oppositely charged polyelectrolytes can improve adhesion between matrix/filler as well as resulting in unique optical effects[113-116].

2.7.5 Electrospinning: an overview

2.7.5.1 Introduction

Electrospinning is a unique process that enables the production of fibers from the micrometer range, which is typical of conventional fibers, down to nanometer range fibers. When the diameter of polymer fiber materials are shrunk from micrometer (e.g. 10-100 μm) to submicrons or nanometers (e.g. $10x10^{-3}$ –$100x10^{-3}$ μm) several amazing characteristics appear, such as a very large surface area to volume ratio (this ratio for the nanofiber can be as large as 103 times of that of a microfiber), flexibility in surface functionalities, and superior mechanical performance (e.g. stiffness and tensile strength) compared with any other known form of the material. Outstanding properties like these make the polymer nanofibers to be most favourable candidates for many important applications such as filtration, electronic, and biomedical applications, etc. These applications are described in an extensive review that was published by Ramakrishna et al. on the use of electrospinning of polymers to produce micro- and nanosized fibers[117]. Electrospinning is therefore becoming one of the most popular processing methods to achieve nanofibers with extremely high surface areas and consequently seems as an attractive method of dispersing nanowhiskers in a polymer matrix ensuring homogeneity.

2.7.5.2 History

Electrospinning of polymer solutions and melts is a process which has already been observed in the late 1800's and first patented in 1934 by Formhals when it first became commercially popular[118]. Taylor set the groundwork for electrospinning in 1969 and in the 1990's Reneker and Chun used a wide range of polymers in order to produce electrospun fiber mats[119]. Electrospinning regained attention in the late 1900's due to the growing interest in nanotechnology.

2.7.5.3 Process and setup

This well established process was termed electrospinning due to the use of electrostatic forces in order fabricate long continuous filaments with diameters in the range of microns down to nanometer scale. Smaller diameters increase the surface area which holds in several advantages of the electrospun fibers. Electrospinning works on the principle that strong repulsive forces which is produced by a direct current (DC) voltage supply, has to overcome the surface tension of the polymer solution. The increase in electrical field cause the surface liquid to form a conical shape called the Taylor cone[117-121]. At a critical point, a charged jet of polymer solution is ejected from the tip of the Taylor cone (see Figure 2.9(b)). The solvent evaporates during a whipping process where the stretched polymer fiber is randomly collected on a grounded metal plate of opposite polarity than the charged jet. A simple schematic representation of the electrospinning setup is shown below in Figure 2.9(a).

The in-house built setup consists of three major components:

1. a high voltage power supply which produces an electrical field (5-50 kV).
2. a spinneret which holds the polymer solution and usually feeds the solution at a controlled rate by a syringe pump.
3. a grounded collecting plate which has opposite polarity to that of the electrode charging the polymer solution in the spinneret.

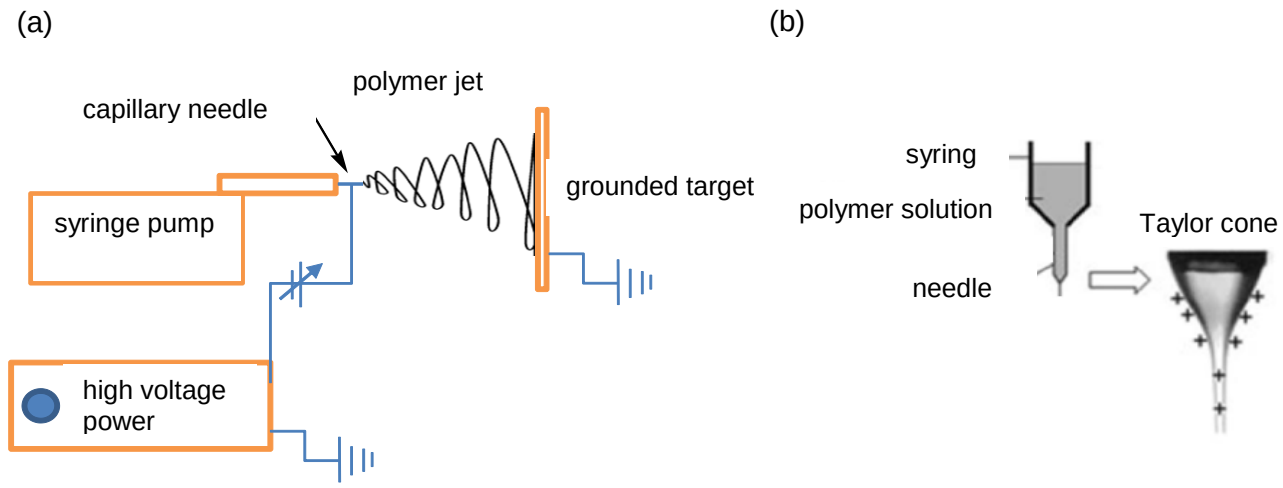

Figure 2.9: (a) Schematic representation of an electrospinning setup and (b) the Taylor cone forming at the tip of a charged needle.

The grounded target can either be stationary collecting randomly directed fibers or rotating on a rotating drum collecting highly aligned fibers as shown in Figure 2.10[122].

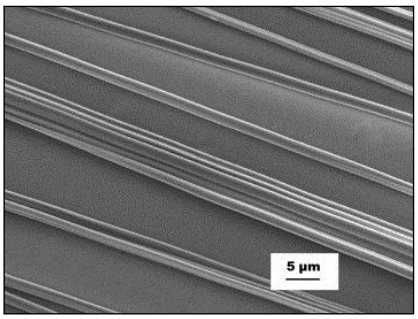

Figure 2.10: Aligned electrospun fibers collected from a rotating collector.

2.7.5.4 Parameter effects

Even though electrospinning seems like a simple technique and set up, the science behind the process is much more complicated and requires proper understanding of the many variables which influence the formation of these fibers. It is important to take into consideration the way in which

the solution properties as well as the process conditions (listed below) affects the morphology and diameter of the electrospun fibers[117,118]. Figure 2.11 illustrates that simply by changing one parameter, for example decreasing solution concentration, the produced fibers have many beads instead of smooth fibers with uniform diameters[10].

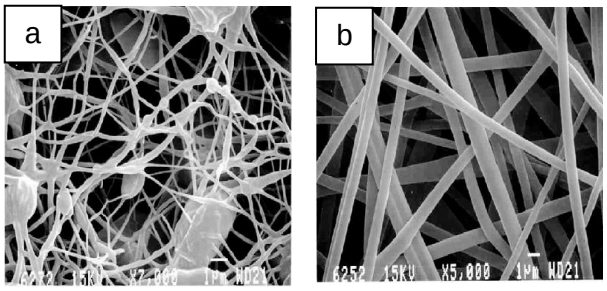

Figure 2.11: SEM images of EVOH fibers spun from solutions of a (a) 5 wt% and (b) 10 wt% concentration (g polymer/ml solvent)[10].

Solution properties which influence fiber morphology:

1. Concentration/viscosity
2. Molecular weight and architecture
3. Conductivity

Processing parameters which influence fiber morphology:

1. Applied voltage
2. Feed rate
3. Tip to collector distance
4. Ambient conditions: atmospheric temperature and humidity

2.7.5.5 Electrospun EVOH nanocomposites

Table 2.1 is a summary of various reported nanocomposites which have successfully been electrospun into fibers as a method of dispersing the cellulose and chitin nanowhiskers as reinforcing phase.

Table 2.1: Electrospun nanocomposites containing cellulose or chitin nanowhiskers reported in literature.

Polymer matrix	*Polysaccharide nanowhisker (nw)*	*Observations*	*Reference*
polyethylene oxide (PEO)	(a) MCC (b) Bacterial cellulose	(a)Increase in mechanical properties and improved alignment of nanowhiksers (b) enhanced mechanical properties	(a)[123] (b)[124]
polystyrene (PS)	Cotton cellulose	Increased strength and elastic modulus	[125]
polyvinyl alcohol (PVA)	(a) Cellulose from Rami fibers (b) Chitin	(a) Enhanced thermo mechanical properties and storage modulus (b) Increased tensile strength and young's modulus	(a)[95] (b)[84]
poly(caprolactone) (PCL)	MCC	Increased storage modulus and nonlinear deformation in strength properties	[126]
poly lactic acid (PLA)	MCC	Increased strength, decreased fiber diameter	[127]
Poly(ethylene-vinyl alcohol) (EVOH)	Bacterial cellulose	More uniform fiber morphology, increased T_g and decreased thermal stability	[128]
Poly methyl methacrylate (PMMA)	(a) Bacterial cellulose (b) Wood pulp cellulose	(a) Increased thermal stability, alignment of cnw, increased T_g and decreased fiber diameter (b) Increased T_g, cnw alignment,and modest increase in mechanical properties	(a)[129] (b)[130]
Chitosan	MCC/chitin blend	Improved structural morphologies	[131]
Poly acrylic acid (PAA)	Cotton cellulose	Decreased fiber diameter, improved uniformity, increased young's modulus and increased strength.	[37]
Lignin/PVA	Cotton cellulose	Improved thermal stability	[132]
Regenerated cellulose	Cellulose	Physical properties of the composites were inferior to the cellulose controlls	[133]

2.8 Characterization of isolated nanowhiskers and nanocomposites

2.8.1 Transmission electron microscopy (TEM) analysis

TEM works on the same principle as a light microscope but uses electrons instead of light which travels through the material. This makes it possible to view objects to the order of a few angstroms and provides us with an extremely powerful tool when studying small detailed structures. Conventional bright field TEM has frequently been used as a tool in characterizing various types of polysaccharide nanocrystals. Cellulose whiskers from sources such as wood, tunicin, ramie, cotton, wheat straw, bacterial cellulose and sugar beet as well as chitin whiskers and starch crystals have been studied[28].

Negative staining is used to enhance the contrast between different phases in order to determine size, shape and crystal aggregation as seen in Figure 2.12[46]. TEM images of nanocomposites (see Figure 2.12(b)) make the study of whisker dispersion within the polymer matrix possible[37,43,124].

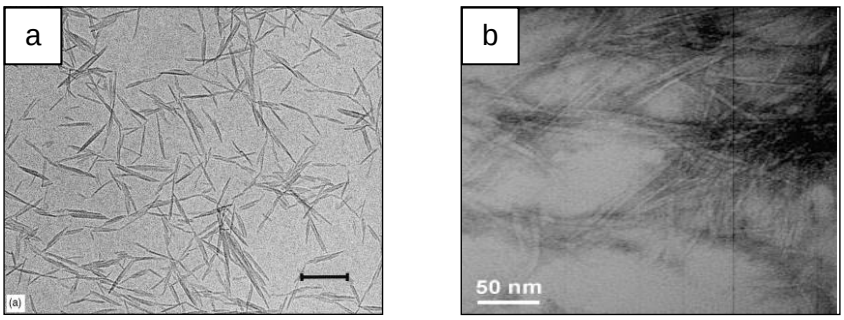

Figure 2.12: TEM images of (a) isolated cellulose nanowhiskers and (b) PLA nanocomposite containing 5 wt% cellulose nanowhiskers[46].

Figure 2.13 illustrates TEM images of PAA imbedded with cellulose nanocrystals. The crystals are observed as rods and spheres. PEO containing bacterial cellulose (BC) was the first nanocomposite to be successfully electrospun into fibers[124] and is illustrated in Figure 2.14. TEM analysis display agglomeration and orientation of bacterial cellulose nanowhiskers inside PEO. It was also observed that the nanofiller increased the mechanical strength of the polymer[124].

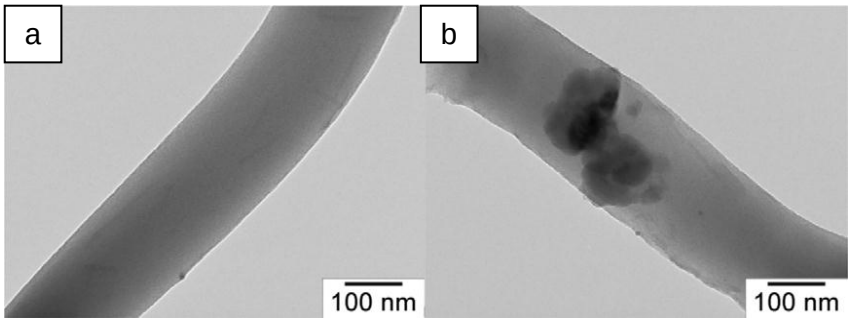

Figure 2.13: TEM images of electrospun PAA/cellulose nanocrystal (cnc) nanocomposites fibers showing entrapped cnc (a) rods and (b) spheres.

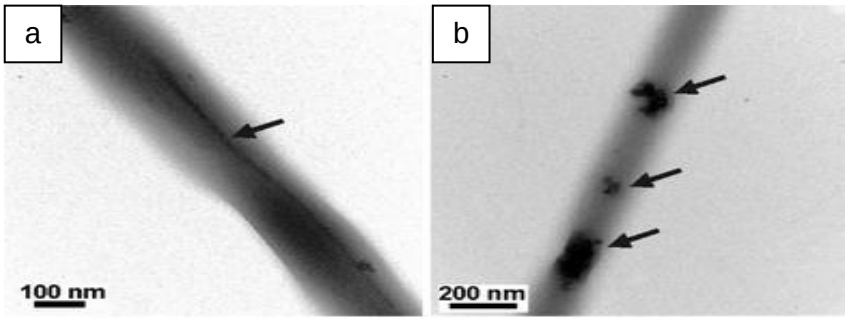

Figure 2.14: TEM images of BC nanowhiskers embedded in PEO electrospun fibers showing (a) orientation and (b) agglomeration of the nanowhiskers[124].

2.8.2 Atomic force microscopy (AFM) analysis

AFM is an attractive tool, in addition to TEM, for studying isolated nanowhiskers. AFM measures attractive or repulsive forces between a cantilever tip and the surface of the sample. These forces cause the cantilever to bend which is sensed by a lazer beam and processed in such a way to provide information on the mechanical properties as well as the morphology of the surface. It is thus possible to determine the elastic modulus and hardness of isolated nanowhiskers of polysaccharides. Structural images created by AFM are seen in Figure 2.15 and differ slightly from TEM and FESEM which may be attributed to the shape of the tip being dragged over the surface. Good contrast and resolution is found with AFM which makes the staining process unnecessary. AFM is a reasonable new approach in the study of nanowhisker based nanocomposites. A recent report from Ingvild Kvien et al. illustrated that ultramicrotomy of nanocomposite films at cryogenic temperatures enable detailed inspection of the cellulose whiskers in PLA matrix as seen in Figure 2.15(b)[43].

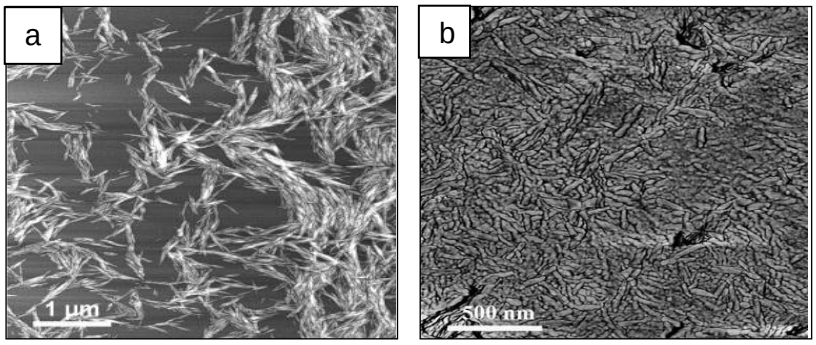

Figure 2.15: AFM topography images of the (a) isolated cellulose nanowhiskers and (b) cryo-microtomed surface of the solution-cast PLA/cellulose whiskers nanocomposite[43].

2.8.3 Flow birefringence

Flow birefringence is a simple method which can be used to investigate whether nanowhiskers are isolated and well dispersed in a suspension. This characterization procedure seems to be a routine in most previous studies after preparation of a nanowhisker suspension. The setup for flow birefringence is shown below in Figure 2.16 and consists of a light source and two polarizing filters which are placed at a 90 degree angle with regard to each other on opposite sides of the suspension. The suspension is stirred in order to observe any patterns which can be related to the flow birefringence of the crystals. The nanowhiskers will align in the direction of flow causing macro domains observed through the polarized filters as a distinct light pattern called flow birefringence. In the case of crystal aggregates in suspension, no flow birefringence will be seen.

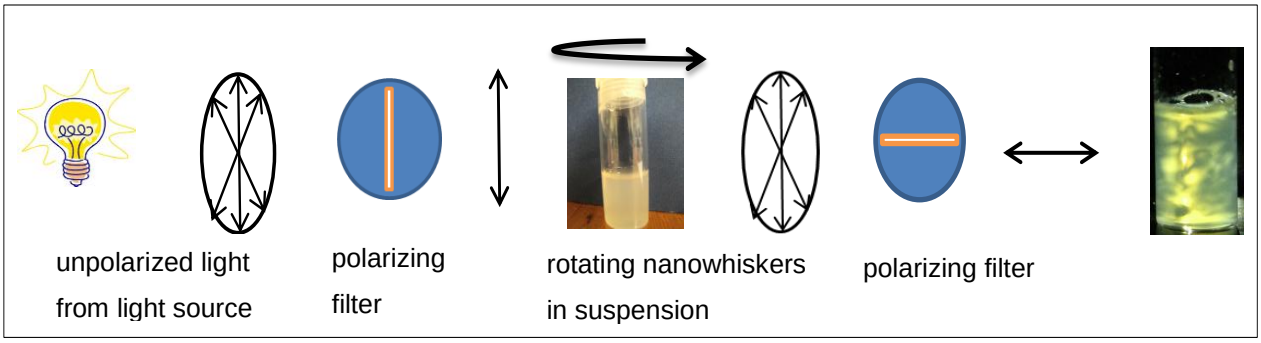

Figure 2.16: Cross polarized setup showing flow birefringence of dispersed nanocrystals.

2.8.4 X-ray diffraction (XRD)

X-ray diffraction is a non-destructive analytical technique which reveals information about the crystal structure, chemical composition and the physical properties of the material. A monochromatic X-ray beam with wavelength, lambda, interacts with the crystalline surface at an angle theta to produce a diffraction pattern. Diffraction occurs only when the distance travelled by the rays reflected from successive planes differs by a complete number *n* of wavelengths. Bragg's law is used to explain the interference pattern of X-rays scattered by crystals. This technique has often been used in previous reports to study the increase in crystallinity when preparing

nanocrystals from cellulose and chitin by acid hydrolysis[69,73,128,134-136]. The change in crystallinity was also quite evident when incorporating these nanowhiskers into the polymer matrix[83,105,136].

2.8.5 Scanning electron microscopy (SEM)

This setup consists of a microscope which scans over the surface with a beam of electrons. As the electrons interact with the surface atoms, information on the surface topography and composition are gathered and often clear structures can be seen on the electron images created by SEM. Elemental analysis and composition can additionally be done with applications such as Energy-dispersive X-ray spectroscopy (EDS). SEM is generally used for extensive morphological inspection. Studies on electrospun nanocomposites as well as fractured surface films at liquid nitrogen temperatures have been done in previous research studies. Conclusions on homogeneity of the composite, presence of voids and whisker aggregates and possible orientation of nanowhiskers have been made using the SEM technique[95,129,134,135,137,138]. Individual nanowhiskers are, however, difficult to spot with conventional SEM but field emission scanning electron microscopy (FESEM) has proven to show much better resolution, observing structures similar to TEM images as well as spotting nanowhiskers dispersed in the polymer matrix. Field emission refers to the filament used to emit electrons which provides images with much higher resolution and makes magnifying to much higher scale possible. A disadvantage of this method is that without coating the acceleration voltage of electrons must be lowered which reduces resolution and with coating, small structures can be misinterpreted or overlooked. It is illustrated in Figure 2.17(b) that the nanowhiskers appear quite large compared to what is seen in TEM images. It is therefore uncertain whether it is individual or clustered nanowhiskers observed in the image[134].

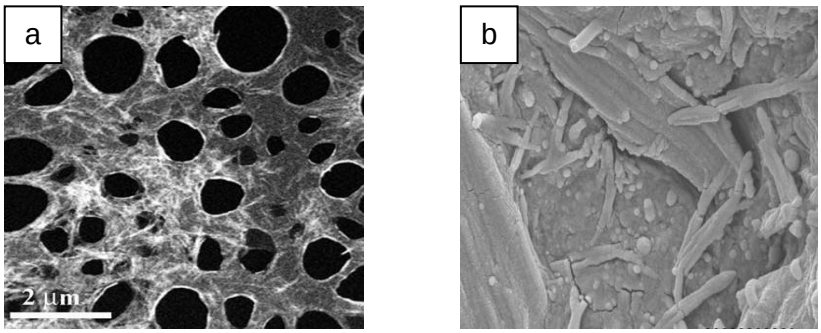

Figure 2.17: FESEM images of (a) individual cellulose nanowhiskers and (b) cellulose nanowhiskers embedded in a polymer matrix[134].

Figure 2.18 shows TEM images of electrospun PVA[95] and PMMA[129] nanocomposites containing cellulose nanowhiskers. The electrospun fibers were fractured and cross sections were imaged in order to study the dispersion of cellulose nanowhiskers. Figure 2.19 illustrates that even though it was not really possible to make out the distinct shape of the whiskers, it was possible to observe nanowhisker dispersion within a polymer matrix by conventional SEM[138].

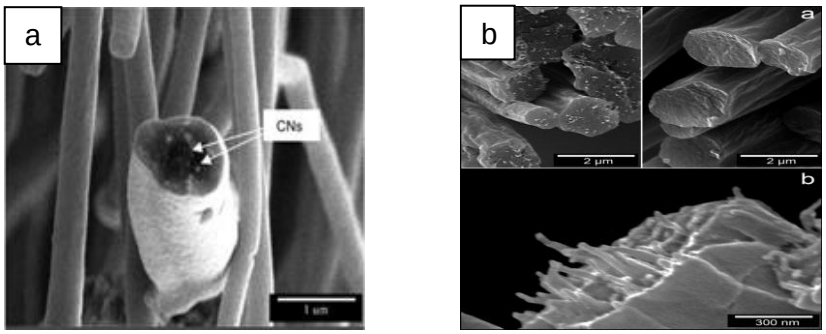

Figure 2.18: FESEM images of electrospun fibers of (a) PVA[95] and (b) PMMA[129] embedded with cellulose nanowhiskers.

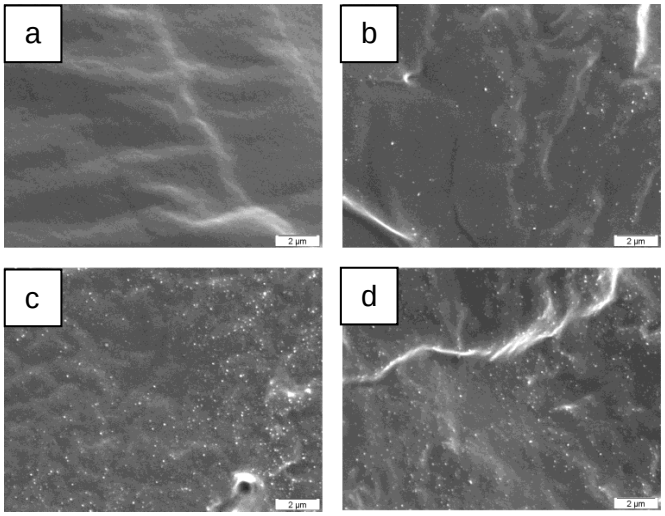

Figure 2.19: SEM images of cryo fractured surfaces of nanocomposites containing (a) 0, (b) 1, (c) 3, (d) 6 wt % tunicin whiskers[138].

2.8.6 Dynamic mechanical analysis (DMA)

DMA is one of the most versatile thermal analysis techniques where it provides a direct correlation between the chemical properties and the mechanical behaviour of the material. Usually an oscillating strain is applied to a sample while varying the temperature and the resulting stress is measured. A suitable program then makes use of mathematical equations generating a DMTA curve in order to get information on the material's elasticity, modulus, viscosity, damping behaviour and glass transition temperature. Favier et al. reported the first demonstration of the reinforcing effect of cellulose whiskers[99]. A big improvement was seen in the storage modulus when incorporating tunican whiskers into a poly(styrene-co-(butyl acrylate)) (poly(S-co-BuA)) matrix. The use of DMTA has been repeatedly proven to be a good tool in establishing the degree of adhesion between matrix and filler[93]. An example of improvement in storage modulus and therefore, enhanced reinforcement by increasing nanofiller loading is presented in Figure 2.20[99].

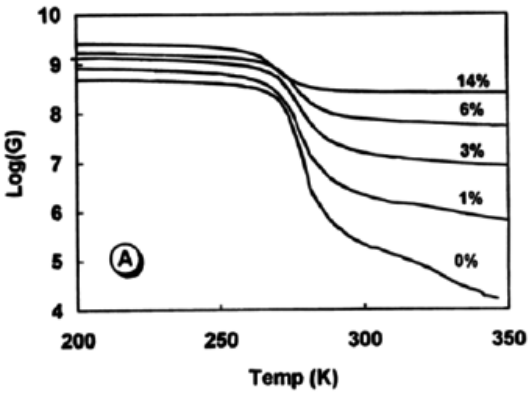

Figure 2.20: Increase in the storage modulus as a function of temperature as the nanowhisker loading in the polymer latex increases[99].

2.8.7 Tensile testing

Mechanical properties of the materials are measured using tensile testing. Tensile testing is a simple and relative inexpensive technique to see how the material will react to forces being applied while under tension. The material gets pulled in a certain direction at ambient temperatures and a set rate. It is then determined how the material will react against the pulling forces by finding its strength along with how much it will elongate before complete fracture. Toughness is a measurement of the area under the stress strain curve which is an indication of the amount of energy absorbed by the material.

The tensile modulus, strength and toughness of a material can be measured and indirectly be related to uniformity of the whisker dispersion and whisker-matrix interaction. The decrease in toughness may be an indication of whisker aggregation forming macro domains. It was previously seen in macro composites that macro reinforcements create large stress concentrations which decrease the ductility in the polymer. Figure 2.21 is an example of enhanced toughness and strength in the cellulose acetate propionate matrix by the addition of cellulose nanowhiskers[139].

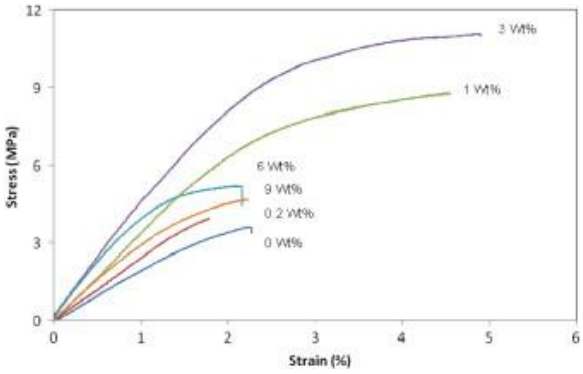

Figure 2.21: The effect of different cellulose nanowhisker loadings on the tensile behaviour of a polymer matrix[139].

2.8.8 Thermogravimetric analysis (TGA)

TGA is a technique used to measure the weight loss of a material as a function of temperature under a controlled atmosphere. These changes in weight at different temperatures are due to decomposition, oxidation or dehydration. TGA is a common procedure to measure the thermal stability of nanowhiskers and nanocomposites. It has been shown that incorporation of cellulose nanowhiskers into some polymer matrix decreases the thermal stability at lower temperature of the nanocomposites due to the cellulose having a much lower degradation temperature and the presence of sulphate groups on the surface of cellulose nanowhiskers[140]. In Figure 2.22 an increase in thermal stability is observed when incorporating the nanowhiskers but only up to a certain loading of nanowhiskers[130].

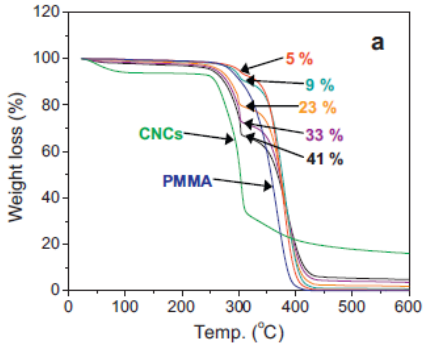

Figure 2.22: The influence of nanowhisker incorporation on the thermal stability of PMMA nanocomposites[130].

2.8.9 Fourier transform infrared (FTIR)

FTIR is an easy way to identify the presence of certain functional groups in a molecule. Different functional groups or bonds absorb infrared radiation at different wavelengths. Also, one can use the unique collection of absorption bands to confirm the identity of a pure compound or to investigate the purity of the sample. Transmission FTIR seems like one of the most effective analysis tools, based on previous nanocomposite studies, in order to chemically prove the presence of nanowhiskers within the nanocomposites. Figure 2.23 illustrates the FTIR spectra of PEO incorporated with different BC loadings[40]. Some authors have used transmission FTIR results to calculate the amount of nanowhiskers effectively incorporated into the nanocomposite by drawing up a calibration curve[128].

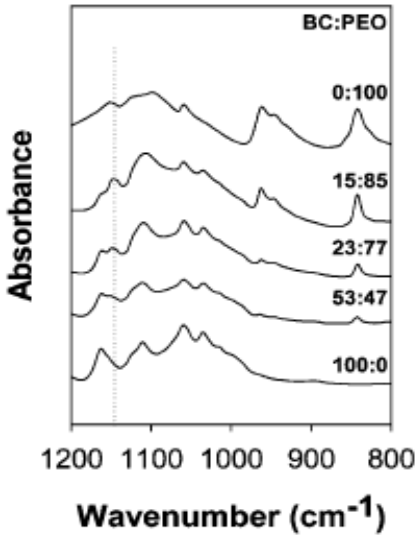

Figure 2.23: FTIR spectra of BC/PEO nanocomposites as a function of the BC/PEO w/w ratio[40].

2.8.10 Differential scanning calorimetry (DSC)

DSC measures the thermal transitions of materials by heating the samples at a certain rate with a manually programmed heating profile. From DSC results, it should then be possible to have an idea of the physical composition of the material. Information on the crystallinity, melting point, polydispersity of crystals and glass transition can be found from the heating/cooling scans. Many DSC studies have recently been done on getting additional interesting information like rate of crystallization etc.[141]. The reports on cellulose and chitin nanowhisker composites have mainly focused on the use of conventional heating/cooling scan information from DCS results in order to complement or clarify results from other mechanical and thermal analysis. One report on EVOH nanocomposites containing bacterial nanowhiskers showed DSC results with a disappearing endotherm as the nanowhisker load increased above 1 wt%. This phenomenon was attributed to nanowhiskers hindering the crystallization of EVOH chains[128]. Similar results were seen with PVA containing chitin nanowhiskers as filler.

2.8.11 Fluorescence microscopy

One of the biggest challenges in nanocomposite analysis is the ability to observe nanowhisker dispersion within the polymer matrix. The resolution of SEM is too low to properly observe the nanowhisker structures and TEM does not always provide enough contrast between the reinforcing phase and nanowhisker phase in order to distinguish between the two. It was therefore suggested to use fluorescence microscopy as an alternative method in studying the nanowhisker distribution. Roman and Dong have developed a three step method for fluorescent labelling of cellulose nanowhiskers[142] for bio-imaging applications and studying the cellulose-nanocrystal interactions (Figure 2.24).

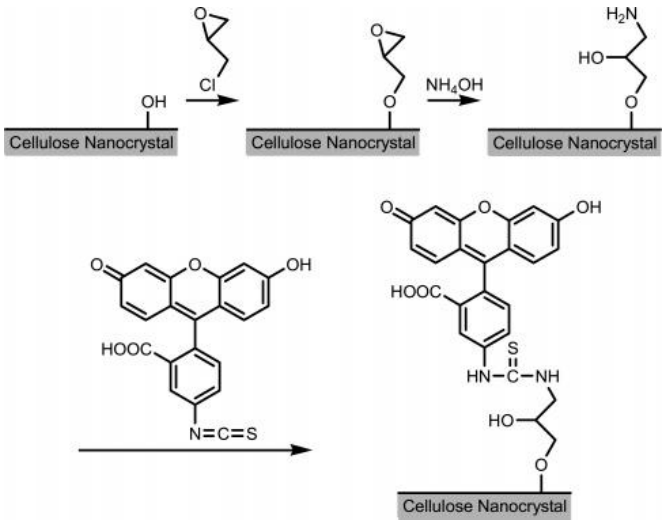

Figure 2.24: Schematic reaction of fluorescent labelling of cellulose[142].

More procedures followed, extending the routes and number of fluorophores available for the labelling of cellulose nanowhiskers[143,144]. The fluorescent labelling of nanoclay particles by rhodamine B (RhB) has been applied in order to investigate the dispersion of clay nanoparticles (cnp) within a polypropylene matrix[145] (Figure 2.25). Particle dispersion in nanocomposites can be viewed with fluorescence microscopy by investigating the homogeneity of the fluorescence intensity[145,146]. It is possible to distinguish agglomerates by the higher local intensities. Thin optical sections can be obtained by using laser scanning microscopy (LSM) - when these are stacked it becomes possible to get a 3D picture (x-, y-, and z direction) of the particle dispersion. The combination of LSM and fluorescence labelling of the nanowhiskers can potentially become very useful for reducing the amount of agglomeration in cellulose nanocomposites.

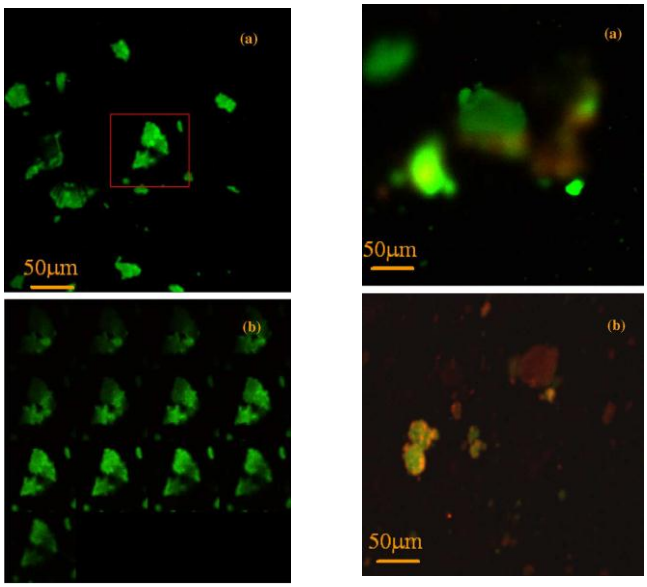

Figure 2.25: Fluorescence confocal images of (a) clay nano particle-RhB (cnp-RhB) and (b) nanocomposites containing cnp-RhB Rod[145].

2.9 References

(1) López-Rubio A, Lagaron JM, Giménez E, Cava D, Hernandez-Muñoz P, Yamamoto T, et al. Morphological Alterations Induced by Temperature and Humidity in Ethylene-Vinyl Alcohol Copolymers. *Macromolecules* 2003;(25)**:9467-9476**.

(2) Mark HF. *Encyclopedia of Polymer Science and Engineering*, Vol. 2, 2nd Ed: John Wiley and Sons Inc; 1985. **188-189**

(3) Zhang F, Zhang Y, Li G, Li H. Preparation and characterization of EVAL hollow fiber membrane adsorbents filled with cation exchange resins. *Frontiers of Chemical Engineering in China* 2009;3(4)**:462-467**.

(4) Lagaron JM, Giménez E, Saura JJ. Degradation of high barrier ethylene-vinyl alcohol copolymer under mild thermal-oxidative conditions studied by thermal analysis and infrared spectroscopy. *Polymer International* 2001;50(6)**:635-642**.

(5) Mokwena KK, Tang J, Laborie M. Water absorption and oxygen barrier characteristics of ethylene vinyl alcohol films. *Journal of Food Engineering* 2011;105(3)**:436-443**.

(6) Cabedo L, Lagarón JM, Cava D, Saura JJ, Giménez E. The effect of ethylene content on the interaction between ethylene-vinyl alcohol copolymers and water—II: Influence of water sorption on the mechanical properties of EVOH copolymers. *Polymer Testing* 2006;25(7)**:860-867**.

(7) Gaucher-Miri V, Jones GK, Kaas R, Hiltner A, Baer E. Plastic deformation of EVA, EVOH and their multilayers. *Journal of Materials Science* 2002;37(13)**:2635-2644**.

(8) López-Rubio A, Lagarón JM, Hernández-Muñoz P, Almenar E, Catalá R, Gavara R, et al. Effect of high pressure treatments on the properties of EVOH-based food packaging materials. *Innovative Food Science & Emerging Technologies* 2005;6(1)**:51-58**.

(9) Artzi N, Narkis M, Siegmann A. EVOH/clay nanocomposites produced by dynamic melt mixing. *Polymer Engineering & Science* 2004;44(6)**:1019-1026**.

(10) Kenawy E, Layman JM, Watkins JR, Bowlin GL, Matthews JA, Simpson DG, et al. Electrospinning of poly(ethylene-co-vinyl alcohol) fibers. *Biomaterials* 2003;24(6)**:907-913**.

(11) Oyane A, Kawashita M, Nakanishi K, Kokubo T, Minoda M, Miyamoto T, et al. Bonelike apatite formation on ethylene-vinyl alcohol copolymer modified with silane coupling agent and calcium silicate solutions. *Biomaterials* 2003;24(10)**:1729-1735**.

(12) Young T-H, Lin C-W, Cheng L-P, Hsieh C-C. Preparation of EVAL membranes with smooth and particulate morphologies for neuronal culture. *Biomaterials* 2001;22(13)**:1771-1777**.

(13) Young T-H, Yao C-H, Sun J-S, Lai C-P, Chen L-W. The effect of morphology variety of EVAL membranes on the behavior of myoblasts in vitro. *Biomaterials* 1998;19(7-9)**:717-724**.

(14) Matsuyama H, Iwatani T, Kitamura Y, Tearamoto M, Sugoh N. Formation of porous poly(ethylene-co-vinyl alcohol) membrane via thermally induced phase separation. *Journal of Applied Polymer Science* 2001;79(13)**:2449-2455**.

(15) Matsuyama H, Kobayashi K, Maki T, Tearamoto M, Tsuruta H. Effect of the ethylene content of poly(ethylene-co-vinyl alcohol) on the formation of microporous membranes via thermally induced phase separation. *Journal of Applied Polymer Science* 2001;82(10)**:2583-2589**.

(16) Shieh M-J, Lai P-S, Young T-H. 5-Aminosalicyclic acid permeability enhancement by a pH-sensitive EVAL membrane. *Journal of Membrane Science* 2002;204(1-2)**:237-246**.

(17) Wen J, Wilkes GL. Surface modification of ethylene-vinyl alcohol (EVOH) copolymer films by the attachment of triethoxysilane functionality. *Polymer Bulletin* 1996;37(1)**:51-57**.

(18) Villalpando-Olmos J, Sánchez-Valdes S, Yáñez-Flores IG. Performance of polyethylene/ethylene-vinyl alcohol copolymer/polyethylene multilayer films using maleated polyethylene blends. *Polymer Engineering & Science* 1999;39(9)**:1597-1603**.

(19) Mark H, Bikales NM, Overberger CG, Menges G. *Encyclopedia of Polymer Science and Engineering*. Vol. 6, 2nd Ed: John Wiley and Sons Inc;1985**:383-521**.

(20) Kroschwitz JI HM. *Encyclopedia of Chemical Technolog.* Vol 17, 4th Ed: John Wiley & Sons Inc;1996**:702 - 781**.

(21) Mark HF. *Encyclopedia of Polymer Science and Technology*. Vol. 2, 3rd Ed.:John Wiley and Sons Inc;1985**:412-440**.

(22) Huang C, Wu J, Huang C, Lin L. Morphological, Thermal, Barrier and Mechanical Properties of LDPE/EVOH Blends in Extruded Blown Films. *Journal of Polymer Research* 2004;11(1)**:75-83**.

(23) Kim S, Chun Y. Barrier property by controlled laminar morphology of LLDPE/EVOH blends. *Korean Journal of Chemical Engineering* 1999;16(4)**:511-517**.

(24) Kulkarni A, Mahanwar P. Effect of dispersion of nanofibers on the properties of LDPE FILMS. *International Journal of Plastics Technology* 2011;15(0)**:77-85**.

(25) Visakh PM, Thomas S. Preparation of bionanomaterials and their polymer nanocomposites from waste and biomass. *Waste and Biomass Valorization* 2010;1(1)**:121-134**.

(26) Updegraff DM. Semimicro determination of cellulose inbiological materials. *Analytical Biochemistry* 1969;32(3)**:420-424**.

(27) Klemm D, Heublein B, Fink H, Bohn A. Cellulose: Fascinating Biopolymer and Sustainable Raw Material. *Angewandte Chemie International Edition* 2005;44(22)**:3358-3393**.

(28) Eichhorn S, Dufresne A, Aranguren M, Marcovich N, Capadona J, Rowan S, et al. Review: current international research into cellulose nanofibres and nanocomposites. *Journal of Materials Science* 2010;45(1)**:1-33**.

(29) Gardner DJ, Oporto GS, Mills R, Samir MASA. Adhesion and Surface Issues in Cellulose and Nanocellulose. *Journal of Adhesion Science & Technology* 2008;22(5)**:545-567**.

(30) Duchemin BJC, Newman RH, Staiger MP. Structure–property relationship of all-cellulose composites. *Composites Science and Technology* 2009;69(7–8)**:1225-1230**.

(31) Vargas NH. Aligned cellulose nanofibers prepared by electrospinning.Masters Thesis, Luleå University of Technology; 2010.

(32) Oke I. Nanoscience in nature: cellulose nanocrystals. *Studies by Undergraduate Researchers at Guelph* 2010;3(2).

(33) Eichhorn SJ. Cellulose nanowhiskers: promising materials for advanced applications. *Soft Matter* 2011;7(2)**:303-315**.

(34) Czaja WK, Young DJ, Kawecki M, Brown RM. The Future Prospects of Microbial Cellulose in Biomedical Applications. *Biomacromolecules* 2007;8(1)**:1-12**.

(35) Loader NJ, Robertson I, Barker AC, Switsur VR, Waterhouse JS. An improved technique for the batch processing of small wholewood samples to α-cellulose. *Chemical Geology* 1997;136(3–4)**:313-317**.

(36) Hubbe MA, Rojas OJ, Lucia LA, Sain M. Cellulosic nanocomposites: A Review. 2008;3(3)**:929-980**.

(37) Lu P, Hsieh Y. Cellulose nanocrystal-filled poly(acrylic acid) nanocomposite fibrous membranes. *Nanotechnology* 2009;20(41)**:415604**.

(38) Azizi Samir MAS, Alloin F, Sanchez J-, Dufresne A. Cellulose nanocrystals reinforced poly(oxyethylene). *Polymer* 2004;45(12)**:4149-4157**.

(39) Bendahou A, Kaddami H, Dufresne A. Investigation on the effect of cellulosic nanoparticles' morphology on the properties of natural rubber based nanocomposites. *European Polymer Journal* 2010;46(4)**:609-620**.

(40) Brown EE, Laborie MG. Bioengineering Bacterial Cellulose/Poly(ethylene oxide) Nanocomposites. *Biomacromolecules* 2007;8(10)**:3074-3081**.

(41) Chazeau L, Cavaillé JY, Canova G, Dendievel R, Boutherin B. Viscoelastic properties of plasticized PVC reinforced with cellulose whiskers. *Journal of Applied Polymer Science* 1999;71(11)**:1797-1808**.

(42) Siró I, Plackett D. Microfibrillated cellulose and new nanocomposite materials: a review. *Cellulose* 2010;17(3)**:459-494**.

(43) Kvien I, Tanem BS, Oksman K. Characterization of cellulose whiskers and their nanocomposites by atomic force and electron microscopy. *Biomacromolecules* 2005;6(6)**:3160-3165**.

(44) Bondeson D, Mathew A, Oksman K. Optimization of the isolation of nanocrystals from microcrystalline cellulose. *Cellulose* 2006;13(2)**:171-180**.

(45) Revol J-, Bradford H, Giasson J, Marchessault RH, Gray DG. Helicoidal self-ordering of cellulose microfibrils in aqueous suspension. *International journal of biological macromolecules* 1992;14(3)**:170-172**.

(46) Dong XM, Revol J, Gray DG. Effect of microcrystallite preparation conditions on the formation of colloid crystals of cellulose. *Cellulose* 1998;5(1)**:19-32**.

(47) Bai W, Holbery J, Li K. A technique for production of nanocrystalline cellulose with a narrow size distribution. *Cellulose* 2009;16(3)**:455-465**.

(48) Rusli R, Shanmuganathan K, Rowan SJ, Weder C, Eichhorn SJ. Stress Transfer in Cellulose Nanowhisker Composites-Influence of Whisker Aspect Ratio and Surface Charge. *Biomacromolecules* 2011;12(4)**:1363-1369**.

(49) Ranby BG. Fibrous macromolecular systems. Cellulose and muscle. The colloidal properties of cellulose micelles. *Discussions of the Faraday Society* 1951;11**:158-164**.

(50) Araki J, Wada M, Kuga S, Okano T. Birefringent Glassy Phase of a Cellulose Microcrystal Suspension. *Langmuir* 2000;16(6)**:2413-2415**.

(51) Elazzouzi-Hafraoui S, Nishiyama Y, Putaux J, Heux L, Dubreuil F, Rochas C. The Shape and Size Distribution of Crystalline Nanoparticles Prepared by Acid Hydrolysis of Native Cellulose. *Biomacromolecules* 2008;9(1)**:57-65**.

(52) Peng BL, Dhar N, Liu HL, Tam KC. Chemistry and applications of nanocrystalline cellulose and its derivatives: A nanotechnology perspective. *The Canadian Journal of Chemical Engineering* 2011;89(5)**:1191-1206**.

(53) Tashiro K, Kobayashi M. Theoretical evaluation of three-dimensional elastic constants of native and regenerated celluloses: role of hydrogen bonds. *Polymer* 1991;32(8)**:1516-1526**.

(54) Eichhorn SJ, Davies GR. Modelling the crystalline deformation of native and regenerated cellulose. *Cellulose* 2006;13(3)**:291-307**.

(55) Bergenstrahle M, Berglund LA, Mazeau K. Thermal Response in Crystalline Iβ Cellulose: A Molecular Dynamics Study. *The Journal of Physical Chemistry B* 2007;111(30)**:9138-9145**.

(56) Šturcová A, Davies GR, Eichhorn SJ. Elastic Modulus and Stress-Transfer Properties of Tunicate Cellulose Whiskers. *Biomacromolecules* 2005;6(2)**:1055-1061**.

(57) Henriette M.C. de A. Nanocomposites for food packaging applications. *Food Research International* 2009;42(9)**:1240-1253**.

(58) Siqueira G, Bras J, Dufresne A. Cellulose Whiskers versus Microfibrils: Influence of the Nature of the Nanoparticle and its Surface Functionalization on the Thermal and Mechanical Properties of Nanocomposites. *Biomacromolecules* 2009;10(2)**:425-432**.

(59) Azizi Samir MAS, Alloin F, Dufresne A. Review of recent research into cellulosic whiskers, their properties and their application in nanocomposite field. *Biomacromolecules* 2005;6(2)**:612-626**.

(60) Pandey JK, Kim C, Chu W, Lee CS, Jang D, Ahn S. Evaluation of morphological architecture of cellulose chains in grass during conversion from macro to nano dimensions. *e-Polymers* 2009**.**

(61) Nair KG, Dufresne A. Crab shell chitin whisker reinforced natural rubber nanocomposites. 1. Processing and swelling behavior. *Biomacromolecules* 2003;4(3)**:657-665**.

(62) Ravi Kumar MNV. A review of chitin and chitosan applications. *Reactive and Functional Polymers* 2000 ;46(1)**:1-27**.

(63) Morin A, Dufresne A. Nanocomposites of Chitin Whiskers from Riftia Tubes and Poly(caprolactone). *Macromolecules* 2002;35(6)**:2190-2199**.

(64) Rinaudo M. Chitin and chitosan: Properties and applications. *Progress in Polymer Science* 2006;31(7)**:603-632**.

(65) Palpandi C, Shanmugam V, Shanmugam A. Extraction of chitin and chitosan from shell and operculum of mangrove gastropod Nerita (Dostia) crepidularia Lamarck. *International Journal of Medicine and Medical Sciences* 2009;1(5)**:198-205**.

(66) Abdou ES, Nagy KSA, Elsabee MZ. Extraction and characterization of chitin and chitosan from local sources. *Bioresource technology* 2008;99(5)**:1359-1367**.

(67) Zeng J, He Y, Li S, Wang Y. Chitin Whiskers: An Overview. *Biomacromolecules* 2012;13(1)**:1-11**.

(68) Einbu A. Characterisation of Chitin and a Study of its Acid-Catalysed Hydrolysis.Thesis for the degree of philosophiae, Norwegian University of Science and Technology; 2007.

(69) Clark GL, Smith AF. X-ray diffraction studies of chitin, chitosan, and derivatives. *Journal of Physical Chemistry* 1936;40(7)**:863-879**.

(70) Gardner KH, Blackwell J. Refinement of the structure of β-chitin. *Biopolymers* 1975;14(8)**:1581-1595**.

(71) Gałat A, Koput J, Popowicz J. Analyses of infrared amide bands of chitin. *Acta Biochimica Polonica* 1979;26(4)**:303-308**.

(72) Pearson FG, Marchessault RH, Liang CY. Infrared spectra of crystalline polysaccharides. V. Chitin. *Journal of Polymer Science* 1960;43(141)**:101-116**.

(73) Darmon SE, Rudall KM. Infra-red and X-ray studies of chitin. *Discussions of the Faraday Society* 1950;9**:251-260**.

(74) Sriupayo J, Supaphol P, Blackwell J, Rujiravanit R. Preparation and characterization of α-chitin whisker-reinforced chitosan nanocomposite films with or without heat treatment. *Carbohydrate Polymers* 2005;62(2)**:130-136**.

(75) Yusof NLBM, Wee A, Lim LY, Khor E. Flexible chitin films as potential wound-dressing materials: Wound model studies. *Journal of Biomedical Materials Research - Part A* 2003;66(2)**:224-232**.

(76) Synowiecki J, Al-Khateeb N. Production, Properties, and Some New Applications of Chitin and Its Derivatives. *Critical reviews in food science and nutrition* 2003;43(2)**:145-171**.

(77) Kato Y, Onishi H, Machida Y. Application of chitin and chitosan derivatives in the pharmaceutical field. *Current Pharmaceutical Biotechnology* 2003;4(5)**:303-309**.

(78) Muzzarelli RAA. Immobilization of enzymes on chitin and chitosan. *Enzyme and microbial technology* 1980;2(3)**:177-184**.

(79) Crini G. Recent developments in polysaccharide-based materials used as adsorbents in wastewater treatment. *Progress in Polymer Science* 2005;30(1)**:38-70**.

(80) Nair KG, Dufresne A, Gandini A, Belgacem MN. Crab Shell Chitin Whiskers Reinforced Natural Rubber Nanocomposites. 3. Effect of Chemical Modification of Chitin Whiskers. *Biomacromolecules* 2003;4(6)**:1835-1842**.

(81) Nair KG, Dufresne A. Crab Shell Chitin Whisker Reinforced Natural Rubber Nanocomposites. 2. Mechanical Behavior. *Biomacromolecules* 2003;4(3)**:666-674**.

(82) Lu Y, Weng L, Zhang L. Morphology and properties of soy protein isolate thermoplastics reinforced with chitin whiskers. *Biomacromolecules* 2004;5(3)**:1046-1051**.

(83) Junkasem J, Rujiravanit R, Grady BP, Supaphol P. X-ray diffraction and dynamic mechanical analyses of α-chitin whisker-reinforced poly(vinyl alcohol) nanocomposite nanofibers. *Polymer International* 2010;59(1)**:85-91**.

(84) Jirawut Junkasem ea. Fabrication of α-chitin whisker-reinforced poly(vinyl alcohol) nanocomposite nanofibres by electrospinning. *Nanotechnology* 2006;17(17)**:4519**.

(85) Paillet M, Dufresne A. Chitin whisker reinforced thermoplastic nanocomposites. *Macromolecules* 2001;34(19)**:6527-6530**.

(86) Minke R, Blackwell J. The structure of α-chitin. *Journal of Molecular Biology* 1978;120(2)**:167-181**.

(87) Goodrich JD, Winter WT. α-Chitin Nanocrystals Prepared from Shrimp Shells and Their Specific Surface Area Measurement. *Biomacromolecules* 2007;8(1)**:252-257**.

(88) Feng L, Zhou Z, Dufresne A, Huang J, Wei M, An L. Structure and properties of new thermoforming bionanocomposites based on chitin whisker-graft-polycaprolactone. *Journal of Applied Polymer Science* 2009;112(5)**:2830-2837**.

(89) Zheng H, Tan Z, Ran Zhan Y, Huang J. Morphology and properties of soy protein plastics modified with chitin. *Journal of Applied Polymer Science* 2003;90(13)**:3676-3682**.

(90) Balazs AC, Emrick T, Russell TP. Nanoparticle Polymer Composites: Where Two Small Worlds Meet. *Science* 2006;314(5802)**:1107-1110**.

(91) Dufresne A. Processing of polymer nanocomposites reinforced with polysaccharide nanocrystals. *Molecules* 2010;15(6)**:4111-4128**.

(92) Krook M, Albertsson A, Gedde UW, Hedenqvist MS. Barrier and mechanical properties of montmorillonite/polyesteramide nanocomposites. *Polymer Engineering & Science* 2002;42(6)**:1238-1246**.

(93) Jordan J, Jacob KI, Tannenbaum R, Sharaf MA, Jasiuk I. Experimental trends in polymer nanocomposites-a review. *Materials Science and Engineering: A* 2005;393(1–2)**:1-11**.

(94) Moon RJ, Martini A, Nairn J, Simonsen J, Youngblood J. Cellulose nanomaterials review: structure, properties and nanocomposites. *Chemical Society Reviews* 2011;40(7)**:3941-3994**.

(95) Peresin MS, Habibi Y, Zoppe JO, Pawlak JJ, Rojas OJ. Nanofiber Composites of Polyvinyl Alcohol and Cellulose Nanocrystals: Manufacture and Characterization. *Biomacromolecules* 2010;11(3)**:674-681**.

(96) Zimmermann T, Bordeanu N, Strub E. Properties of nanofibrillated cellulose from different raw materials and its reinforcement potential. *Carbohydrate Polymers* 2010;79(4)**:1086-1093**.

(97) Wang Y, Cao X, Zhang L. Effects of Cellulose Whiskers on Properties of Soy Protein Thermoplastics. *Macromolecular Bioscience* 2006;6(7)**:524-531**.

(98) Favier V, Canova GR, Cavaillé JY, Chanzy H, Dufresne A, Gauthier C. Nanocomposite materials from latex and cellulose whiskers. *Polymers for Advanced Technologies* 1995;6(5)**:351-355**.

(99) Favier V, Chanzy H, Cavaille JY. Polymer Nanocomposites Reinforced by Cellulose Whiskers. *Macromolecules* 1995;28(18)**:6365-6367**.

(100) Garcia de Rodriguez NL, Thielemans W, Dufresne A. Sisal cellulose whiskers reinforced polyvinyl acetate nanocomposites. *Cellulose* 2006;13(3)**:261-270**.

(101) Elmabrouk AB, Wim T, Dufresne A, Boufi S. Preparation of poly(styrene-co-hexylacrylate)/cellulose whiskers nanocomposites via miniemulsion polymerization. *Journal of Applied Polymer Science* 2009;114(5)**:2946-2955**.

(102) Helbert W, Cavaillé JY, Dufresne A. Thermoplastic nanocomposites filled with wheat straw cellulose whiskers. Part I: Processing and mechanical behavior. *Polymer Composites* 1996;17(4)**:604-611**.

(103) Dufresne A, Cavaillé J, Helbert W. Thermoplastic nanocomposites filled with wheat straw cellulose whiskers. Part II: Effect of processing and modeling. *Polymer Composites* 1997;18(2)**:198-210**.

(104) Carlmark A, Larsson E, Malmström E. Grafting of cellulose by ring-opening polymerisation – A review. *European Polymer Journal* 2012;48(10)**1649-1659**.

(105) de Menezes AJ, Siqueira G, Curvelo AAS, Dufresne A. Extrusion and characterization of functionalized cellulose whiskers reinforced polyethylene nanocomposites. *Polymer* 2009;50(19)**:4552-4563**.

(106) Lu J, Askeland P, Drzal LT. Surface modification of microfibrillated cellulose for epoxy composite applications. *Polymer* 2008;49(5)**:1285-1296**.

(107) Goussé C, Chanzy H, Excoffier G, Soubeyrand L, Fleury E. Stable suspensions of partially silylated cellulose whiskers dispersed in organic solvents. *Polymer* 2002;43(9)**:2645-2651**.

(108) Grunert M, Winter WT. Nanocomposites of Cellulose Acetate Butyrate Reinforced with Cellulose Nanocrystals. *Journal of Polymers and the Environment* 2002;10(1)**:27-30**.

(109) Ljungberg N, Bonini C, Bortolussi F, Boisson C, Heux L, Cavaillè. New Nanocomposite Materials Reinforced with Cellulose Whiskers in Atactic Polypropylene: Effect of Surface and Dispersion Characteristics. *Biomacromolecules* 2005;6(5)**:2732-2739**.

(110) Chauve G, Heux L, Arouini R, Mazeau K. Cellulose Poly(Ethylene-co-vinyl Acetate) Nanocomposites Studied by Molecular Modeling and Mechanical Spectroscopy. *Biomacromolecules* 2005;6(4)**:2025-2031**.

(111) Ljungberg N, Cavaillé J-, Heux L. Nanocomposites of isotactic polypropylene reinforced with rod-like cellulose whiskers. *Polymer* 2006;47(18)**:6285-6292**.

(112) Wågberg L, Hägglund R. Kinetics of Polyelectrolyte Adsorption on Cellulosic Fibers. *Langmuir* 2001;17(4)**:1096-1103**.

(113) Jean B, Dubreuil F, Heux L, Cousin F. Structural Details of Cellulose Nanocrystals/Polyelectrolytes Multilayers Probed by Neutron Reflectivity and AFM. *Langmuir* 2008;24(7)**:3452-3458**.

(114) Jean B, Heux L, Dubreuil F, Chambat G, Cousin F. Non-Electrostatic Building of Biomimetic Cellulose-Xyloglucan Multilayers. *Langmuir* 2009;25(7)**:3920-3923**.

(115) de Mesquita JP, Donnici CL, Pereira FV. Biobased Nanocomposites from Layer-by-Layer Assembly of Cellulose Nanowhiskers with Chitosan. *Biomacromolecules* 2010;11(2)**:473-480**.

(116) Larsson P, Wågberg L. Influence of fibre–fibre joint properties on the dimensional stability of paper. *Cellulose* 2008;15(4)**:515-525**.

(117) Huang Z, Zhang Y-, Kotaki M, Ramakrishna S. A review on polymer nanofibers by electrospinning and their applications in nanocomposites. *Composites Science and Technology* 2003;63(15)**:2223-2253**.

(118) Bhardwaj N, Kundu SC. Electrospinning: A fascinating fiber fabrication technique. *Biotechnology Advances* 2010;28(3)**:325-347**.

(119) Reneke DH, Chun I. Nanometre diameter fibres of polymer, produced by electrospinning. *Nanotechnology* 1996;7(3)**:216**.

(120) Li D, Xia Y. Electrospinning of Nanofibers: Reinventing the Wheel? *Advanced Materials* 2004;16(14)**:1151-1170**.

(121) Schiffman JD, Schauer CL. A Review: Electrospinning of Biopolymer Nanofibers and their Applications. *Polymer Reviews* 2008;48(2)**:317-352**.

(122) Pan H, Li L, Hu L, Cui X. Continuous aligned polymer fibers produced by a modified electrospinning method. *Polymer* 2006;47(14)**:4901-4904**.

(123) Zhou C, Chu R, Wu R, Wu Q. Electrospun Polyethylene Oxide/Cellulose Nanocrystal Composite Nanofibrous Mats with Homogeneous and Heterogeneous Microstructures. *Biomacromolecules* 2011;12(7)**:2617-2625**.

(124) Park W, Kang M, Kim H, Jin H. Electrospinning of Poly(ethylene oxide) with Bacterial Cellulose Whiskers. *Macromolecular Symposia* 2007;249-250(1)**:289-294**.

(125) Rojas OJ, Montero GA, Habibi Y. Electrospun nanocomposites from polystyrene loaded with cellulose nanowhiskers. *Journal of Applied Polymer Science* 2009;113(2)**:927-935**.

(126) Zoppe JO, Peresin MS, Habibi Y, Venditti RA, Rojas OJ. Reinforcing Poly(Îµ-caprolactone) Nanofibers with Cellulose Nanocrystals. *ACS Applied Materials & Interfaces* 2009;1(9)**:1996-2004**.

(127) Xiang C, Taylor AG, Hinestroza JP, Frey MW. Controlled release of nonionic compounds from poly(lactic acid)/cellulose nanocrystal nanocomposite fibers. *Journal of Applied Polymer Science* 2012;127(1)**:79-86**.

(128) Martinez-Sanz M, Olsson R, Lopez-Rubio A, Lagaron J. Development of electrospun EVOH fibres reinforced with bacterial cellulose nanowhiskers. Part I: Characterization and method optimization. *Cellulose* 2011;18(2)**:335-347**.

(129) Olsson RT, Kraemer R, Lopez-Rubio A, Torres-Giner S, Ocio MJ, LagaroÌ• n JM. Extraction of Microfibrils from Bacterial Cellulose Networks for Electrospinning of Anisotropic Biohybrid Fiber Yarns. *Macromolecules* 2010;43(9)**:4201-4209**.

(130) Dong H, Strawhecker KE, Snyder JF, Orlicki JA, Reiner RS, Rudie AW. Cellulose nanocrystals as a reinforcing material for electrospun poly(methyl methacrylate) fibers: Formation, properties and nanomechanical characterization. *Carbohydrate Polymers* 2012;87(4)**:2488-2495**.

(131)Jacobs V, Rajesh D. Anandjiwala, Maya John, Aji P. Mathew and Kristina Oksman. Studies on electrospun chitosan based nanobibres reinforced with cellulose and chitin nanowhiskers. *TAPPI International Conference on Nanotechnology for the Forest Products Industry*; 27-29 September 2010; .

(132) Ago M, Okajima K, Jakes JE, Park S, Rojas OJ. Lignin-Based Electrospun Nanofibers Reinforced with Cellulose Nanocrystals. *Biomacromolecules* 2012;13(3)**:918-926**.

(133) MagalhaÌƒes W,Luiz Esteves, Cao X, Lucia LA. Cellulose Nanocrystals/Cellulose Core-in-Shell Nanocomposite Assemblies. *Langmuir* 2009;25(22)**:13250-13257**.

(134) Kvien I, Tanem BS, Oksman K. Investigation of the Structure of Cellulose Whiskers and Its Nanocomposites using TEM, SEM, AFM and X-ray Diffraction : *8th International Conference on Woodfiber-Plastic Composites*. 2005.

(135) Lu P, Hsieh Y. Preparation and properties of cellulose nanocrystals: Rods, spheres, and network. *Carbohydrate Polymers* 2010;82(2)**:329-336**.

(136) Gindl W, Martinschitz KJ, Boesecke P, Keckes J. Structural changes during tensile testing of an all-cellulose composite by in situ synchrotron X-ray diffraction. *Composites Science and Technology* 2006;66(15)**:2639-2647**.

(137) Visakh PM, Thomas S, Oksman K, Mathew AP. Crosslinked natural rubber nanocomposites reinforced with cellulose whiskers isolated from bamboo waste: Processing and mechanical/thermal properties. *Composites Part A: Applied Science and Manufacturing* 2012;43(4)**:735-741**.

(138) Azizi Samir M,Ahmed Sa, Alloin F, Sanchez J, El Kissi N, Dufresne A. Preparation of Cellulose Whiskers Reinforced Nanocomposites from an Organic Medium Suspension. *Macromolecules* 2004;37(4)**:1386-1393**.

(139) Pooyan P, Tannenbaum R, Garmestani H. Mechanical behavior of a cellulose-reinforced scaffold in vascular tissue engineering. *Journal of the Mechanical Behavior of Biomedical Materials* 2012;7(0)**:50-59**.

(140) Uddin AJ, Araki J, Gotoh Y. Characterization of the poly(vinyl alcohol)/cellulose whisker gel spun fibers. *Composites Part A: Applied Science and Manufacturing* 2011;42(7)**:741-747**.

(141) De Santis F, Pantani R, Titomanlio G. Nucleation and crystallization kinetics of poly(lactic acid). *Thermochimica Acta* 2011;522(1–2)**:128-134**.

(142) Dong S, Roman M. Fluorescently Labeled Cellulose Nanocrystals for Bioimaging Applications. *Journal of the American Chemical Society* 2007;129(45)**:13810-13811**.

(143) Yang Q, Pan X. A facile approach for fabricating fluorescent cellulose. *Journal of Applied Polymer Science* 2010;117(6)**:3639-3644**.

(144) Nielsen LJ, Eyley S, Thielemans W, Aylott JW. Dual fluorescent labelling of cellulose nanocrystals for pH sensing. *Chemical Communications* 2010;46(47)**:8929-8931**.

(145) Aloisi GG, Costantino U, Latterini L, Nocchetti M, Camino G, Frache A. Preparation and spectroscopic characterisation of intercalation products of clay and of clay–polypropylene composites with rhodamine B. *Journal of Physics and Chemistry of Solids* 2006;67(5-6)**:909-914**.

(146) Langat J, Bellayer S, Hudrlik P, Hudrlik A, Maupin PH, Gilman Sr. JW, et al. Synthesis of imidazolium salts and their application in epoxy montmorillonite nanocomposites. *Polymer* 2006;47(19)**:6698-6709**.

Chapter 3:
Experimental Work

3.1 Materials

Poly(ethylene-co-vinyl alcohol) copolymers (EVOH) differing in ethylene content (EVOH27 with 27 mole% ethylene and EVOH44 with 44 mole% ethylene) were purchased in pellet form from Sigma-Aldrich. The appropriate solvent used throughout this study was a water/isopropanol blend that was used in 30:70 ratio (v/v). The isopropanol was supplied by Merck. Microcrystalline cellulose (MCC), from which cellulose nanowhiskers were isolated, was provided by JRS Pharma under the product name VIVAPUR101. Chitin was purchased from Sigma Aldrich and originates from shrimp shells. Low density polyethylene (LDPE) was supplied by Sasol South Africa. Poly(ethylene-graft-(maleic anhydride) with 0.04 wt% maleic anhydride (determined by NMR) was used as compatibilizer for the LDPE/EVOH composites and was obtained from Sigma-Aldrich. Rhodamine B and 5(6)-fluorescein isothiocyanate mixed isomer (FITC) used for fluorescent labelling was purchased from Sigma-Aldrich. Concentrated sulphuric acid (96 wt%) and concentrated hydrochloric acid (32 wt%) was supplied by Merck.

3.2 Preparation of nanowhiskers

3.2.1 Cellulose

Cellulose nanowhiskers were prepared by way of acid hydrolysis of MCC using 64 wt% sulphuric acid with slight modification of the same method that was used by Bondeson et al.[1]. The hydrolysis of MCC was carried out by way of vigorous stirring at 45 °C using a ratio of 1 g:8.75 ml (cellulose:sulphuric acid). The suspension was diluted with deionized water after 120 minutes in order to cool down and end the hydrolysis process.

Remaining acid as well as dissolved amorphous regions from the MCC were removed by way of centrifugation as well as solvent exchange. The solvent exchange involved replacement of the supernatant with deionised water and this step was repeated until the supernatant turned turbid. The turbid suspension containing the nanowhiskers was then dialyzed for a couple of days to remove

further traces of acid until the pH was between four and five. The suspension was then treated with 0.1 M NaOH until the pH was nine and dialyzed further to remove any excess base and salt. The neutralised cellulose nanowhisker suspension was then either freeze dried in order to isolate the nanowhiskers in solid powder form or kept as an aqueous nanowhisker suspension.

The concentration of the nanowhiskers in suspension was increased by using rotor evaporation at 23 bar and 40 °C. The use of a concentrated PEG (20 000 g/mole molecular weight) solution was also investigated as a possible method to increase the nanowhisker concentration by using the osmotic pressure principle[2,3].

3.2.2 Chitin

Chitin nanowhiskers were prepared using a similar method to that for cellulose nanowhiskers. Hydrochloric acid (3 N) was used to hydrolyze chitin powder at 105 °C for 4 hours. The acid hydrolysis was followed by centrifugation of the suspension followed by dialysis in order to remove excess acid. The next step in the isolation process involved sonication in order to obtain well dispersed nanowhiskers in suspension[4]. The suspension was then finally either freeze dried or kept as an aqueous nanowhisker suspension as obtained after dialysis and sonication. The concentration of the suspension was increased by using rotor evaporation.

3.3 Preparation of EVOH nanocomposites

The EVOH27 and EVOH44 copolymers were dissolved in a water/isopropanol solvent combination (30:70 ratio) forming a 5-6 wt% solution. Two different methods were used to incorporate the nanowhiskers into the EVOH polymer matrix. The first method involved redispersing the freeze dried nanowhiskers into water and adding the suspension as 1, 3, 5, 8, 10 wt% with regard to the weight of the EVOH copolymer. The second method entailed the addition of the nanowhisker suspension (without freeze drying and redispersing) into the polymer solution in the same weight fractions as mentioned above. The nanocomposite mixture was stirred for approximately two hours before further processing using solution casting and electrospinning to produce the nanocomposite materials.

3.3.1 Solution casting

The nanocomposite mixtures with different nanofiller loadings were dried in glass petri dishes at ambient conditions and ground into powder form when completely dry. The EVOH27 and EVOH44 nanocomposites with cellulose nanowhiskers incorporated in either a freeze dried (fd) form or as a

suspension (sus) will from here on respectively be referred to as EVOH27/cnw(fd) (or EVHO44/cnw(fd)) and EVOH27/cnw(sus) (or EVOH44/cnw(sus)). A similar abbreviated labelling was used for the EVOH/chitin nanocomposites, for example EVOH27/chnw(fd) refers to an EVOH/chitin nanocomposite consisting of EVOH27 as matrix and chitin nanowhiskers incorporated into the matrix as a freeze dried product.

3.3.2 Electrospinning

Electrospinning of 5-6 wt% (wt polymer/wt solution) EVOH nanocomposite solutions was carried out on a horizontal electrospinning setup as illustrated in Figure 3.1. This in-house build device consists of a high voltage supply unit (0-50 kV), a syringe pump, a spinneret connected to the positive terminal as well as a grounded collector plate connected to the negative terminal of the power supply unit. The voltage was kept at 10 kV and the flow rate at 0.01 ml/min during electrospinning. The tip to collector distance was 15 cm. All the different EVOH/cnw and EVOH/chnw nanocomposites containing different nanowhisker loadings were electrospun at these conditions.

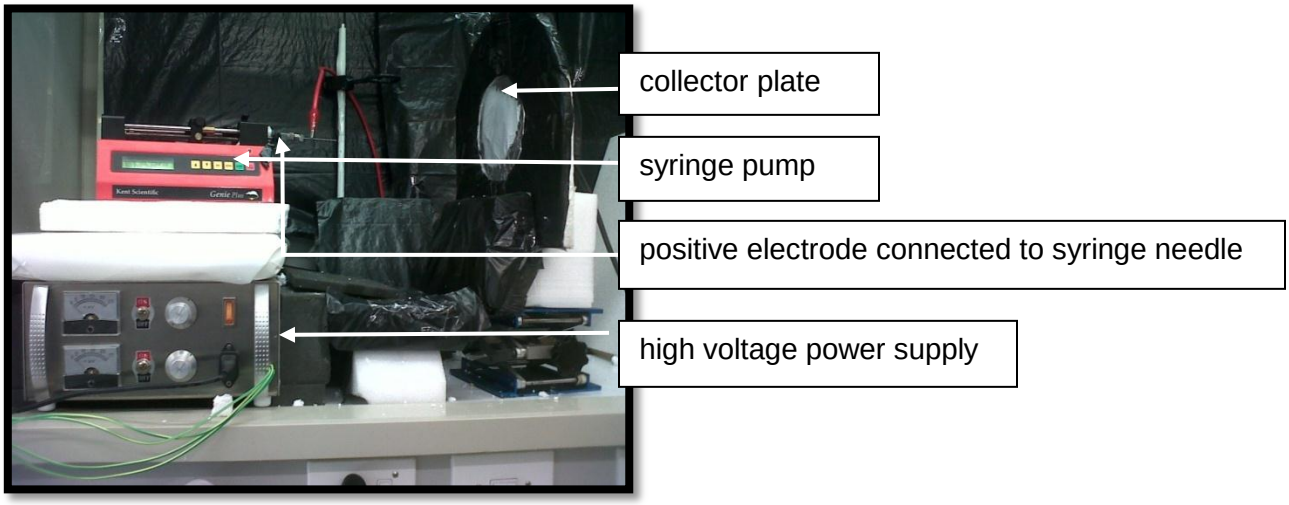

Figure 3.1: Electrospinning setup used to prepare EVOH nanocomposites fibers.

3.4 Fluorescent labelling of cellulose nanowhiskers

Two different fluorescent dyes (Rhodamine B and FITC) were used for labelling of the cellulose nanowhiskers in order to study the dispersion of these nanocrystals within the EVOH matrix.

Rhodamine B was dissolved in water forming a very dilute solution. A certain mass of nanowhiskers were added to the diluted Rhodamine B solution (2.5 mg:1 mg; nanowhiskers:Rhodamine B) and stirred at 45 °C for 2 hours. The nanowhisker suspension was dialyzed in clean water for two days in order to wash out the Rhodamine B which did not bond to the surface hydroxyl groups. The freeze dried nanowhiskers had a very light pink tint colour after being labelled with Rhodamine B.

FITC was used as an alternative fluorescent dye and fluorescent labelling was done according to a one-step procedure used by Nielsen et al. This procedure is illustrated in Figure 3.3 and involves addition of 250 mg freeze dried cellulose nanowhiskers to 25 ml of 0.1 N NaOH. Thereafter 10 mg of FITC was added to the solution and the mixture was stirred for 3 days in the dark[5].

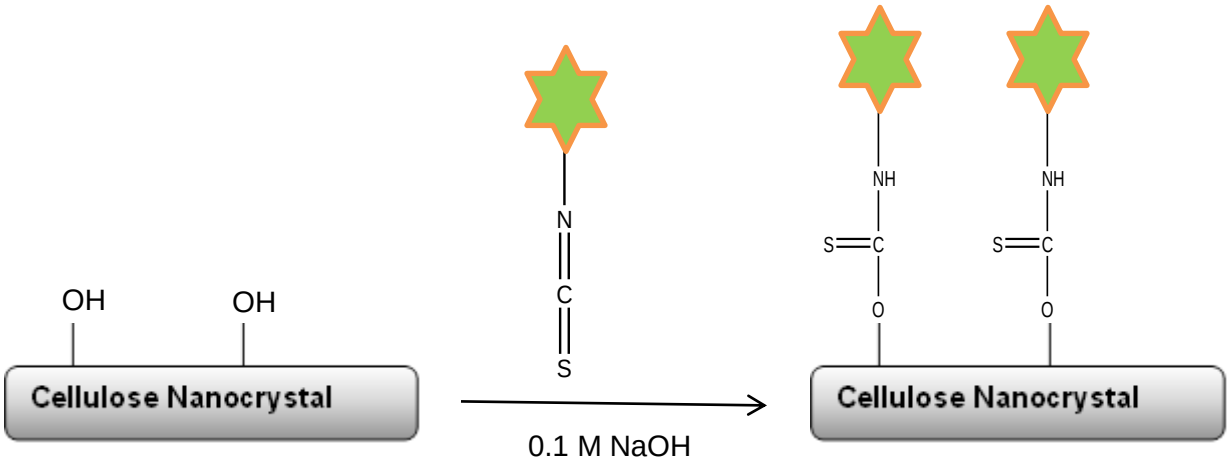

Figure 3.2: Reaction of FITC and cellulose nanowhiskers.

3.5 Preparation of LDPE nanocomposites

EVOH electrosopun nanofibers containing 0, 3, 8 and 10 wt% cellulose nanowhiskers were used to prepare LDPE nanocomposite films. The electrospun fiber mat was placed between two LDPE films followed by melt pressing the ‘sandwich’ at 120 °C which is higher than the melting temperature of LDPE but lower than the melting temperature of EVOH. The samples were pressed with a force of 2 ton.

3.6 Characterization of nanowhiskers and EVOH nanocomposites

3.6.1 Transmission electron microscopy (TEM) analysis

TEM analysis was used to characterize isolated cellulose and chitin nanowhiskers. Sample preparation was done by depositing a drop of diluted nanowhisker suspension onto a carbon coated TEM grid, negatively stained with urinal acetate and allowed to dry. The EVOH solution cast nanocomposite samples as well as the EVOH nanocomposites fibers were embedded in agar resin and ultra microtomed in order to study the nanowhisker dispersion within the EVOH matrix by way of TEM analysis. Staining with urinal acetate was done after placing the microtomed samples on the carbon coated copper grids. All the sample grids were observed in a LEO 912 EM TEM instrument. Images of lower and higher magnification were taken.

3.6.2 Atomic force microscopy (AFM) analysis

Characterization of the isolated nanowhiskers was done on an EasyScan 2 AFM from Nanosurf (Switzerland) using a non-contact Si cantilever with a spring constant of 50 N/m and a resonance frequency of 330 kHz. Sample preparation involved drying a dilute nanowhisker suspension on a mica surface.

3.6.3 Polarized optical light (POL) microscopy analysis

Birefringence of individual dispersed nanocrystals in suspension was studied using a setup consisting of cross polarized filters and a light source as described previously in Section 2.8.3. The cellulose nanowhiskers in suspension as well as the redispersed cellulose (after being freeze dried) and chitin nanowhiskers were characterized in this way. Images were taken with a digital camera.

3.6.4 Scanning electron microscopy (SEM) analysis

All samples were gold coated before analysis with a Leo® 1430VP scanning electron microscope. At least one lower (X1000) and one higher magnification (X4000-6000) were taken for each electrospun nanocomposite sample.

3.6.5 Field emission scanning microscopy (FESEM) analysis

FESEM was done using a FEI Nova nano FEG SEM 230 instrument. Samples were carbon coated before imaging.

3.6.6 Fourier transform infrared (FTIR) analysis

Transmission FTIR data were recorded using a Thermo Fisher Nicolet iS10 instrument. The spectra were recorded at a minimum number of scans set at 32 and with a resolution of 4 cm^{-1}. Neat EVOH samples, all nanocomposites as well as isolated nanowhiskers were all analysed as thin films.

3.6.7 Differential scanning calorimetry (DSC) analysis

Crystallization and melting behaviour of all EVOH nanocomposite samples were studied using a Q100 DSC (TA instruments) instrument. Calibration of the instrument was carried out with an indium metal standard, according to standard procedures. Three heating cycles with a fixed heating/cooling ramp of 10 °C/min was used.

The first step was programmed to heat the sample up to 180 °C for EVOH44 and 200 °C for EVOH27 and then kept isothermally at that temperature for 5 minutes before cooling down to 25 °C. The purpose was to remove the thermal history. The third step consisted of reheating the sample to the same respective temperatures in order to obtain the crystallization and melting point data. The second melting endotherm of each sample was recorded and discussed in the results section of Chapter 5.4.

3.6.8 Thermogravimetric analysis (TGA)

Thermal stability of all samples was studied using a Perkin Elmer TGA7 instrument. The samples were heated under nitrogen flow from room temperature to 900 °C at a rate of 20 °C/min.

3.6.9 Tensile testing

Tensile testing was done on a LRX (LLOYD instruments) tensile tester. Dumbbell shaped samples were prepared by using the melt pressed LDPE nanocomposites films. Tests were performed with a starting force of 1 N and a test speed of 50.0 mm/min. Sample dimensions were chosen as follow: gauge length: 23 mm, width: 5 mm and thickness: varied between 0.1-0.16 µm. Thickness was measured before every test for accuracy. Tensile testing of each nanocomposite was repeated 5 times in order to record an average stress strain curve.

3.6.10 Dynamic mechanical analysis (DMA)

DMA was done on the EVOH44 solution cast nanocomposites containing freeze dried cellulose nanowhiskers and cellulose nanowhiskers in suspension respectively. The instrument that was used is a Perkin Elmer Diamond DMA. The analysis was carried out at a constant frequency of 1 Hz with force amplitude of 1500(mN). The test speed was set at a rate of 3 °C/min and the temperature range was set from -5 °C to 140 °C.

3.6.11 Fluorescence microscopy analysis

Thin film samples of the solution cast EVOH/cnw and EVOH/chnw nanocomposites were prepared by melt pressing. Thin electrospun EVOH/cnw and EVOH/chnw nanocomposite fiber mats were also subjected to fluorescence microscopy. An Olympus Cell'R, attached to an IX-81 inverted fluorescence microscope and equipped with an F-view-II cooled CCD camera (Soft imaging Systems) was used for analysis of prepared samples. A Xenon-Arc burner (Olympus Biosystems GMBH) was used as the light source. The excitation filters were: 360 nm (for blue staining), 492 nm (for green staining) and 572 nm (for red staining) and emission was collected with a UBG triple-bandpass emission filter cube (Chroma). It is important to mention that when the background was subtracted, Z-stacks have been deconvoluted. Most samples were recorded with two magnifications (60X and 100X).

3.7 References

(1) Bondeson D, Mathew A, Oksman K. Optimization of the isolation of nanocrystals from microcrystalline cellulose. *Cellulose* 2006;13(2):**171-180**.

(2) Araki J, Wada M, Kuga S, Okano T. Birefringent Glassy Phase of a Cellulose Microcrystal Suspension. *Langmuir* 2000;16(6):**2413-2415**.

(3) Uddin AJ, Araki J, Gotoh Y. Characterization of the poly(vinyl alcohol)/cellulose whisker gel spun fibers. *Composites Part A: Applied Science and Manufacturing* 2011;42(7):**741-747**.

(4) Morin A, Dufresne A. Nanocomposites of Chitin Whiskers from Riftia Tubes and Poly(caprolactone). *Macromolecules* 2002;35(6)**:2190-2199**.

(5) Nielsen LJ, Eyley S, Thielemans W, Aylott JW. Dual fluorescent labelling of cellulose nanocrystals for pH sensing. *Chemical Communications* 2010;46(47):**8929-8931**.

Chapter 4:
Characterization of Nanowhiskers

4.1 Introduction

Cellulose and Chitin nanowhiskers were produced through acid hydrolysis as described in Section 3.2.1. Some of the nanowhiskers were isolated from suspension by way of freeze drying and the rest was kept in suspension in order to make it possible to incorporate the nanowhiskers into the matrix as a suspension. Nanowhiskers incorporated directly as a suspension has been shown to retain better dispersion within a polymer matrix when compared to incorporation of freeze dried nanowhiskers[1,2]. The dialysed nanowhisker suspensions were calculated gravimetrically, before and after water evaporation, to contain between 0.4 and 0.5 wt% nanowhiskers. Techniques such as TEM, AFM, FTIR, POL and Fluorescence were used to characterize the produced nanowhiskers and the results are discussed in this chapter. Cellulose nanowhiskers will be referred to as **cnw** and chitin nanowhiskers will be referred to as **chnw** in the remainder of this chapter.

4.2 Transmission electron microscopy (TEM) analysis

The dimensions and agglomeration of cellulose and chitin nanowhiskers were determined using TEM. As already mentioned, the nanowhiskers were either kept in suspension after dialysis or freeze dried and then redispersed into a water solution. The freeze dried product was alternatively redispersed in a water/isopropanol blend which is the solvent used for dissolving the EVOH that was used as matrix further on. Cnw were also dispersed in a water/isopropanol blend by means of solvent exchange during centrifugation. The advantage of solvent exchange is avoiding the freeze drying process and therefore avoiding possible aggregation of cnw during redispersion in solvent. Figure 4.1(a) displays a clear TEM image of cnw with dimensions in the range of 50–150 nm (length) and 5-10 nm (width) and Figure 4.1(b) displays a TEM image of individual dispersed chnw with lengths in the range of 50-200 nm and widths of 5-15 nm.

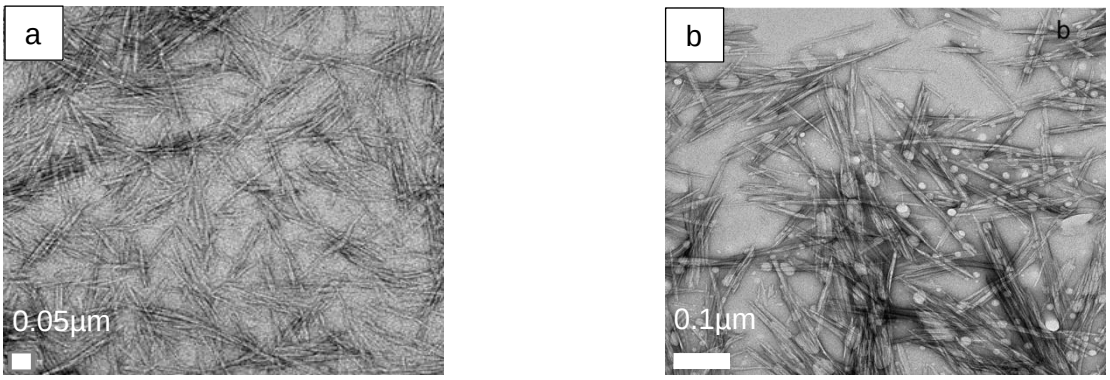

Figure 4.1: TEM images of (a) cellulose nanowhiskers and (b) chitin nanowhiskers from the samples in suspension.

TEM images of freeze dried chnw redispersed in water and a water/isopropanol blend are shown in Figure 4.2 (a) and (b) as well as images of freeze dried cnw redispersed in water and water/isopropanol are shown in Figure 4.3 (a) and (b). These images of redispersed nanowhiskers, either in water or in water/isopropanol, indicate somewhat more agglomeration than in the case of cnw and chnw displayed in Figure 4.1. The isolated nanowhiskers observed in Figure 4.1 (a) and (b) was prepared from a nanowhisker suspension sample that was kept after dialysis. During the sulphuric acid hydrolysis process, some degree of surface modification takes place where ester sulphate groups are grafted onto the cellulose molecule. These negatively charged sulphate groups on the nanowhisker surface repel each other and keep whiskers well dispersed in the suspension. The agglomeration may be owing to the loss in ester sulphate groups during the process of freeze drying. Once these crystals are dried they also agglomerate forming strong hydrogen bonds which are much harder to completely separate again when redispersing them into water[3,4].

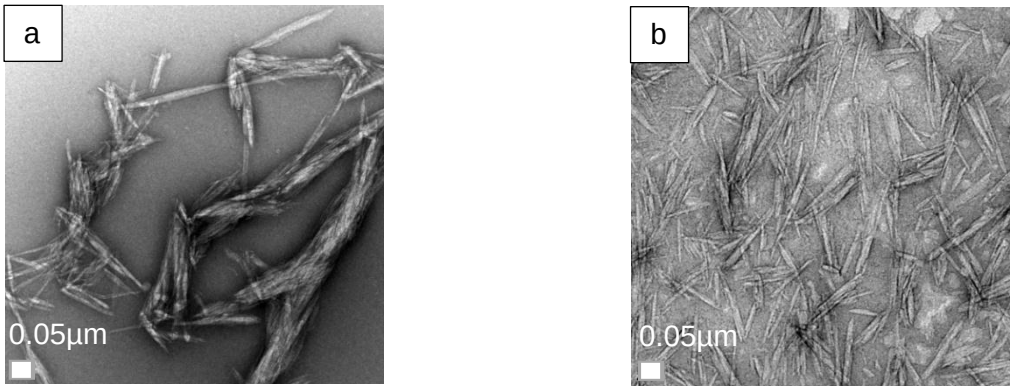

Figure 4.2: TEM images of redispersed freeze dried chnw in (a) water and (b) water/isopropanol.

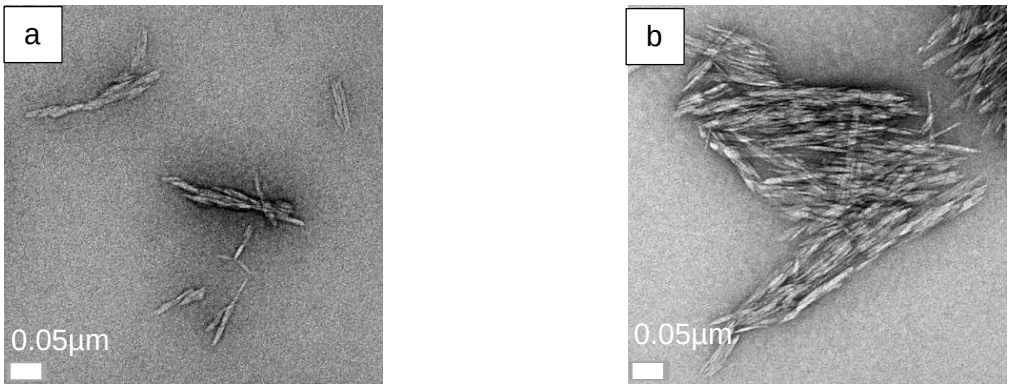

Figure 4.3: TEM images of redispersed freeze dried cnw in (a) water and (b) water/sopropanol.

Figure 4.4 displays the TEM image and Figure 4.5(a) displays a digital image of the nanowhiskers which were dispersed in the water/isopropanol blend using the solvent exchange method during centrifugation

Figure 4.5 illustrates a digital image of nanowhisker suspensions after extensive sonication and left to stand overnight. The polytop containing cnw redispersed in a water/isopropanol blend (Figure 4.5(c)) was the only mixture separating into two distinct phases. Better dispersion is observed for the samples which contained cnw which were kept in suspension compared to freeze dried cnw redispersed into the water/isopropanol blend. The well dispersed cnw in water/isopropanol using the solvent exchange method is partly due to the presence of the excess sulphuric acid on the nanowhisker surface. Dialysis was not done in order to remove the excess acid after centrifugation due to the water/isopropanol medium which would result in too much solvent waste. Nanowhiskers dispersed in water rather than in the water/isoproanol blend was therefore incorporated into the matrix as a nanowhisker suspension.

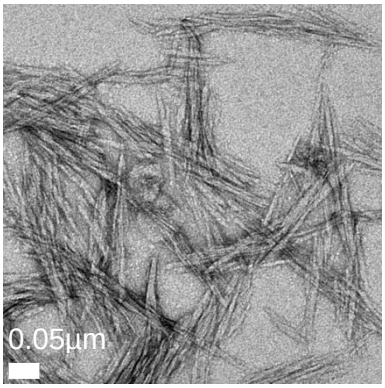

Figure 4.4: TEM image of cnw which was solvent exchanged during centrifugation.

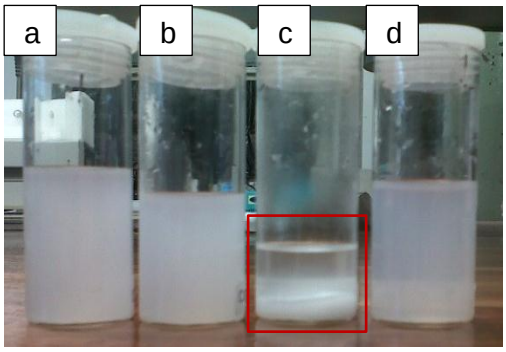

Figure 4.5: Digital image of (a) cnw in water/isopropanol obtained by solvent exchange, (b) redispersed cnw in water (c) redispersed cnw in water/isopropanol and (d) cnw suspension as obtained after dialysis.

Two methods were investigated to increase the nanowhisker concentration in suspension. The weight percentage of the nanowhiskers was increased using a concentrated PEG (20 000 g/mole molecular weight) solution as well as through rotary evaporation. Both methods were successful in increasing the nanowhisker concentration. TEM analysis was necessary to prove that the nanocrystal morphology remained unchanged during both these processes. Possible attachment of low molecular weight PEG may have penetrated through the dialysis membrane changing the size and structure of the nanowhiskers. According to TEM images in Figure 4.6 and Figure 4.7 the cellulose and chitin nanocrystals retain their rodlike structure known as nanowhiskers.

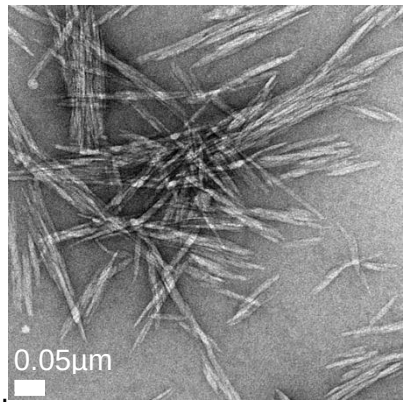

Figure 4.6: TEM image of cnw after increasing the weight percentage of the suspension using a concentrated PEG solution.

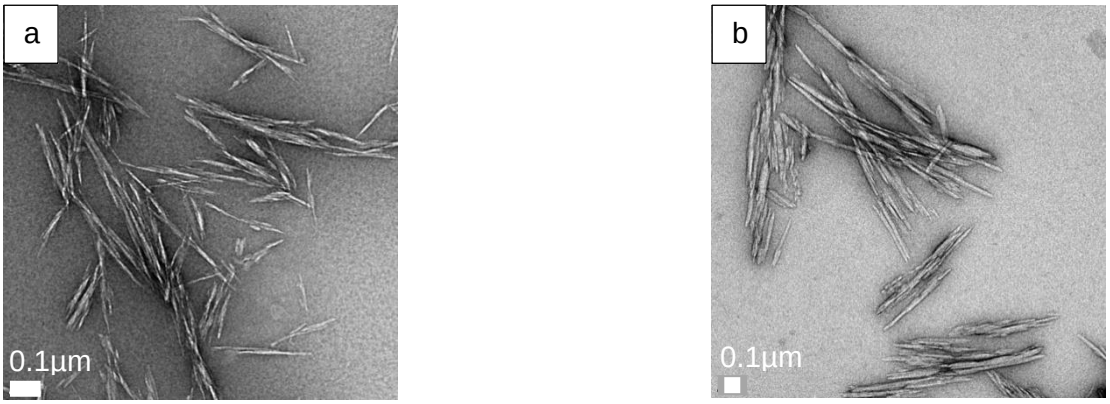

Figure 4.7: TEM images of (a) cnw and (b) chnw after rotor evaporation of water.

4.3 Atomic force microscopy (AFM) analysis

Figure 4.8 and Figure 4.9 illustrate phase and topography images of cellulose and chitin nanowhiskers respectively obtained by AFM and dimensions seen here agreed well with TEM results. The structure of chitin nanowhiskers looks somewhat different on the AFM phase image compared to what we see according to TEM analysis. This is due to the method of imaging compared to electrons being transmitted through the sample.

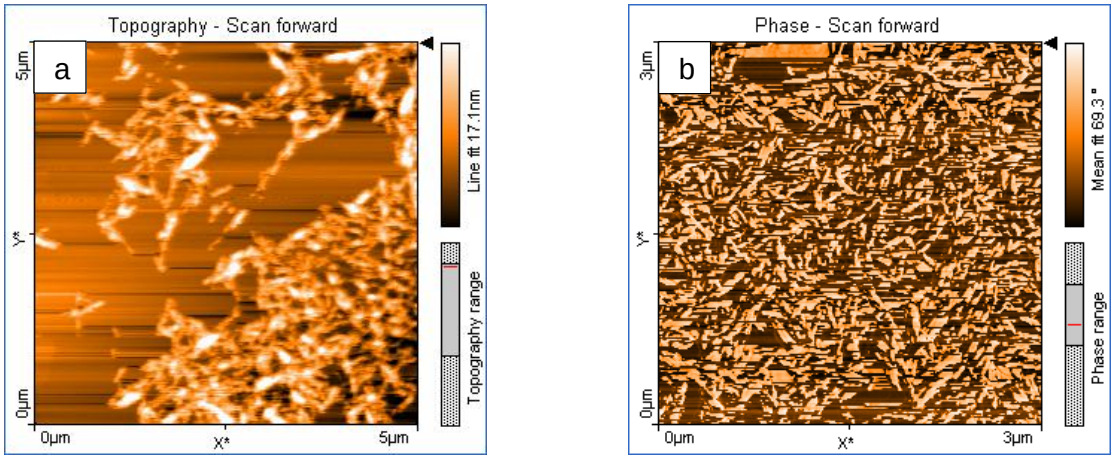

Figure 4.8: AFM (a) topography and (b) phase images of cellulose nanowhiskers.

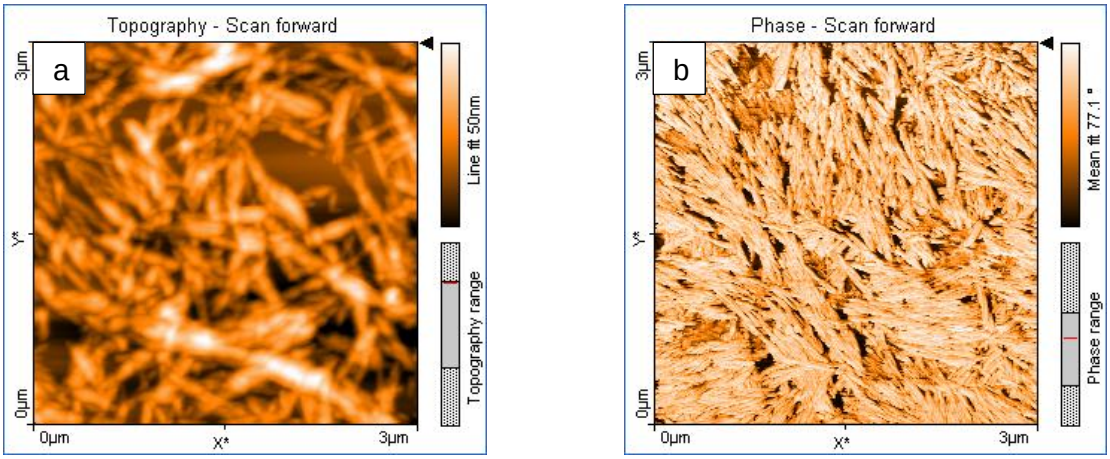

Figure 4.9: AFM (a) topography and (b) phase images of chitin nanowhiskers.

4.4 Polarized optical light (POL) microscopy analysis

The nanowhisker suspensions obtained after sonication were imaged using the POL setup. Figure 4.10 shows POL microscopy images displaying clear birefringence of individual well dispersed nanowhiskers present in water for both cellulose and chitin nanowhiskers.

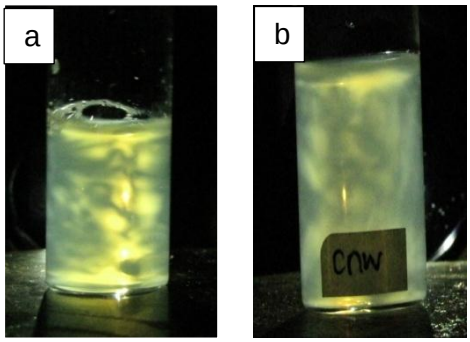

Figure 4.10: POL microscopy images of (a) chnw and (b) cnw water suspensions.

Figure 4.11 represents POL microscopy images of redispersed cnw as well as chnw in water and in water/isopropanol blends.

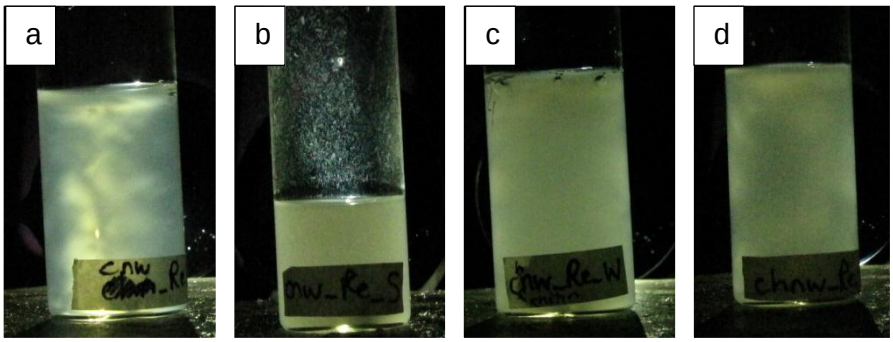

Figure 4.11: POL microscopy images of redispersed (a) cnw in water, (b) cnw in water/isopropanol, (c) chnw in water and (d) chnw in water/isopropanol.

According to these images, the redispersed nanowhiskers in water and water/isopropanol did not show the same colourful pattern except the sample of cnw redispersed in water (Figure 4.11(a)). The lack of birefringence or poor birefringence is ascribed to agglomeration of nanowhiskers[3]. Diluting the sample and increasing the sonication time did, however, increase the birefringence slightly. Figure 4.12 shows a POL microscopy image of cnw that underwent solvent exchanged during centrifugation. The mentioned cnw display clear birefringence in the water/isopropanol solution blend (Figure 4.12).

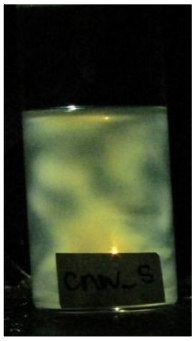

Figure 4.12: POL microscopy image of cnw dispersed in a water/isopropanol blend during a solvent exchange centrifugation process.

4.5 Thermogravimetric analysis (TGA)

Figure 4.13 displays the derivative weight loss curves of cellulose, cnw, chitin and chnw. Comparison of the TGA results for cellulose nanowhiskers and MCC, show that the onset in degradation starts at a much lower temperature for the nanowhiskers which is due to the acid hydrolysed cellulose containing sulphate groups attached to them (Figure 4.13(a))[3,5].

TGA results of cellulose nanowhiskers before and after dialysis were compared to cellulose nanowhiskers treated with 0.1 M NaOH in order to neutralize the remaining acid. The thermal stability of cellulose nanowhiskers before dialysis clearly showed a lower as well as broader

degradation temperature curve than in the case of the rest of the samples. Figure 4.14 illustrates the sample treated with base resulted in the sample with the highest thermal stability. This increase in thermal stability agrees with previous reports where nanowhiskers containing a higher amount of acid traces result in thermally less stable crystals[1,5-7].

Chitin and chnw have very close onset temperatures of degradation (Figure 4.13(b)). This observation differs from that of cellulose. Chitin is treated with hydrochloric acid which is thermally much more stable than sulphuric acid. The hydrogen bonding between chitin molecules is also known to be extremely strong due to the amide moiety present in the backbone[8].

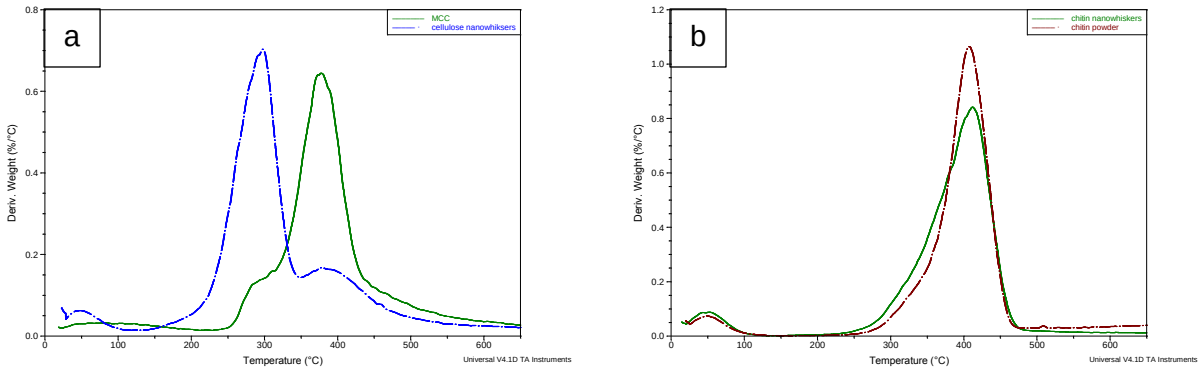

Figure 4.13: Overlaid derivative weight loss curves of (a) cnw and MCC (b) chnw and chitin.

The TGA curve of cnw, concentrated in the water using a concentrated PEG solution, indicated that the nanowhiskers contained some PEG (not displayed in this chapter). The onset degradation temperature in the higher temperature region corresponds to that of PEG homopolymer and differs from neat cnw. Except for the possibility of using a dialysis membrane with a very low molecular weight cut off, the whole process using a concentrated PEG solution is rather time consuming. Rotor evaporation under vacuum was, therefore, used in the remainder of the study in order to increase the cellulose concentration in the water suspension.

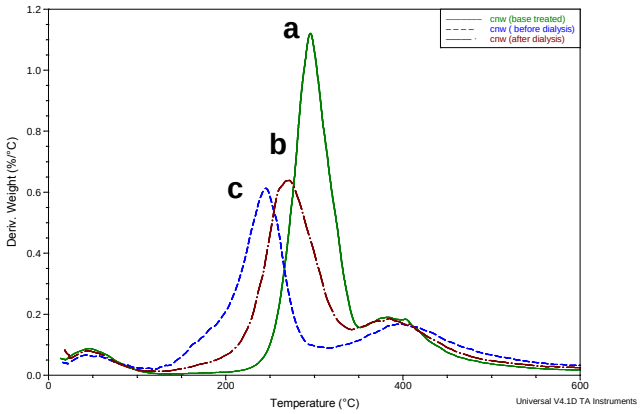

Figure 4.14: Overlaid derivative weight loss curves of (a) cnw treated with base (NaOH), (b) cnw after dialysis and (c) cnw before dialysis.

4.6 Fourier transform infrared (FTIR) spectroscopy

FTIR spectra of cellulose and chitin nanowhiskers are shown below in Figure 4.15 and Figure 4.16 respectively. The cellulose peaks were identified as follow: the region 3100-3600 cm^{-1} is attributed to hydrogen bond hydroxyl stretching; the peak at 1031 cm^{-1} is due to C-OH deformation mode and 664 cm^{-1} show the presence of C-OH out of plane bending mode. The peak in the region of 1160 cm^{-1} is due to asymmetric stretching of C-O-C and has previously been used as the characteristic peak of cellulose in nanocomposites containing bacterial cellulose[1]. In this current investigation where EVOH is used as polymer matrix, it was decided to use the peak at 1031 cm^{-1} and 1160 cm^{-1} for identifying cellulose in the nanocomposite spectrum.

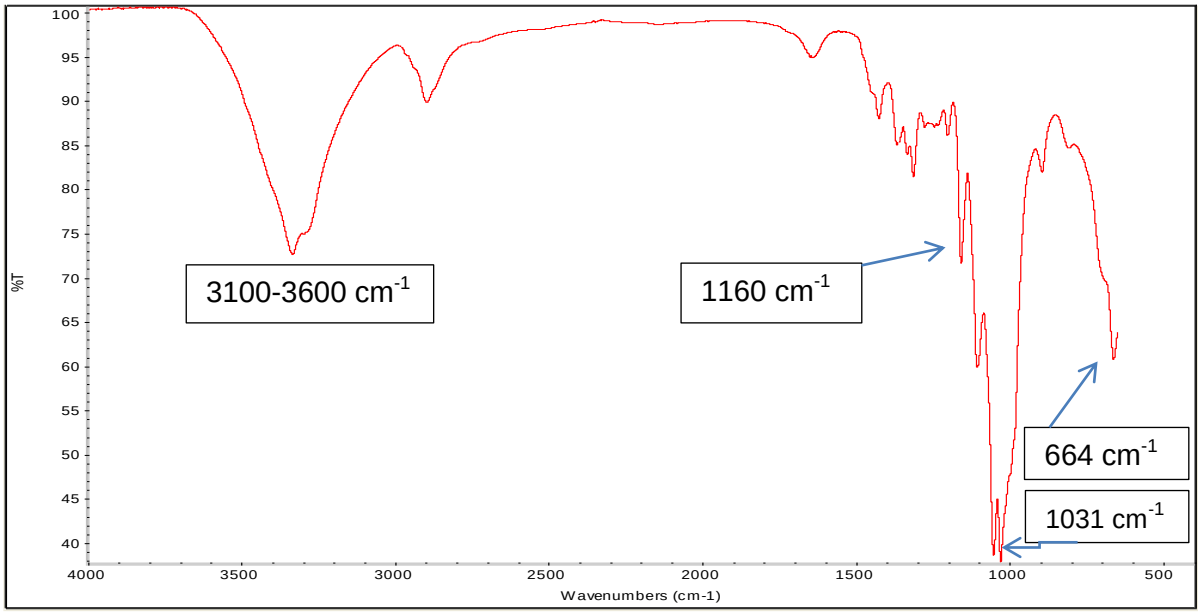

Figure 4.15: ATR-FTIR of cellulose nanowhiskers.

Chitin has the characteristic amide I and II bands in the IR region of 1500-1660 cm^{-1} which are ascribed to the carbonyl stretching of the amide moiety[9]. The amide I band is split into two peaks of which the peak at 1656 cm^{-1} is attributed to C=O which is hydrogen bonded to a nearby NH-group. The peak at 1621 cm^{-1} is speculated to be due to the presence of a hydrogen bond between C=O and a hydroxymethyl group of another chitin molecule[9].

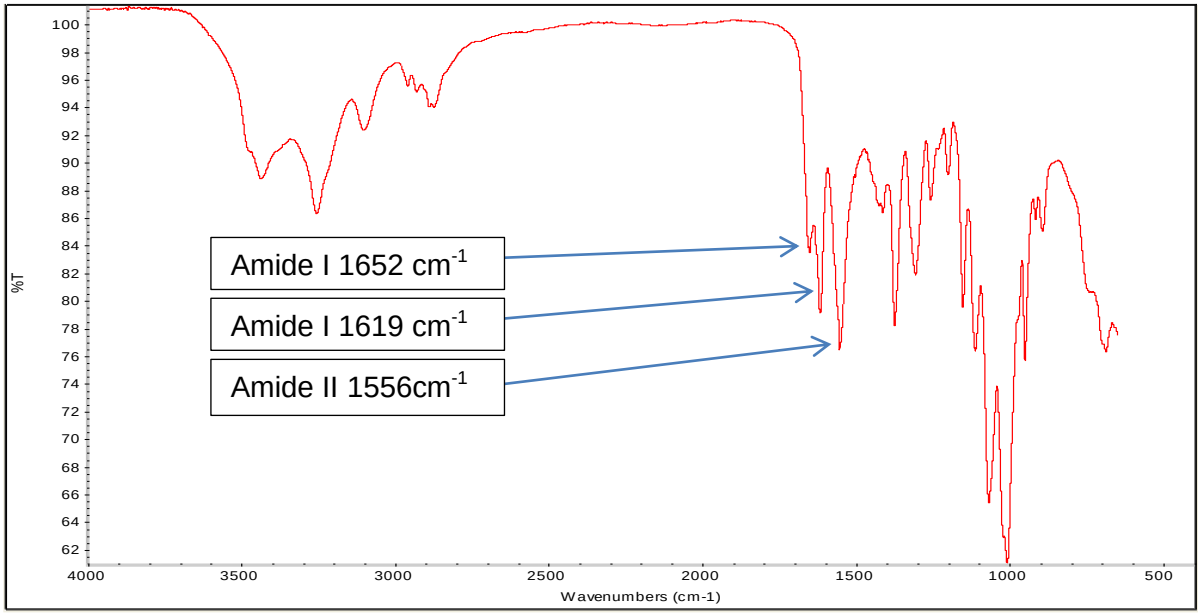

Figure 4.16: ATR-FTIR of chitin nanowhiskers.

Figure 4.17 illustrates the ATR- FTIR spectra for the qualitative analysis of MCC and cnw. The MCC was treated with sulphuric acid in order to remove the more amorphous areas and ended up with a highly crystalline structure. This was proven qualitatively by analysing the FTIR spectra of MCC and cellulose nanowhiskers. According to Oh et al. a sharpening of certain bands seen after acid hydrolysis is an indication of a more crystalline material. The broadening of especially the bands with wavenumbers at 4000-2995, 2900, 1430, 1375 and 900 cm^{-1} are related to the amount of molecular disorder and therefore the ratio A_{1430}/A_{900} can be used to estimate the crystalline versus amorphous fractions in the cellulose material as seen in previous studies[10]. The peak height tool from the OMNIC software was used to automatically create a baseline between two adjacent points and find the absorbance value at 1427 cm^{-1} (see the insert in Figure 4.17). According to the calculation of the height, the band ratio for cellulose nanowhiskers increased from 1.07 for MCC to 1.23 which indicates the efficiency of the acid hydrolysis process in creating a more crystalline structure.

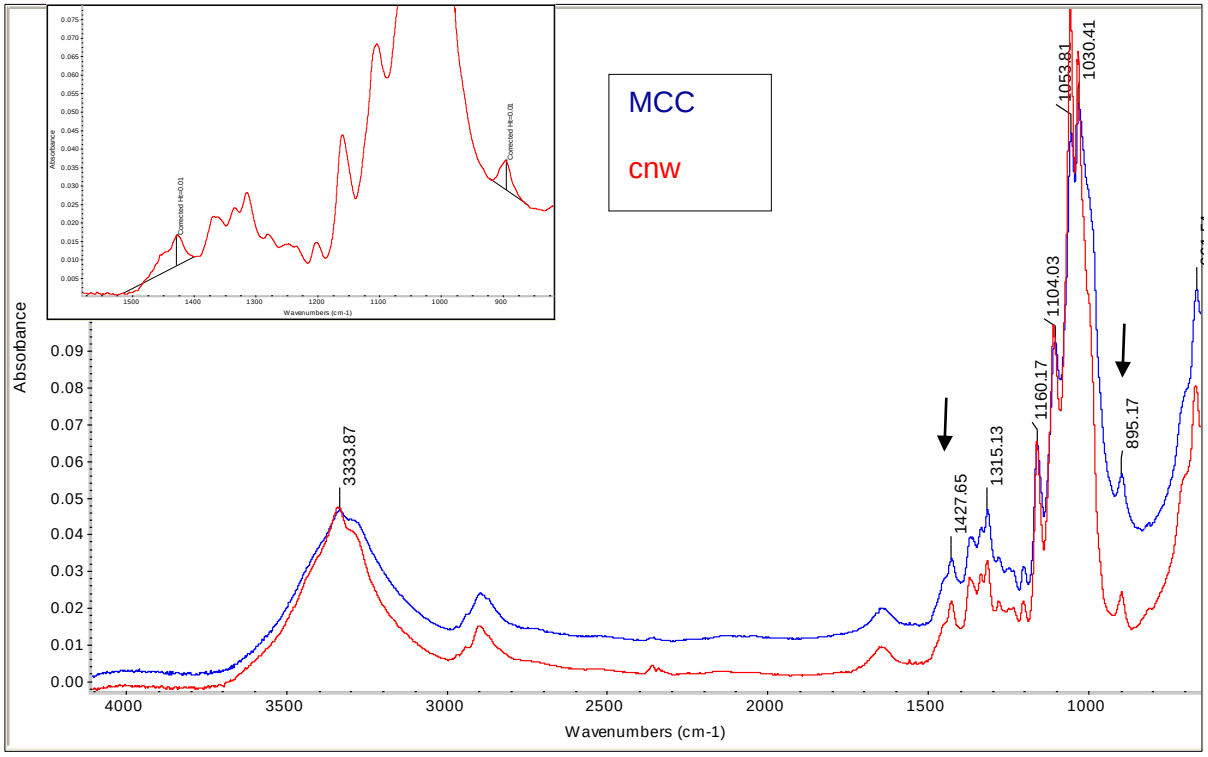

Figure 4.17: ATR-FTIR spectrum of MCC and celulose nanowhiskers

4.7 Differential scanning calorimetry (DSC) analysis

DSC thermograms of cellulose and chitin did not deliver any melting or crystallization peaks during the heating run of 25-200 °C due to the fact that degradation takes place before any melting can occur. This phenomenon is because of the strong intra- and inter-hydrogen bonding between the molecules.

4.8 Fluorescence microscopy analysis

Fluorescence images of the dyed cellulose in suspension were obtained. Figure 4.18 shows large agglomerates for nanowhiskers labelled with FITC. Smaller Rhodamine B-whisker bundles, measuring between 0.35 µm and 3.69 µm, were observed.

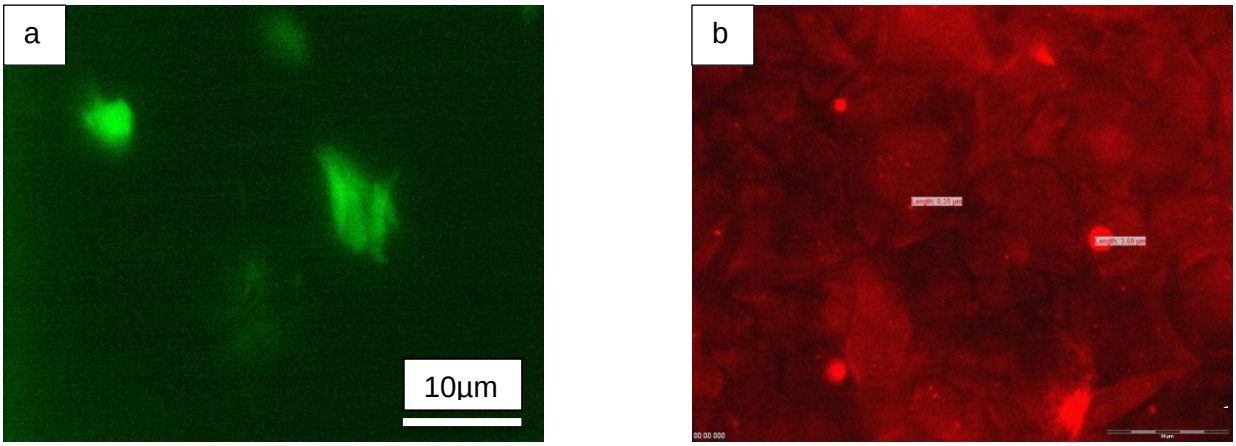

Figure 4.18: Fluorescence images of cnw in suspension dyed with (a) FITC and (b) Rhodamine B.

4.9 Conclusions

TEM and AFM images clearly show that the chitin and cellulose nanowhiskers were successfully isolated and measured dimensions are in good agreement with results found in literature. TEM and POL microscopy results indicate that freeze dried cellulose nanowhiskers do not redisperse as well in water and even worse in the water/isopropanol blend which might be due to strong hydrogen bonding once the whiskers have dried or the loss of ester sulphate groups from the freeze drying process. The poor dispersion and clear phase separation in the case of the redispersed cnw in solvent may be due to the presence of isopropanol. The reason being that isopropanol competes with cellulose nanowhiskers for hydrogen bonding with water, resulting in increased intermolecular bonding and aggregation of the nanowhiskers. In pure water, the cellulose molecules have a greater tendency to form hydrogen bonds with water and disperse slightly better than with the water/isopropanol blend.

The chitin also displayed agglomeration according to TEM as well as POL images and this is attributed to even stronger hydrogen bonding between molecules. Fluorescence was done on freeze dried cellulose nanowhiskers dispersed in water, which also confirmed the presence of agglomerates. TGA confirmed the production of nanowhiskers by comparing the thermal degradation temperatures to the cellulose and chitin source. The results agree with what has already been reported in literature for obtained nanowhiskers.

One of the most important features in producing nanowhiskers from macro sources is the increase in crystallinity. It is this property increase which gives the nanowhiskers superior mechanical properties. The increase in crystallinity for the obtained nanowhiskers was proven using the absorbance spectrum from FTIR.

4.10 References

(1) Martínez-Sanz M, Olsson R, Lopez-Rubio A, Lagaron J. Development of electrospun EVOH fibres reinforced with bacterial cellulose nanowhiskers. Part I: Characterization and method optimization. *Cellulose* 2011;18(2):**335-347**.

(2) Zhou C, Chu R, Wu R, Wu Q. Electrospun Polyethylene Oxide/Cellulose Nanocrystal Composite Nanofibrous Mats with Homogeneous and Heterogeneous Microstructures. *Biomacromolecules* 2011;12(7):**2617-2625**.

(3) Lu P, Hsieh Y. Preparation and properties of cellulose nanocrystals: Rods, spheres, and network. *Carbohydrate Polymers* 2010;82(2):**329-336**.

(4) Eichhorn SJ. Cellulose nanowhiskers: promising materials for advanced applications. *Soft Matter* 2011;7(2):**303-315**.

(5) Roman M, Winter WT. Effect of Sulfate Groups from Sulfuric Acid Hydrolysis on the Thermal Degradation Behavior of Bacterial Cellulose. *Biomacromolecules* 2004; 5(5):**1671-1677**.

(6) Martínez-Sanz M, Olsson RT, Lopez-Rubio A, Lagaron JM. Development of bacterial cellulose nanowhiskers reinforced EVOH composites by electrospinning. *Journal of Applied Polymer Science* 2012;124(2):**1398-1408**.

(7) Uddin AJ, Araki J, Gotoh Y. Characterization of the poly(vinyl alcohol)/cellulose whisker gel spun fibers. *Composites Part A: Applied Science and Manufacturing* 2011;42(7):**741-747**.

(8) Kameda T, Miyazawa M, Ono H, Yoshida M. Hydrogen Bonding Structure and Stability of α-Chitin Studied by 13C Solid-State NMR. *Macromolecular Bioscience* 2005;5(2):**103-106**.

(9) Rinaudo M. Chitin and chitosan: Properties and applications. *Progress in Polymer Science* 2006;31(7):**603-632**.

(10) Oh SY, Yoo DI, Shin Y, Seo G. FTIR analysis of cellulose treated with sodium hydroxide and carbon dioxide. *Carbohydrate Research* 2005;340(3):**417-428.**

Chapter 5:
Results and Discussion of EVOH Nanocomposites

5.1 Introduction

In this chapter the analysis and characterization results of EVOH27 and EVOH44 nanocomposites containing different amounts of cellulose and chitin nanowhiskers are discussed. These nanocomposites were obtained by way of solvent evaporation as described in Section 3.3.1. Cellulose nanowhiskers will be abbreviated as cnw and chitin nanowhiskers as chnw. The numbers 27 and 44 refer to ethylene content (mole %) in the EVOH copolymer. The nanocomposite made with freeze dried nanowhiskers will from here on be referred to as EVOH/cnw(fd) (or EVOH/chnw(fd)) and the nanocomposites made with nanowhiskers in suspension will be referred to as EVOH/cnw(sus) (or EVOH/chnw(sus)). TEM is a technique used to characterise the nanocomposites by investigating the dispersion of the cellulose and chitin nanowhiskers within the EVOH matrix. Transmission FTIR was done to chemically prove the incorporation of the nanopolysaccharides by observing the characteristic peaks of cellulose and chitin appearing as the nanofiller loads increase in the EVOH matrix. Preliminary results from DMA are discussed in order to study the dynamic mechanical properties of the nanocomposites. Finally fluorescence microscopy was investigated as a possible technique to study the incorporation and dispersion of the nanowhiskers.

5.2 Transmission electron microscopy (TEM) analysis

Microtomed nanocomposite samples containing different loadings of cellulose and chitin nanowhiskers were examined. The uranyl acetate staining procedure made it possible to observe the nanowhiskers within the matrix by increasing the contrast between the different phases. Figure 5.1 illustrates the TEM images of EVOH27/chnw containing 10 and 3 wt% chnw respectively. According to these images the higher chnw loadings such as 10 wt% tend to agglomerate slightly more than the lower loadings such as 3 wt%, but there is still a good measure of dispersion present in both samples. This observation was seen in the case of the nanocomposites containing chnw as well as cnw. Figure 5.2 shows more examples of cnw dispersed in EVOH as freeze dried nanowhiskers and as whiskers in suspension. It is clearly visible that there is still a good measure of dispersion even in the case of EVOH/5%cnw(fd).

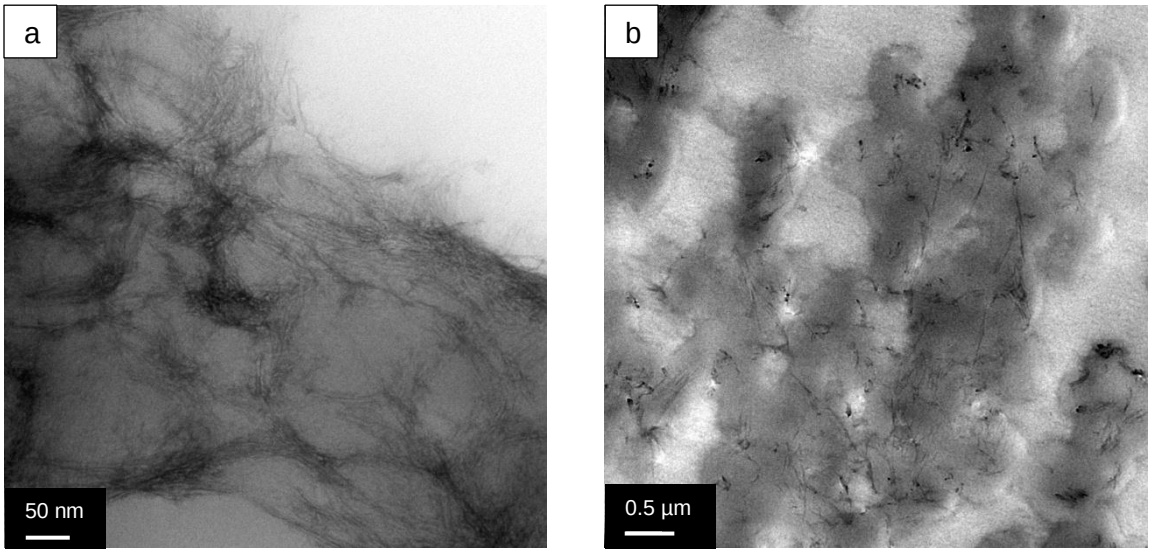

Figure 5.1: TEM images of (a) EVOH27/10%chnw(sus) and (b) EVOH27/3%chnw(sus).

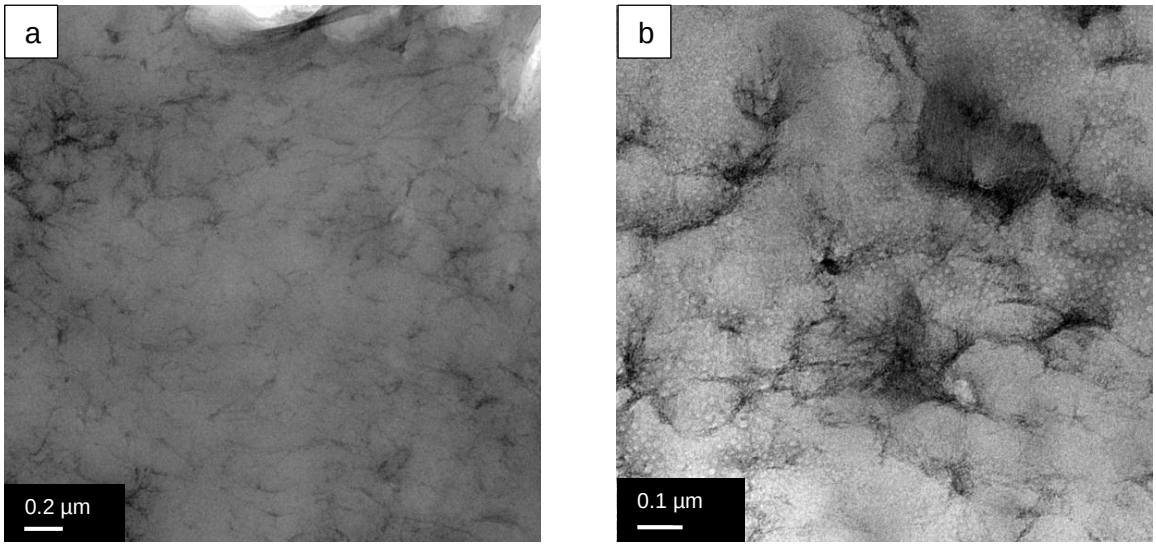

Figure 5.2: TEM images of (a) EVOH27/5%cnw(fd) and (b) EVOH44/10%cnw(sus).

5.3 Fourier transform infrared (FTIR) spectroscopy

Cellulose consists of C, H and O atoms only and the IR bands overlap with most of those of EVOH which makes it difficult to isolate and quantify individual peaks that contribute exclusively to the cellulose nanowhiskers within the nanocomposites.

Transmission FTIR results indicate in Figure 5.3 the appearance of characteristic cellulose peaks at 1031 cm^{-1} and 1060 cm^{-1}, as the nanowhisker load increases from 0 wt% to 10 wt%. Only the spectra for EVOH27/cnw(sus) nanocomposites are shown below but similar results were observed in the case of EVOH27/cnw(fd), EVOH44/cnw(sus) and EVOH44/cnw(fd) nanocomposites.

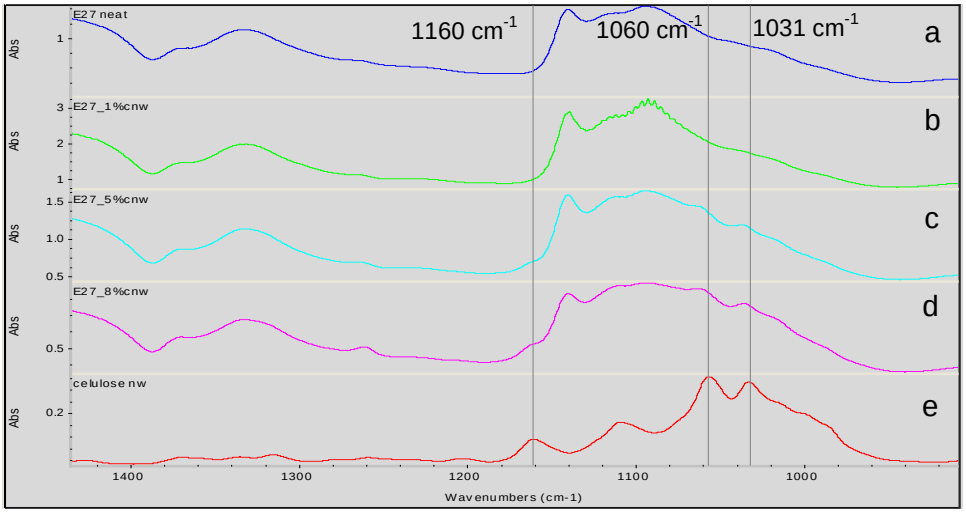

Figure 5.3: FTIR spectra of EVOH27 nanocomposites containing (a) 0, (b) 1, (c) 5, (d) 8 wt% cnw(sus) and (e) isolated cnw.

Chitin nanowhiskers were much easier to identify by way of FTIR within the nanocomposite samples due to the prominent amide moiety from the Amide I bands at 1660 cm^{-1} and 1619 cm^{-1} and the Amide II band at 1556cm^{-1} [1]. These bands appear in all the different EVOH samples loaded with nanowhiskers. Figure 5.4 shows an example of spectra that were observed for all the other samples containing chitin nanowhiskers.

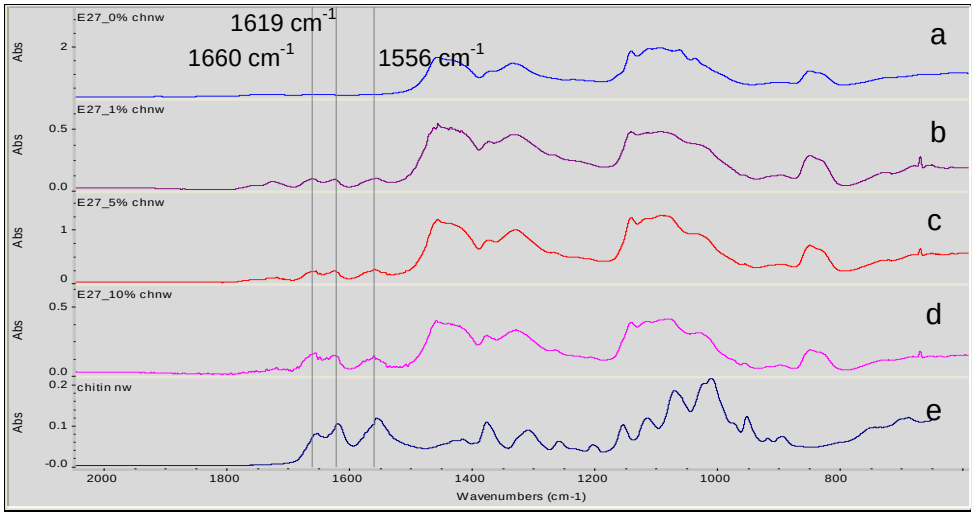

Figure 5.4: FTIR spectra of EVOH27 nanocomposites containing (a) 0, (b) 1, (c) 5, (d) 10 wt% chnw(fd) and (e) isolated chnw.

5.4 Thermogravimetric analysis (TGA)

The thermal stabilities of EVOH27 and EVOH44 nanocomposites containing cnw and chnw were investigated by comparing the maximum peak degradation temperature as well as the onset in degradation temperatures. The maximum peak degradation temperature is obtained by finding

the temperature corresponding to the highest and most prominent peak associated with the neat EVOH matrix.

5.4.1 Degradation effects

Degradation of nanocomposites was suspected when a brown/yellowish colour was observed after heating the nanocomposite samples to a temperature above their melting point. One suggestion for this observation may be due to the presence of cellulose nanowhiskers which have an onset in degradation temperature of 180-200 °C. This temperature range falls in the same region as the melting points of EVOH27 and EVOH44. Secondly, the presence of acid traces could still be present which could possibly catalyse dehydration followed by chain scission reactions and the formation of conjugated double bonds. In order to investigate whether acid traces are responsible for the early degradation of the nanocomposites, a strong base known as a proton sponge (1,8-bis(dimethylamino)naphthalene), was dissolved in acetone and blended with the dried nanocomposite powders. This mixture was left to dry properly under vacuum.

The improvement in degradation for the nanocomposites containing the proton sponge was visually noticeable. The colour change was less evident compared to the nanocomposites without the proton sponge. The surface of the hot pressed film was less brittle, smooth and more transparent. These observations lead to the neutralization of the nanowhisker suspensions before addition to the EVOH matrix. The nanowhisker suspensions were neutralized by addition of 0.1 M NaOH to the suspension and dialysed until a neutral suspension was obtained as already described in Sections 3.2.1 and 4.4.

Figure 5.5 illustrates derivative weight loss curves of neat EVOH27, EVOH27/cnw treated with a proton sponge and EVOH27 nanocomposites containing either neutralized cnw or cnw without any base treatment. According to the results from Figure 5.5 there is a significant increase in the thermal stability of the EVOH nanocomposites containing cnw that was not treated with any base compared to the neat EVOH27 as well as EVOH27/cnw nanocomposites which were treated with either a proton sponge or cnw treated with NaOH. It is unexpected to find a decrease in the thermal stability of the nanocomposites when the nanowhiskers are neutralized before incorporation into EVOH. The presence of ester sulphate groups is expected to decrease the thermal stability as seen in the TGA results of neat cellulose nanowhiskers (Section 4.4).

The thermal degradation of polyvinyl alcohol (PVA) has been extensively investigated and many degradation mechanisms have been proposed[3,4]. The presence of acid in PVA results in chemical modification of the PVA homopolymer[3] and the mechanism for this modification may be used to explain similar conditions for the EVOH nanocomposites in the presence of acid.

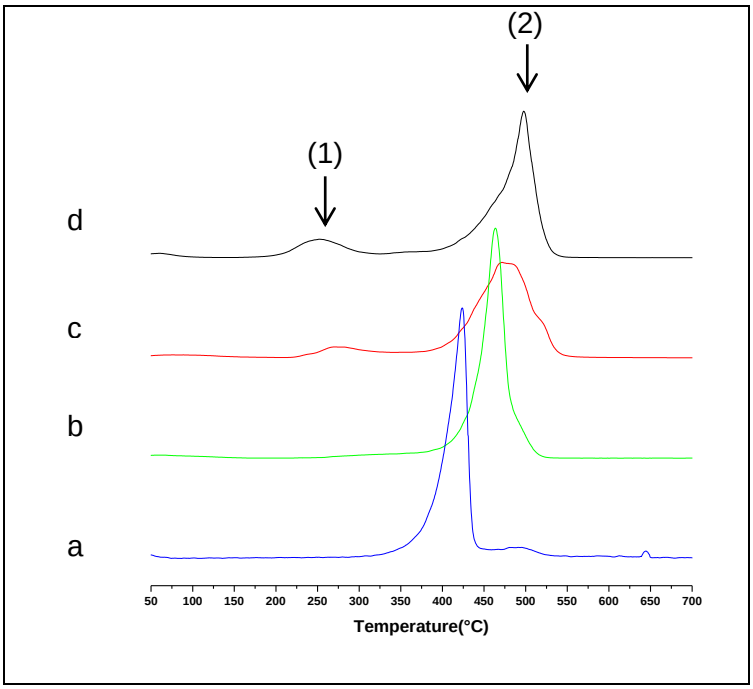

Figure 5.5: Derivative weight loss curves of (a) neat EVOH27 (b) EVOH27 containing 8 wt% neutralized cnw (c) EVOH27/8%cnw (proton sponge) and (d) EVOH27/8%cnw (no base treatment).

In order to over exaggerate and simulate the mechanism of acid catalysed degradation of EVOH44 and EVOH27, the neat polymer solutions were mixed with a few drops of 64 wt% sulphuric acid and left to dry. TGA was done in order to compare the derivative weight loss curves of the neat EVOH44 to that of the EVOH44/cnw nanocomposite. The same analysis was done for an EVOH27/H_2SO_4 combination. Figure 5.6 illustrates the TGA results of EVOH44/H_2SO_4 and EVOH27/H_2SO_4 compared to that of neat EVOH44 and EVOH27 respectively. Peak 1 that is observed in the lower temperature region of 185-235 °C in Figure 5.6(a) and (b) is probably due to the elimination of alcohol groups from the PVA segments in EVOH[3]. The sudden appearance of this lower temperature Peak 1 in Figure 5.6 corresponds very well with results for the nanocomposites containing cnw that was not treated with a base (Figure 5.5). A large increase in thermal stability for the higher region peaks (Peak 2) at 476 °C and 487 °C for EVOH44 and EVOH27 respectively is clearly visible in Figure 5.6 and again corresponds to the large increase observed in the case of the EVOH27/cnw in Figure 5.5(d) of which the cnw were not treated with any base.

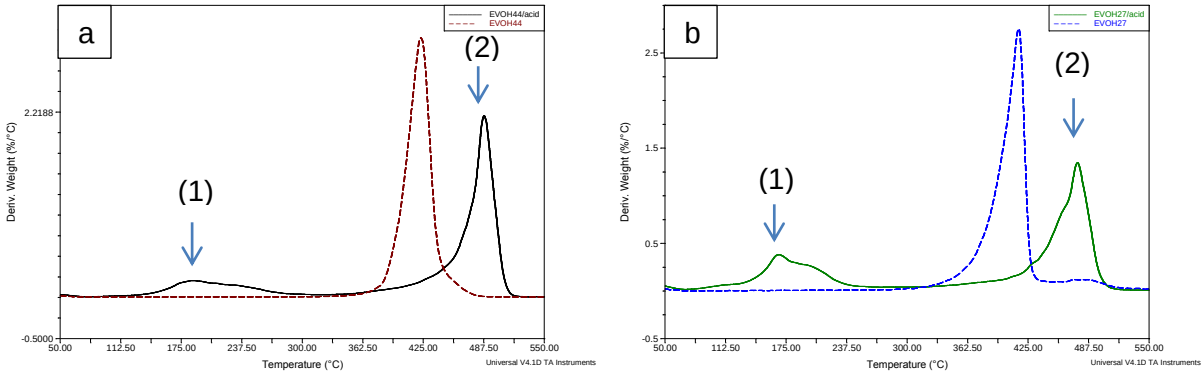

Figure 5.6: Derivative weight loss curves of (a) EVOH44 and EVOH44/H_2SO_4 (b) EVOH27 and EVOH27/H_2SO_4.

Table 5.1 displays the peak maximum temperatures of the two derivative weight loss peaks obtained from heating EVOH and EVOH/cnw.

Table 5.1: Table of the maximum peak degradation temperatures of EVOH in the presence of acid.

Material	Peak 1 (°C)	Peak 2 (°C)
EVOH44/acid	185-238	487
EVOH27/acid	165-190	475
EVOH27/8% cnw	244	482
EVOH27/8%cnw(proton sponge)	265	457
EVOH27/8%cnw(base treated)	No peak observed	439

These findings already give a significant indication that the nanowhiskers still contain traces of acid as well as ester sulphate groups, even after dialysis for several days, and that the presence of acid results in increased thermal stability of nanocomposites.

This degradation mechanism of the EVOH/cnw nanocomposites was investigated further in order to understand whether acid may be responsible for increasing the thermal stability of the material by chemical modifications of the EVOH molecules. One proposed mechanism is the early dehydration of alcohol groups by acid catalysis forming polyene structures. The formation of double bonds and possible crosslinks require more energy to be broken and may be the reason why a second degradation peak (Peak 2) is observed at much higher temperatures than that for the original EVOH peak.

EVOH27/cnw and EVOH44/cnw as well as EVOH treated with 64 wt% sulphuric acid display a peak in the higher temperature region (475-490 °C) corresponding to the thermal degradation temperature of polyethylene[5]. Sulphuric acid does, however, increase the thermal stability of EVOH by first increasing the rate of dehydration of the alcohol groups present in EVOH and possibly also cellulose forming chemical alterations which lead to higher stability when compared to the neat EVOH copolymer. It is, therefore, questionable whether the appearance of the small peak at around 200 °C must be attributed only to the depolymerisation and degradation of the cellulose nanowhiskers in the EVOH as previously reported[6] and not also to the degradation of PVA segments in the EVOH copolymer.

According to the present results, it seems that well dispersed cellulose nanowhiskers only play a small role in the increase of the thermal stability. Acid catalyses the degradation of EVOH which eventually leads to chemical alterations resulting in an increase in thermal stability as well as very low onset of degradation for the PVA segments in the EVOH copolymer.

5.4.2 EVOH27/cnw nanocomposites

Table 5.2 displays information on the maximum peak degradation temperatures of EVOH27 nanocomposites containing different loadings of cnw. The table is followed by Figure 5.7 (a) and (b) which display the derivative TGA curves to illustrate a visual representation of the onset in degradation temperatures.

Table 5.2: Maximum peak degradation temperatures (°C) for EVOH27/cnw nanocomposites.

wt% cnw	EVOH27(fd)	EVOH27(sus)
0	415.20	415.20
1	423.36	414.04
3	441.00	434.80
5	441.65	443.04
8	439.26	439.75
10	440.70	439.94

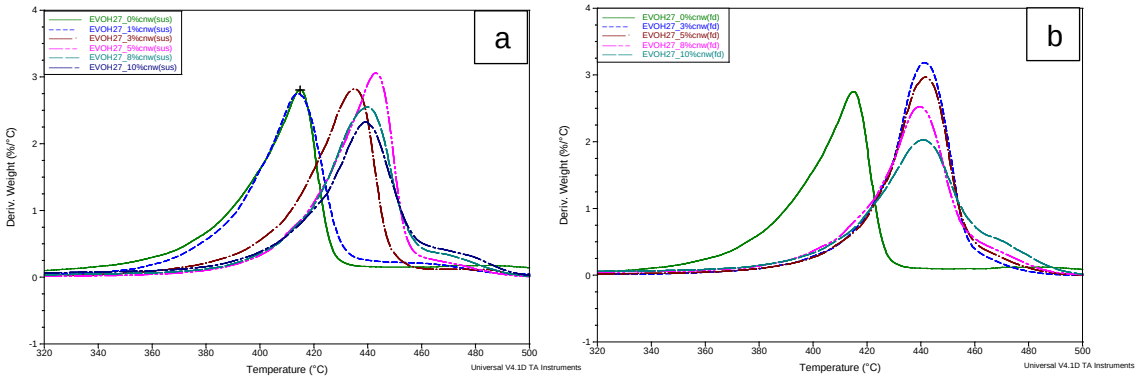

Figure 5.7: Derivative weight loss curves of (a) EVOH27/cnw(sus) and (b) EVOH27/cnw(fd).

The results from Table 5.2 and Figure 5.7 show that the nanocomposites reveal an increase in thermal stability with an increase in nanowhisker loading. The difference in degradation temperatures between neat EVOH27 and the EVOH27/10%cnw(sus) is 24.7 °C. The EVOH27/10%cnw(fd) shows a 25.5 °C increase in thermal stability with regards to the thermal stability of neat EVOH. The overall degradation temperatures of both EVOH nanocomposites (freeze dried and suspended) are extremely close and increase the thermal stability of the neat polymer significantly. The reason for this increased thermal stability may be that nanowhiskers are well dispersed within the matrix and therefore cause stronger and more effective hydrogen bonding between the EVOH chains and the cellulose nanowhiskers.

5.4.3 EVOH44/cnw nanocomposites

Table 5.3 displays information on the maximum peak degradation temperatures of EVOH44 nanocomposites containing different loadings of cnw. The table is followed by Figure 5.8 (a) and (b) which display the derivative TGA curves, giving a visual representation of the onset in degradation temperatures.

Table 5.3: Maximum peak degradation temperatures (°C) of EVOH44/cnw nanocomposites.

wt% cnw	EVOH44 (fd)	EVOH44(sus)
0	421.84	421.84
1	420.14	432.58
3	415.00	429.64
5	420.14	426.37
8	424.50	430.62
10	428.00	452.42

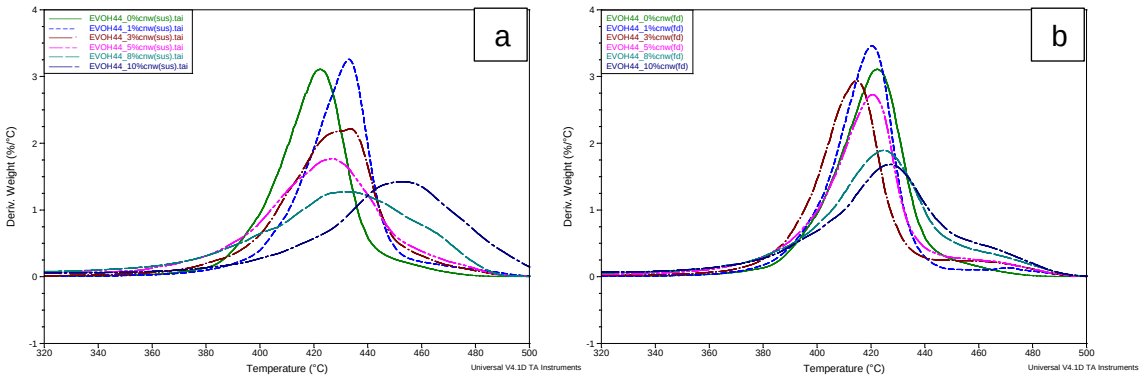

Figure 5.8: Derivative weight loss curves of (a) EVOH44/cnw(sus) and (b) EVOH44/cnw(fd).

EVOH44/cnw nanocomposites showed an increase in thermal stability with an increase in cellulose nanowhisker loading. The increased thermal stability is according to the overall increase in the maximum peak degradation temperature displayed in Table 5.3 and Figure 5.8. The EVOH4/cnw(sus) nanocomposites containing 8 wt% and 10 wt% cnw display high increases in maximum peak degradation temperatures. The onset in degradation temperature for the

EVOH44/cnw(sus) and EVOH44/cnw(fd) is lower compared to neat EVOH44, with exception to the EVOH44/1%cnw nanocomposites. The weight loss curves of EVOH44/cnw(sus) (containing 3-10 wt% cnw) are broader compared to the EVOH44/cnw(fd) nanocomposites, which may be due to a different degradation mechanism. It is possible that the EVOH44/cnw(fd) nanocomposites contain less sulphate groups on the cnw surface which cause a slight increase in thermal stability of the lower temperature region compared to EVOH44/cnw(sus) nanocomposites. An explanation for the low thermal stability for the main EVOH44/cnw(fd) peak when compared to EVOH44/cnw(sus) may be that freeze dried nanowhiskers do not disperse as well and rather agglomerate within the EVOH44 matrix compared to when cnw are incorporated as a suspension.

EVOH44 contains fewer alcohol groups than EVOH27 which makes this polymer less hydrophilic than EVOH27. Less compatibility between EVOH44 and cellulose nanowhiskers is, therefore, expected which explains the different trend seen in EVOH44/cnw(fd) compared to EVOH27/cnw(fd) nanocomposites. Another reason for the higher thermal stability of the EVOH44/cnw(sus) nanocomposites may be attributed to chemical modification of the EVOH molecules due to acid traces in the cellulose that are absent or less in the case of EVOH44/cnw(fd)[2].

5.4.4 EVOH27/chnw nanocomposites

Table 5.4 lists the degradation temperatures of the maximum peak intensities for EVOH27 containing different chnw loadings. There is a 16°C difference between the maximum thermal degradation temperature of EVOH27/8%chnw(fd) and EVOH27/8%chnw(sus). The EVOH27/chnw(sus) indicates a much higher onset in degradation temperature and there is a general increase in thermal stability observed with the addition of up to 8 wt% chnw. Chitin nanowhiskers are synthesized using HCl instead of sulphuric acid as in the case of cellulose nanowhiskers. The nanowhiskers therefore do not contain sulphate groups which may cause a decrease in onset degradation temperature as seen in nanocomposites containing cellulose. In this case it may be that the chnw in suspension dispersed better in the EVOH27 matrix compared to freeze dried chnw.

Table 5.4: Maximum peak degradation temperatures (°C) of EVOH27/chnw nanocomposites.

wt% chnw	EVOH27(fd)	EVOH27(sus)
0	414.97	414.97
1	434.48	436.92
3	437.61	440.04
5	424.76	441.78
8	443.22	459.14
10	429.27	427.88

Chitin nanowhiskers are more hydrophobic than cellulose nanowhiskers and stronger hydrogen bonding exists between molecules due to the acetamide groups. This behaviour could result in no definite trends when incorporated into a hydrophilic matrix. The EVOH27/10%chnw nanocomposites display a decrease in thermal stability compared to the rest which might be caused by too much agglomeration of the chitin nanowhiskers.

5.4.5 EVOH44/chnw nanocomposites

Table 5.5 displays information on the maximum peak degradation temperatures of EVOH44 nanocomposites containing different loadings of chnw. Figure 5.9 follows the table and displays the derivative weight loss curves of EVOH44/chnw nanocomposites therefore giving a visual representation of the onset in degradation temperatures.

Table 5.5: Maximum peak degradation temperatures (°C) of EVOH44/chnw(fd) nanocomposites.

wt% chnw	EVOH44 (fd)
0	422.33
1	433.09
3	441.78
5	448.38
8	456.02
10	448.03

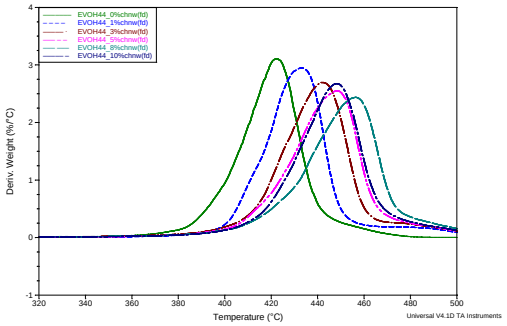

Figure 5.9: Derivative weight loss curves of EVOH44/chnw(fd).

The thermal stability increased with 34 °C with incorporation of 8 wt% chnw as a redispersed freeze dried product into the neat EVOH44 matrix (Table 5.5). Chnw have strong interactions with the EVOH44 chains therefore increasing the degradation temperature of EVOH44 by protecting the polymer chains from thermal degradation. It is interesting to observe that the EVOH44/10%chnw(fd) display a decrease in thermal stability which is similar to the results for the EVOH27/10%chnw(fd) (Table 5.4). The decreased thermal stability may in this case also be attributed to nanowhisker agglomeration beyond an optimum nanowhisker loading.

5.5 Differential scanning calorimetry (DSC) analysis

Table 5.6 and Table 5.7 display the DSC results of the second heating and cooling run for all the EVOH/cnw nanocomposites. The results are compared to that for neat EVOH samples in order to investigate the change in percentage crystallization and melting point of the nanocomposites after erasing the thermal history. The results displayed in the tables are corrected for the cnw content, assuming a representative sample with regards to the wt% cnw.

Table 5.6: Melting points (°C) of EVOH27/cnw and EVOH44/cnw nanocomposites.

wt% cnw	EVOH27(sus)	EVOH27(fd)	EVOH44(sus)	EVOH44(fd)
0	188	188	165	165
1	187	188	164	164
3	187	187	164	163
5	187	186	163	163
8	187	187	163	163
10	187	186	163	163

Table 5.7: Percentage crystallization of EVOH27/cnw and EVOH44/cnw nanocomposites.

wt% cnw	EVOH27(sus)	EVOH27(fd)	EVOH44(sus)	EVOH44(fd)
0	70	70	75	75
1	77	74	75	77
3	71	71	77	78
5	71	70	75	78
8	69	68	75	76
10	64	70	68	74

5.5.1 EVOH27/cnw nanocomposites

The results of the EVOH27/cnw nanocomposites showed an increase in percentage crystallization for the samples containing 1 wt% cnw (Table 5.7). Most of the EVOH27/cnw nanocomposites displayed crystallization results which did not vary significantly except for the EVOH/10%cnw(sus) nanocomposite. The melting point stayed relatively constant with a slight decrease as the nanowhisker loading increases (Table 5.6).

The EVOH27/cnw(sus) nanocomposites showed a clearer trend than EVOH27/cnw(fd) in terms of crystallization and melting behaviour. Redispersed freeze dried nanowhiskers still contained agglomerates and it may have been that cnw added in suspension therefore disperse better between the EVOH27 molecules. It seems that in both samples, the 1 wt% cnw act as nucleating agents thus increasing the percentage crystallization. The extremely small change in melting temperature may be attributed to the formation of smaller crystals compared to the case in neat EVOH27

5.5.2 EVOH44/cnw nanocomposites

Figure 5.10 displays initial DSC thermogram results of the EVOH44/cnw(fd) nanocomposites that were analysed using different programmed heating runs. The first analysis set was carried out to a maximum temperature of 180 °C and the second set was heated to 200 °C in the heating runs. Large differences in terms of the melting endotherms are observed. The thermogram with a heating profile up to 200 °C showed a much larger decrease in percentage crystallization as well as in melting point compared to the thermograms programmed with heating runs up to 180 °C. A white to yellow colour change of some samples were observed after the DSC runs (maximum temperature of 200°C). This observation together with the difference in thermal results for the two sets of EVOH44/cnw nanocomposites, indicate that degradation is taking place during exposure to high temperatures.

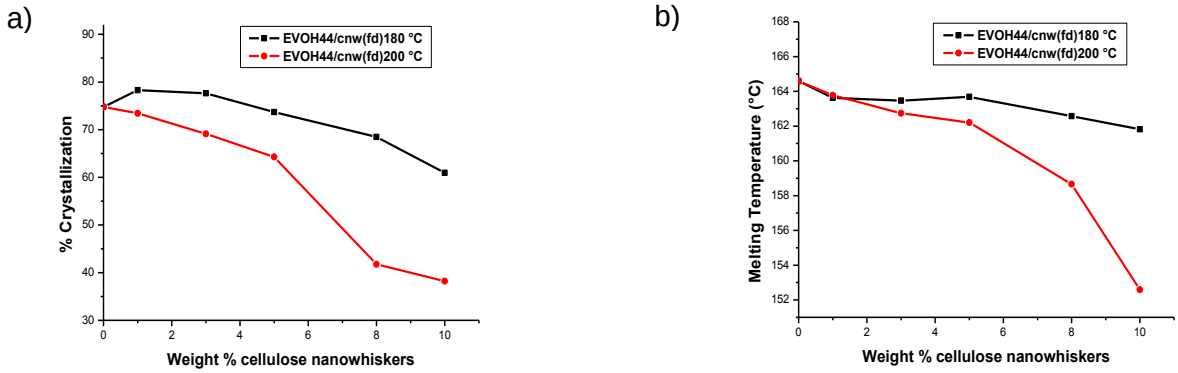

Figure 5.10: Comparisons of the (a) crystallization and (b) melting behaviour of EVOH44/cnw(fd) nanocomposites.

The degraded samples were recovered after the DSC runs were finished and added to a water/isopropanol blend as well as DMSO, DMF and other less polar solvents (xylene and TCB) in order to test the solubility. The degraded samples were found insoluble in all the tested solvents. This insolubility suggested possible chemical changes especially some degree of crosslinking. It was clear that incorporated nanowhiskers still contained a large amount of acid traces which was not washed out during dialysis. The acid is enough to catalyse oxidative degradation of the hydroxyl groups causing chemical changes such as formation of carbonyl groups, conjugated double bonds and possible crosslinking. Therefore, the severe decrease in percentage crystallization during the heating run of 200 °C is not entirely owing to the nanowhiskers preventing EVOH chains to crystallize, but most possibly due to the loss of alcohol groups which causes a decrease in the amount of hydrogen bonding between the chains. These findings point out that it is necessary to improve neutralization of nanowhiskers. One method investigated was the addition of a base as mentioned in previous studies[2,6-8] as well as in Section 3.3. All nanocomposite samples were then reprocessed with a new neutralized nanowhisker batch and further analysis was done on the new neutralized nanocomposite materials. Comparison of the DCS results for the

neutralized batch and the original batch of nanocomposites is illustrated in Figure 5.11. Less change in percentage crystallization and melting point behaviour is observed for EVOH44 nanocomposites containing neutralized cnw.

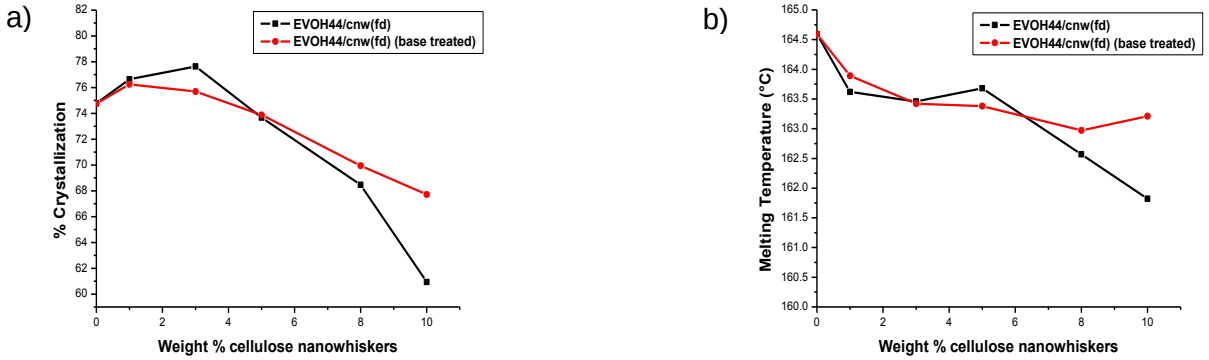

Figure 5.11: Comparisons of the (a) crystallization and (b) melting behaviour of EVOH44/cnw nanocomposites with and without base treatment of cnw.

Thermal behaviour of EVOH44/cnw(sus) and EVOH44/cnw(fd) nanocomposites were compared as seen Table 5.7 and Table 5.8 The small decrease in melting point behaviour is similar for EVOH44/cnw(sus) and EVOH44/cnw(fd). The increase in percentage crystallization was slightly larger for EVOH44/cnw(fd) than for EVOH44/cnw(sus). Addition of nanowhiskers as a suspension seems to result in better dispersion and perhaps causing greater hindering for crystallization of EVOH44.

5.5.3 EVOH/chnw nanocomposites

The results of the second heating run of EVOH27 and EVOH44 nanocomposites containing chnw were compared to that of neat EVOH samples in order to investigate the change in percentage crystallization and melting point of the nanocomposites after erasing the thermal history. These results are displayed in Table 5.8 and Table 5.9. The results displayed in the tables are corrected for the chnw content, assuming a representative sample with regards to the wt% chnw.

Table 5.8: Melting points (°C) of EVOH27/chnw and EVOH44/chnw nanocomposites.

wt% chnw	EVOH27(sus)	EVOH27(fd)	EVOH44(fd)
0	188	188	165
1	188	188	163
3	188	188	163
5	188	188	163
8	188	188	164
10	188	188	164

Table 5.9: Percentage crystallization of EVOH27/chnw and EVOH44/chnw nanocomposites.

wt% chnw	EVOH27(sus)	EVOH27(fd)	EVOH44(fd)
0	70	70	75
1	75	71	79
3	67	72	78
5	72	70	79
8	73	68	75
10	73	73	78

5.5.4 EVOH27/chnw nanocomposites

The incorporation of chnw cause no significant change in melting temperature (Table 5.8) but the change in crystallization (Table 5.9) is quite significant for the EVOH27/chnw(sus) and EVOH27/chnw(fd) nanocomposites. EVOH27/chnw(sus) showed an overall increase in percentage crystallization except for the sample containing 3 wt% chnw where an decrease in crystallization is observed. The results of the EVOH27/chnw(fd) do not show a clear trend but overall it seems that by increasing the nanowhisker load, the crystallization is somewhat increased or relatively constant. A possible explanation may be that the agglomeration of freeze dried incorporated cnw does not affect the crystallization process.

5.5.5 EVOH44/chnw nanocomposites

The incorporation of chitin nanowhiskers only as freeze dried product was investigated. The change in melting temperature (Table 5.8) was once again extremely small in comparison to the change in crystallization (Table 5.9). A slight decrease is observed with the first nanowhisker loading and as the wt% increases the melting temperature starts to increase again. An overall increase in crystallization is observed which does not change significantly as the cne load increases up to 10wt%. It seems that the chnw act as nucleating agents, creating smaller crystals with lower melting points.

5.6 Nuclear magnetic resonance (NMR) spectroscopy

In the present study, solid state NMR was carried out in order to characterize and compare the degradation products from EVOH44/sulphuric acid mixtures and EVOH44/cnw(fd) nanocomposites. EVOH44 were mixed with a drop of 64 wt% sulphuric acid and dried. The dried product was heated to 180 °C and kept isothermally for 6 minutes. The same was done for an EVOH44/10%cnw nanocomposite. The EVOH44 samples without exposure to heat as well as the heat exposed EVOH44 samples were analysed using solid state NMR.

Figure 5.12 illustrates the NMR spectra of all four different samples in order to compare the change in peak intensities as well as the formation of new peaks. The main ^{13}C chemical shifts for EVOH, cellulose and decomposition products are listed in Table 5.10[9-12].

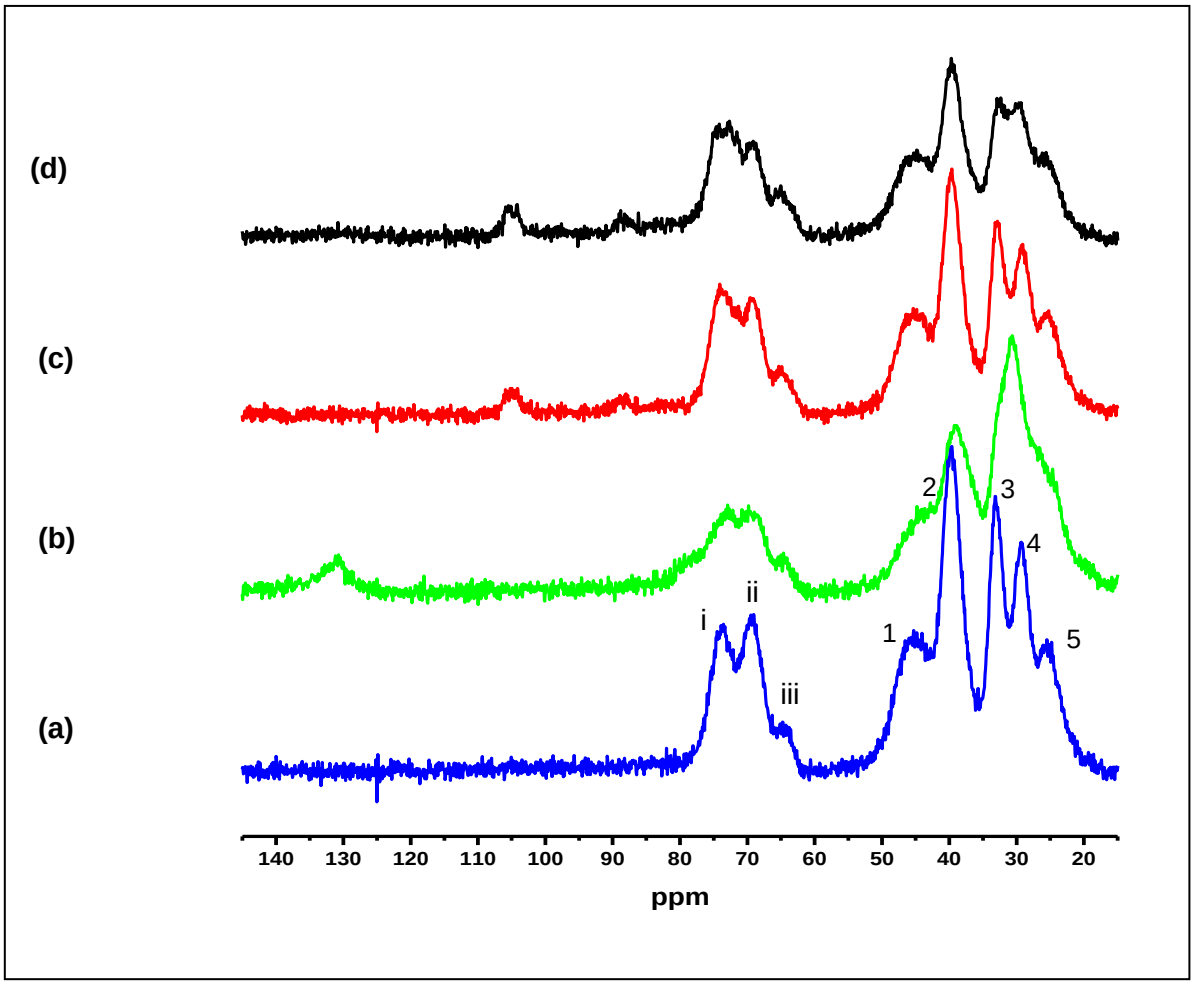

Figure 5.12: CP/MAS ^{13}C NMR spectra of (a) EVOH44/acid, (b) EVOH44/acid after heat exposure, (c) EVOH44/8%cnw and (d) EVOH44/8%cnw after heat exposure, all normalized to the same total intensity.

Table 5.10: ^{13}C Chemical shifts of EVOH and cellulose

δ(^{13}C)/ppm	**Assignment**
~10-50	Aliphatic (1)CH_2-CHOH-$\underline{C}H_2$-CHOH (2) CH_2-CHOH-$\underline{C}H_2$-CH_2 (3) CH_2-CH_2-$\underline{C}H_2$-CH_2-CH_2 (4) CHOH-CH_2-$\underline{C}H_2$-CH_2-CH_2 (5)CHOH-CH_2-$\underline{C}H_2$-CH_2-CHOH
~45	Methylene (1)
~120-140	Olefinic/aromatic
~60-77	Alcohol carbons i) two intra/inter H-bonds ii) one intra/inter H-bond iii) no H-bonding
 ~105 ~80-92 ~72-79 ~64	Cellulose C atoms C1 C4 C2, C3, C5 C6

The progressive loss of alcohol carbons (~70 ppm) with the gain in aromatic/olefinic carbons (~120-140 ppm) was clearly visible as the degradation temperature was increased[11]. The formation of aromatic and olefinic structures during the proposed Diels Alder reaction has also been reported in another study of acid catalysed decomposition of PVA[3].

In the present study, it is observed that for both EVOH44/acid and EVOH44/cnw the alcohol carbon peaks decrease in intensity relative to the aliphatic carbons and are much less defined after thermal treatment (Figure 5.12(b) and (d)) compared to the same samples before thermal treatment (Figure 5.12(a) and (c)). The appearance of a peak in the 130-140 ppm region is assigned to the formation of olefin/aromatic groups as seen in the proposed PVA pyrolysis mechanisms from previous articles[11]. The formation of decomposition products is not as severe as what was observed in the case of the PVA study, suggesting that the decomposition of EVOH is

catalysed by sulphuric acid but to a much lesser extent. The peaks in the region of 20-35 ppm from aliphatic carbons seem to become less defined and the formation of one broad peak is observed. A definite gain in aliphatic carbons due to chain scission and dehydration is observed, as well as a decrease in the methylene peak at ~45 ppm due to chemical conversions into decomposition products.

NMR spectra of EVOH44/cnw(fd) nanocomposites containing possible acid traces on the surface of the incorporated cnw were seen to give similar changes in the peak definitions and intensities of the alcohol and the aliphatic carbons after thermal treatment. The appearance of the cellulose C1 and C4 peak is seen at 105 ppm and 87 ppm respectively. The cellulose peaks did not seem to disappear or decrease in intensity after thermal treatment, which supports the idea that the degradation observed in the EVOH/cnw nanocomposites is not only due to the decomposition of the cnw. It has been proven in a previous article that the main decomposition products in the first step of a two-step decomposition process, were aldehydes and methylketones[4]. No carbonyl carbon peaks from aldehydes or ketones were observed downfield in the NMR spectra of either the EVOH44 acid mixture or the EVOH44/cnw(fd) nanocomposite after thermal treatment. The peaks may be extremely small and hidden in the noise of the solid state baseline. It has also been reported that polyethylene act as a thermal stabilizer in EVOH copolymers[5] and may therefore be a reason for not observing the same degradation products as in the case of the decomposition of neat PVA. The extent of the thermal treatment was also less severe compared to previous studies on PVA. The NMR results have thus shown that the EVOH44 containing cellulose nanowhiskers(fd) do not undergo extensive acid degradation

5.7 Dynamic mechanical analysis (DMA)

Preliminary data was recorded for some of the nanocomposites and the following results were obtained for EVOH44/cnw(sus) and EVOH44/cnw(fd) nanocomposites containing different amounts of cnw. The modulus and tan(δ) results are displayed in Figure 5.13 and Figure 5.14.

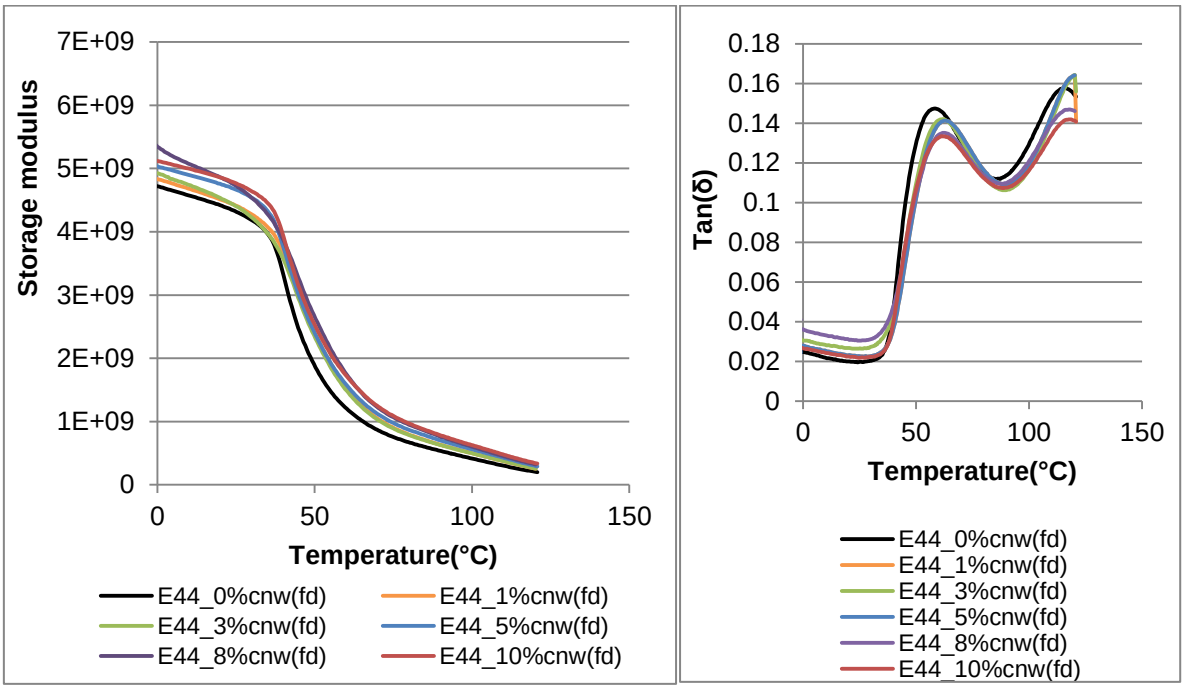

Figure 5.13: Storage modulus and tan(δ) graphs of EVOH44/cnw(fd) nanocomposites.

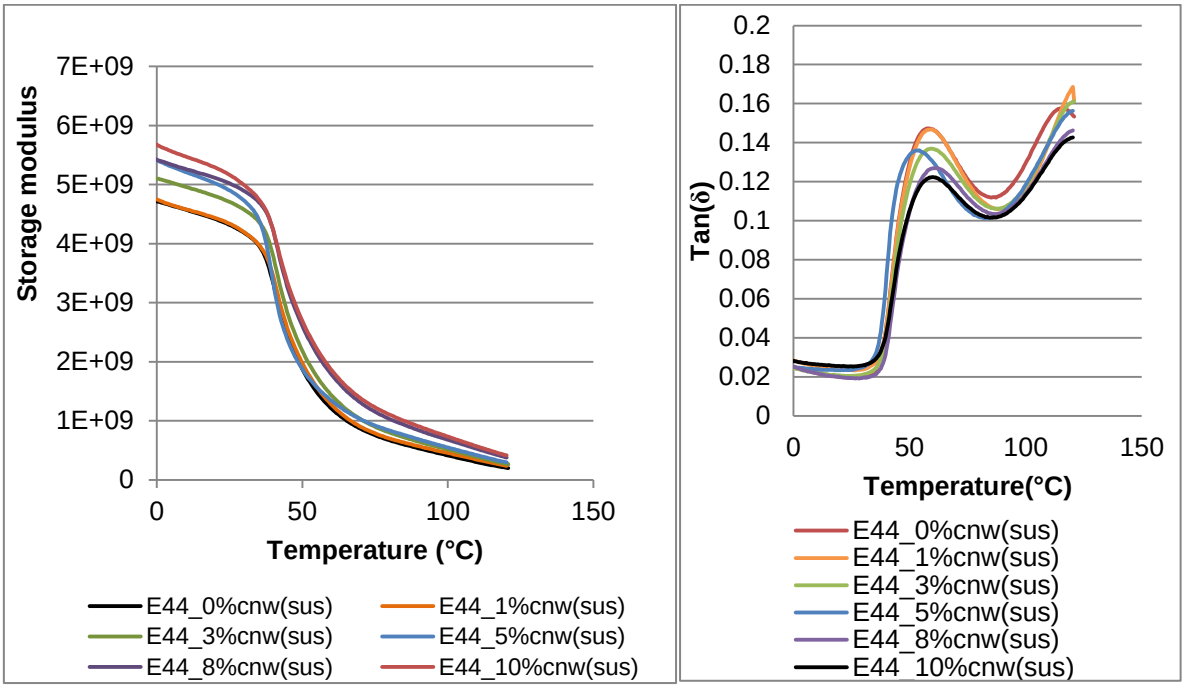

Figure 5.14: Storage modulus and tan(δ) graphs of EVOH44/cnw(sus) nanocomposites.

A definite increase in the storage modulus for both methods of incorporation is illustrated in Figure 5.13 and Figure 5.14. The EVOH44/cnw(sus) nanocomposites show a much larger and definite increase in storage modulus especially for the 10 wt% cellulose nanowhisker load which increases significantly. This suggests that the presence of cellulose nanowhiskers reduces the flexibility of the EVOH chains leading to an increase in storage modulus.

There are also clear differences in the intensities of the tan(δ) peaks. Table 5.11 displays the change in T_g as a function of cnw content. EVOH44/cnw(sus) nanocomposites display a much larger drop (50-60 °C) in peak intensity. The temperature shift in the different peaks is not as significant for the EVOH44/cnw(sus) nanocomposites compared to the EVOH44/cnw(fd) nanocomposites. It seems that the EVOH44/cnw(fd) samples display a larger increase in T_g compared with the neat polymer

Table 5.11: The change in Tg (°C) of EVOH44/cnw(sus) and EVOH44/cnw(fd) nanocomposites as a function of the cnw content.

wt% cnw	EVOH44(sus)	EVOH(fd)
0	52.30	52.30
1	52.31	58.02
3	53.54	56.9
5	46.98	56.37
8	53.58	56.68
10	52.76	54.86

5.8 Fluorescence microscopy analysis

EVOH44/cnw(fd) and EVOH27/cnw(fd) nanocomposites were subjected to fluorescent spectroscopy in order to investigate whether this technique may be useful in studying the dispersion of nanowhiskers within the matrix polymer.

Figure 5.15(b) shows an image that was obtained for the EVOH44/10%cnw(fd) nanocomposite. This image is a good representation of the EVOH44/cnw nanocomposites containing high nanofiller loadings. The intense fluorescence areas which measures dimensions in the range 2-6 µm indicates that the nanowhiskers are agglomerated. These measurements are much larger than single nanowhiskers. The fluorescing aggregates are, however, still seen to be evenly spread through the sample.

Figure 5.15(a) shows an image of EVOH27/8%cnw which seems, according to measurements, to contain much smaller aggregates of nanowhiskers. The fluorescing bundles were measured to be in the range of 0.45-6 µm in length. The appearance of these agglomerates was confirmed by similar observation when the cnw were labelled with Rhodamine B. (Figure 5.16).

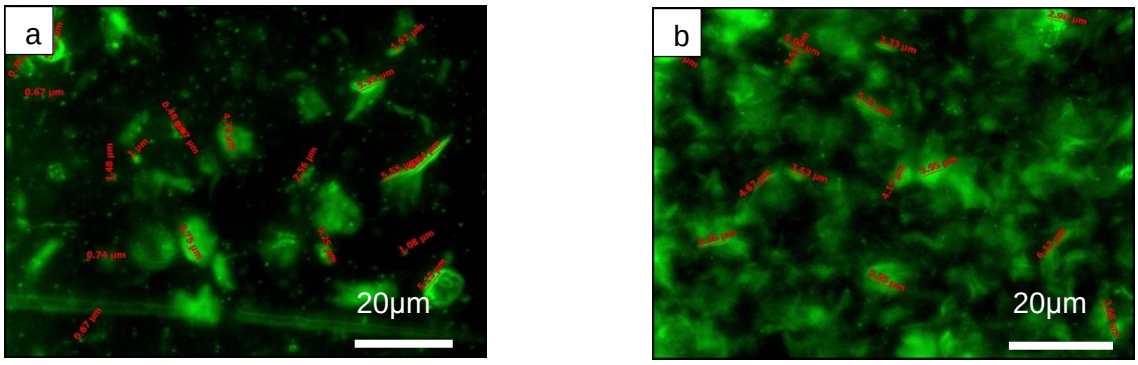

Figure 5.15: Fluorescent images of (a) EVOH27/8%cnw(fd) and (b) EVOH44/10%cnw(fd) of which the cnw are labelled with FITC.

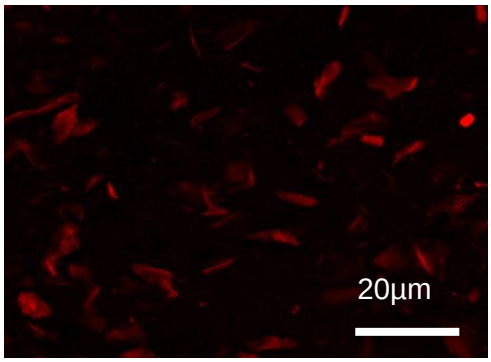

Figure 5.16: Fluorescent image of EVOH27 containing 8wt% cnw labelled with Rhodamine B.

5.9 Conclusions

TEM and FTIR analysis results of the produced EVOH/cnw and EVOH/chnw nanocomposites show successful incorporation of cellulose and chitin nanowhiskers. TEM images indicate good dispersion of nanowhiskers but agglomeration is definitely present at higher nanowhisker loadings.

Agglomeration of nanowhiskers is extremely difficult to overcome. The small size and strong hydrogen bonding between the nanowhisker molecules cause challenges for proper dispersion. A general trend is, however, seen with the addition of nanowhiskers: an increase in thermal stability is observed as well as an increase in percentage crystallisation of EVOH up to certain nanowhisker loadings. One suggestion is that the nanowhiskers disperse between the EVOH chains in such a way acting as nucleating agents until a certain nanowhisker load where the nanowhiskers start hindering crystallization of molecules or even changing the formation of crystallization. The chitin nanowhiskers seem to behave more unpredictable than the cellulose nanowhiskers due to their more hydrophobic character as well as stronger hydrogen bonding between chitin molecules than in the case of cellulose.

Thermal analysis results of the nanocomposites show that the increase in thermal stability at high temperatures could be partly attributed to the presence of acid, causing chemical modifications such as conjugated double bonds and crosslinking. NMR results have indicated that

the amount of acid traces present cannot have such a significant effect on the temperature increase and therefore the nanowhiskers must also contribute to the enhanced thermal stability of the nanocomposite samples.

DMA analyses reveal an increase in the storage modulus of the EVOH44/cnw nanocomposite samples which indicates that the cellulose nanowhiskers are increasing the stiffness of the matrix by decreasing the mobility of EVOH polymer chains. The mechanical analysis results also indicate greater improvement in the storage modulus for the EVOH44/cnw(sus) nanocomposites which may be explained in terms of good dispersion of the nanowhiskers within the matrix.

Agglomeration of the nanowhiskers was observed during fluorescent microscopy. The agglomerates, however, seem to be evenly dispersed throughout the nanocomposite sample. From the images obtained it seems that the cellulose nanowhiskers inside the EVOH27 form much smaller agglomerates than within the EVOH44 matrix.

5.10 References

(1) Rinaudo M. Chitin and chitosan: Properties and applications. *Progress in Polymer Science* 2006;31(7):**603-632**.

(2) Uddin AJ, Araki J, Gotoh Y. Characterization of the poly(vinyl alcohol)/cellulose whisker gel spun fibers. *Composites Part A: Applied Science and Manufacturing* 2011;42(7):**741-747**.

(3) Alexy P, Káchová D, Kršiak M, Bakoš D, Šimková B. Poly(vinyl alcohol) stabilisation in thermoplastic processing. *Polymer Degradation and Stability* 2002;78(3):**413-421**.

(4) Tsuchiya Y, Sumi K. Thermal decomposition products of poly(vinyl alcohol). *Journal of Polymer Science* Part *A-1: Polymer Chemistry* 1969;7(11):**3151-3158**.

(5) Alvarez VA, Ruseckaite RA, Vázquez A. Kinetic analysis of thermal degradation in poly(ethylene vinyl alcohol) copolymers. *Journal of Applied Polymer Science* 2003;90(11):**3157-3163**.

(6) Martínez-Sanz M, Olsson RT, Lopez-Rubio A, Lagaron JM. Development of bacterial cellulose nanowhiskers reinforced EVOH composites by electrospinning. *Journal of Applied Polymer Science* 2012;124(2):**1398-1408**.

(7) Jiang L, Morelius E, Zhang J, Wolcott M, Holbery J. Study of the poly(3-hydroxybutyrate-co-3-hydroxyvalerate)/cellulose nanowhisker composites prepared by solution casting and melt processing. J*ournal of Composite Materials* 2008;42(24):**2629-2645**.

(8) Bahar E, Ucar N, Onen A, Wang Y, Oksüz M, Ayaz O, et al. Thermal and mechanical properties of polypropylene nanocomposite materials reinforced with cellulose nano whiskers. *Journal of Applied Polymer Science* 2012;125(4):**2882-2889**.

(9) Kanekiyo M, Kobayashi M, Ando I, Kurosu H, Amiya S. A structural study of (ethylene-vinyl alcohol) copolymers by high- resolution solid-state 13C NMR. *Polymer* 2000;41(7):**2391-2404.**

(10) Masson JF, Manley RS. Solid-state NMR of some cellulose/synthetic polymer blends. *Macromolecules* 1992;25(2):**589-592**.

(11) Gilman JW, VanderHart DL, Takashi K. Thermal Decomposition Chemistry of Poly(vinyl alcohol). *American Chemical Society* 1995;**161-185.**

(12) Bhattacharya D, Germinario LT, Winter WT. Isolation, preparation and characterization of cellulose microfibers obtained from bagasse. *Carbohydrate Polymers* 2008;73(3):**371-377**.

Chapter 6: Results and Discussion of Electrospun EVOH Nanocomposites

6.1 Introduction

Electrospinning of EVOH27 and EVOH44 with different cellulose and chitin nanowhisker loadings was done in order to produce electrospun nanocomposite fibers as discussed in Section 3.3.2. These nanocomposites were characterised and analysed with various techniques in order to get a better understanding of the properties of the nanocomposites. Cellulose and chitin nanowhiskers will be referred to as cnw and chnw respectively. The numbers 44 and 27 represents the ethylene mole% content present in the EVOH copolymer. The EVOH copolymer containing freeze dried nanowhiskers that were incorporated by way of electrospinning will further on be referred to as EVOH/cnw(fd) ((or EVOH/chnw(fd)) fibers and the EVOH copolymer containing nanowhiskers that was left in suspension (also processed by way of electrospinning) will be referred to as EVOH/cnw(sus) ((or EVOH/chnw(sus)) nanocomposites fibers. The purpose of utilizing electrospinning as an experimental technique to incorporate nanowhiskers into an EVOH matrix was to gain a better dispersion of the nanowhiskers inside EVOH. A uniform dispersion of the nanowhiskers within the EVOH matrix was important with the aim of introduction of these well dispersed nanowhiskers via EVOH into highly hydrophobic LDPE. SEM analysis was used to study the morphology of the electrospun nanocomposites. TEM and FE-SEM characterization techniques were used to prove the incorporation of the nanowhiskers within the EVOH matrix and investigate the dispersion thereof. Thermal analysis data were obtained from TGA and DSC analysis in order to investigate the change in thermal stability and crystallization behaviour respectively.

6.2 Scanning electron microscopy (SEM) analysis

SEM images of all the electrospun EVOH nanocomposite fibers were obtained. It was possible to incorporate all the different loadings (1%, 3%, 5%, 8%, 10%) of cnw as well as chnw and successfully retain decent fiber morphology. The idea was not to optimize the fiber morphology by detailed variable investigation but rather to produce fiber diameters as close as possible to the nanometer range. Smaller diameter fibers result in materials with increased surface areas. The nanocomposites were all spun at the same conditions in order to produce electrospun

nanocomposites with decent fiber morphology. Most electrospun nanocomposite fibers produced diameters in the range of 0.2- 0.6µm depending on the EVOH solution concentration.

SEM images of some of the EVOH nanocomposite fibers are shown in Figure 6.1, 6.2 and 6.3. These EVOH nanocomposite fibers were all electrospun from 6 wt% EVOH solutions.

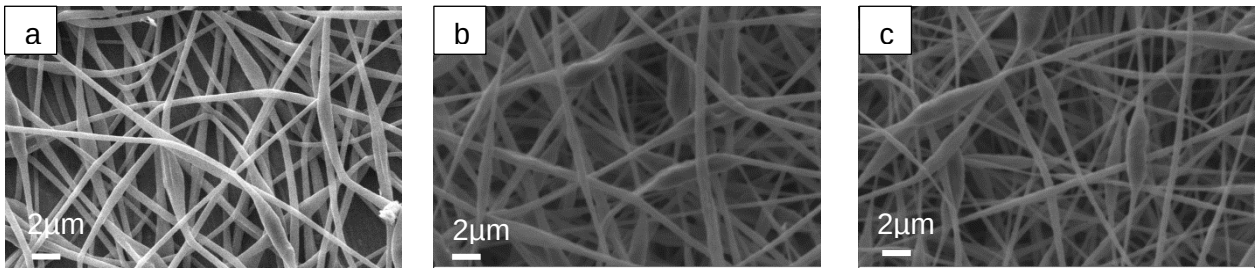

Figure 6.1: SEM images of electrospun EVOH44/cnw fibers containing (a) no cnw, (b) 3 wt% cnw(sus) and (c) 10 wt% cnw(fd).

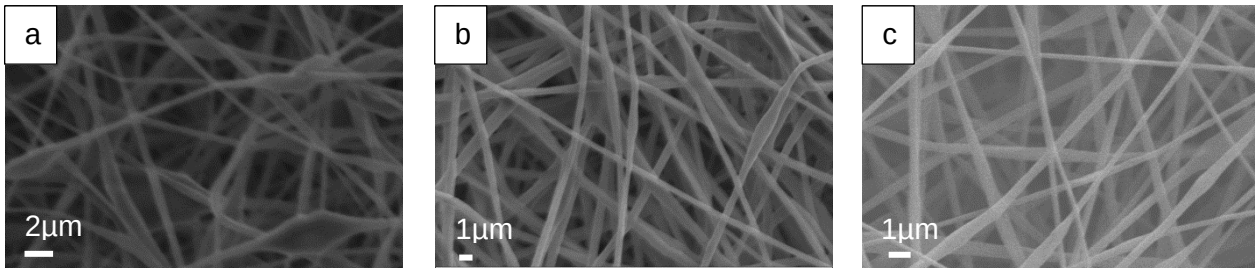

Figure 6.2: SEM images of electrospun EVOH27/cnw fibers containing (a) no nw, (b)10 wt% cnw(sus) and (c) 10 wt% cnw(fd).

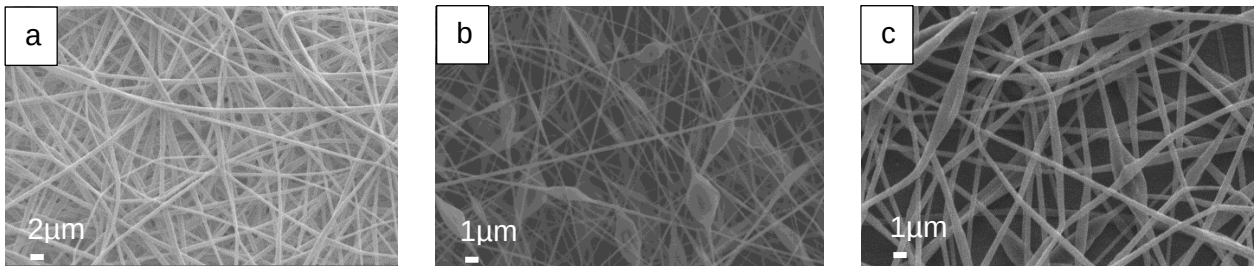

Figure 6.3: SEM images of electrospun (a) EVOH44/5%chnw(fd) fibers, (b) EVOH27/10%chnw(fd) fibers and (c) EVOH27/8%chnw(sus) fibers.

The influence of cnw content on the specifically EVOH27 fiber diameter was investigated by keeping the temperature constant at 23.5-24 °C and the percentage humidity between 48 and 54. The EVOH solution concentration was 5.5 wt% and the rest of the process parameters were all

kept constant. The average fiber diameters as a function of EVOH solution concentration are displayed in Figure 6.4. The average fiber diameter increases with an increase in the nanowhisker content. The beading also tends to decrease with an increase in the fiber diameter.

The increase in fiber diameter is more prominent for EVOH27/cnw(fd) nanocomposite fibers in comparison with EVOH27/cnw(sus) nanocomposite fibers. The reason for the changes in fiber diameter may be assigned to viscosity and conductivity properties of the nanocomposites. An increase in the conductivity usually results in smaller diameters whereas an increase in viscosity causes larger fiber diameters[1]. Figure 6.4 illustrates the EVOH27/cnw fiber diameters as a function of cnw loading

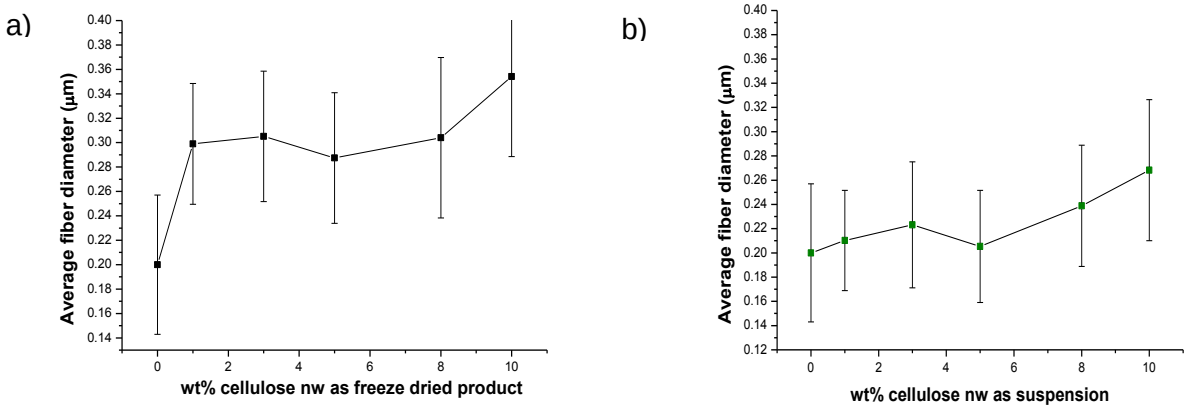

Figure 6.4: The average fiber diameter and standard deviations of (a) EVOH27/cnw(fd) and (b) EVOH27/cnw(sus) as a function of cnw content.

Table 6.1 displays conductivity and viscometry results which were only carried out on some EVOH27/cnw solutions. According to what is observed from Figure 6.4, it seems as if the conductivity effect is over powering the viscosity effect in the EVOH27/cnw(sus) fiber samples whereas the same effect but to a lesser extent is observed for the EVOH27/cnw(fd) fiber samples. The results from the viscometry analysis show the opposite effect from what is predicted. The EVOH27/cnw(sus) fibers were found to display a higher viscosity than the EVOH27/cnw(fd) fibers, resulting in smaller fiber diameters. This finding agrees with a previous investigation where bacterial cellulose was added to EVOH[2]. They reported a decrease in the average fiber diameter with an increase in the viscosity. The conductivity for neat EVOH27 is low according to the conductivity results presented in Table 6.1 and the addition of cellulose nanowhiskers does not seem to increase the conductivity significantly. The presence of negative ester sulphate groups on cnw in suspension is probably slightly more than what is found on the freeze dried cnw. The presence of negative ions should increase the conductivity of the solution as shown in previous

reports[2-4]. The small increase in conductivity indicated by Table 6.1 is ascribed to the effective neutralization of cellulose nanowhiskers.

Table 6.1 : Conductivity and viscosity measurements of EVOH27/cnw nanocomposites fibers**.**

Nanocomposite fiber	Conductivity (µS/m)	Viscosity(cP)
EVOH27 neat	6.0	39.5
EVOH27/1%cnw(sus)	6.8	42.5
EVOH27/10%cnw(sus)	8.6	57.5
EVOH27/1%cnw(fd)	6.7	40.5
EVOH27/10%cnw(fd)	7.6	43.0

.

The conductivity increase upon addition of 10 wt% cnw is however more in the case of the EVOH27/cnw(sus) fibers than in the case of the EVOH27/cnw(fd) fibers. The greater increase in conductivity as well as viscosity in the case of the EVOH27/cnw(sus) fibers therefore contributes to the smaller fiber diameters when compared to the EVOH27/cnw(fd) fibers.

EVOH27/cnw fibers furthermore produced smaller fiber diameters than in the case of the EVOH44/cnw fibers. The smaller fiber diameters for the EVOH27/cnw fibers may be attributed to the different ethylene mole % within the copolymers. Secondly, the EVOH27 was observed to stay in solution much longer than EVOH44 at room temperature which could also have an indirect impact on the fiber diameter during electronspinning.

6.3 Field emission scanning electron microscopy (FESEM) analysis

Field Emission SEM was investigated as an alternative for observing the nanowhiskers inside the fibers and perhaps to learn something about the dispersion of the different loadings. Several different approaches were explored in order to achieve this objective but due to challenging fiber mats and small diameters, this method was not as successful as TEM. The fibers were submerged in liquid nitrogen and broken in order to study the cross sections. Structures which agree with the nanowhisker dimensions (less than 10 nm) were however measured in some images of low filler nanocomposites fibers. Figure 6.5 presents FESEM images of EVOH27/1%cnw and EVOH/8%cnw nanocomposites fibers. Nanofiber diameters of more than 1 µm were observed which made it easier to observe possible nanowhiskers within the electrospun fibers.

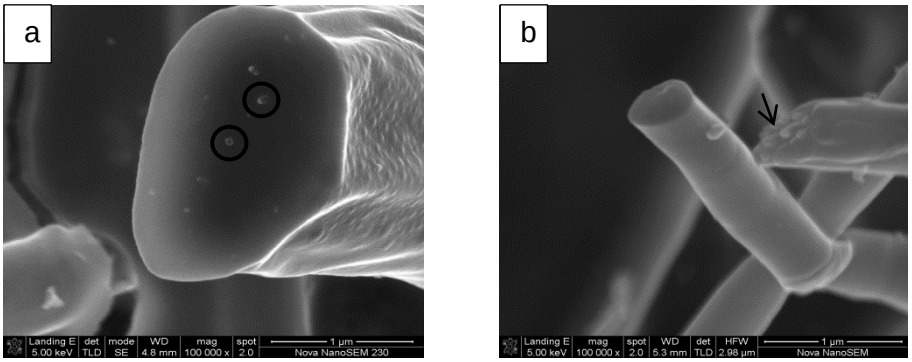

Figure 6.5: FESEM images of (a) EVOH27/1%cnw and (b) EVOH27/8%cnw nanocomposite fibers.

6.4 Transmission electron microscopy (TEM) analysis

Individual electrospun EVOH/cnw nanocomposite fibers were initially studied without embedding them in resin and without ultra microtoming and staining them. It was extremely difficult to observe nanowhiskers within the EVOH matrix and especially difficult to get an idea of degree of nanowhisker dispersion within the matrix. The small size of the nanowhiskers and lack of contrast between the nanowhiskers and the EVOH matrix made this characterization method time consuming and ineffective. Figure 6.6 illustrates EVOH27/cnw fibers containing 0% cnw, 3% cnw and 8% cnw respectively. The individual nanowhiskers are observed Figure 6.6(b) and (c) and are orientated along the direction of the fiber length as well as forming agglomerated structures.

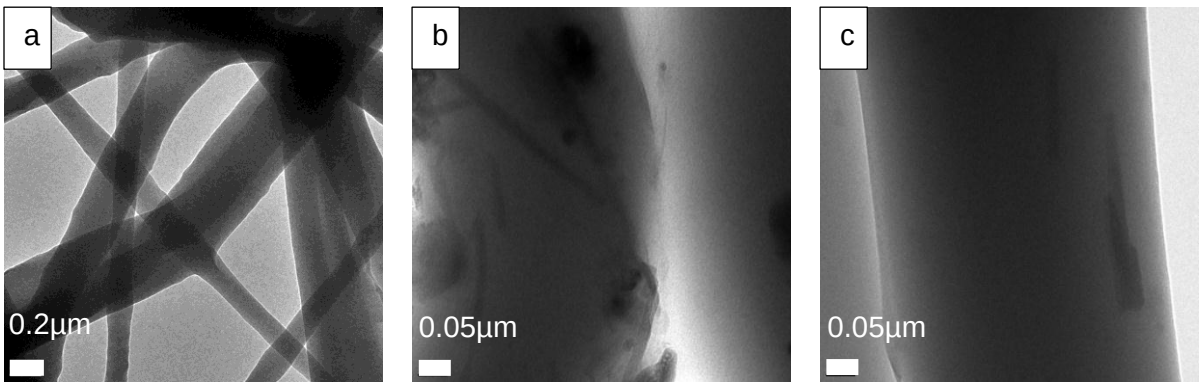

Figure 6.6: TEM images of individual EVOH27/cnw nanocomposite fibers containing (a) 0% cnw, (b) 8% cnw and (c) 3% cnw.

The TEM charactization method was improved by embedding the electrospun fibers in resin, followed by ultra microtoming the fibers and lastly staining the fibers with uranyl acetate. The

improved preparation of the nanofiber samples provided much better results in terms of resolution and contrast and the dispersion of the nanowhiskers within the EVOH fiber matrix was also easier to investigate through this method.

TEM analysis of electrosopun nanocomposite fibers is, howeve,r still much more challenging when compared to analysis of nanocomposites in the form of powders or films. Sample preparation is extremely important when analysing nanocomposite fibers by way of TEM analysis. The area of the fiber which is observed during TEM analysis is much smaller when compared to what is seen when looking at microtomed powder samples. Staining also seems to be less effective in the case of nanocomposite fiber samples when compared to the staining of powder samples. Figures 6.8, 6.9 and 6.10 present TEM images of EVOH27/8%cnw, EVOH44/8%cnw and EVOH44/3%cnw nanocomposite fibers. Figure 6.7 and Figure 6.8 display images of the EVOH nanocomposite fibers sectioned in length and clearly show that nanowhiskers incorporated into the EVOH fibers are well dispersed and well orientated in the direction of the fiber axis. Drawing of the nanocomposite fibers during the electrospinning process seems to align the incorporated nanowhiskers in the same direction as the electrostatic pull.

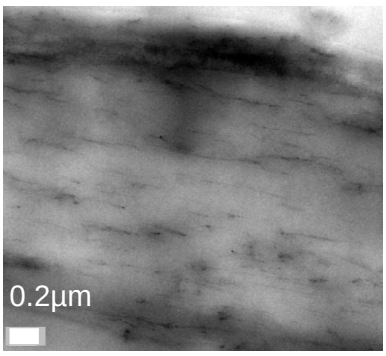

Figure 6.7: TEM image of a microtomed sample of EVOH27/8%cnw nanocomposite fibers.

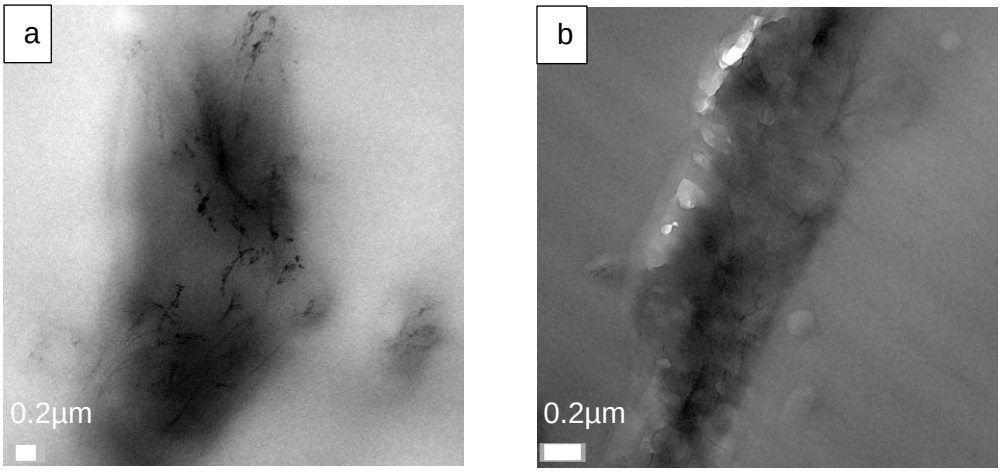

Figure 6.8: TEM images of microtomed samples of (a) EVOH44/8%cnw fibers (b) EVOH44/3%cnw.

Figure 6.9 shows an example of the cross section of electrospun nanocomposite fibers containing 8 wt% cnw imaged at different magnifications. The nanowhisker orientation as well as nanowhisker dispersion are less clearly visible unless the cross section have dimensions much larger than the average fiber diameter.

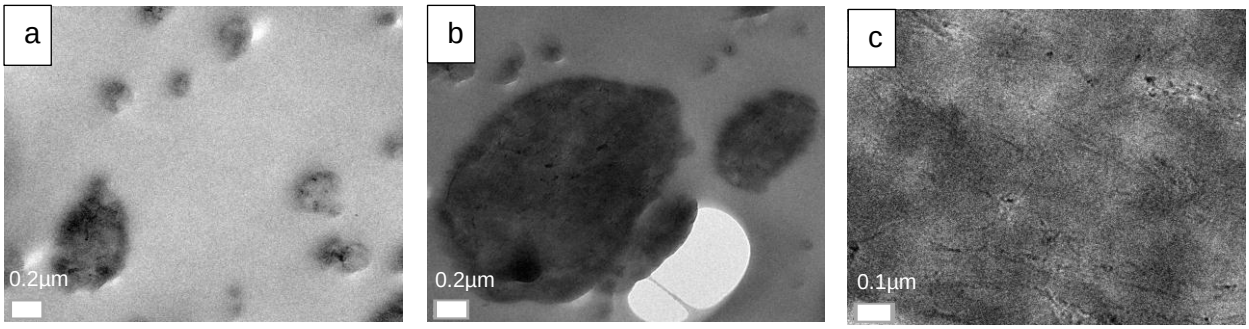

Figure 6.9: TEM images of EVOH27/cnw nanocomposite fibers taken at a (a) low magnification, (b) high magnification and (c) higher magnification in order to study dispersion of the nanowhiskers.

6.4 Fourier transform infrared (FTIR) spectroscopy

Figure 6.10 presents the transmission FTIR results of EVOH27/cnw(sus) fibers and indicates the appearance of characteristic cellulose peaks at 1031 cm^{-1} and 1060cm^{-1}, as the cnw load increases from 0 wt% to 10 wt%. Similar results were observed for both EVOH27 and EVOH44 nanocomposite fibers containing freeze dried cnw and cnw kept in suspension.

As discussed previously in Section 5.2, the overlapping of IR bands of EVOH and cellulose makes it difficult to isolate and quantify individual peaks that contribute exclusively to the cellulose nanowhiskers within the nanocomposites.

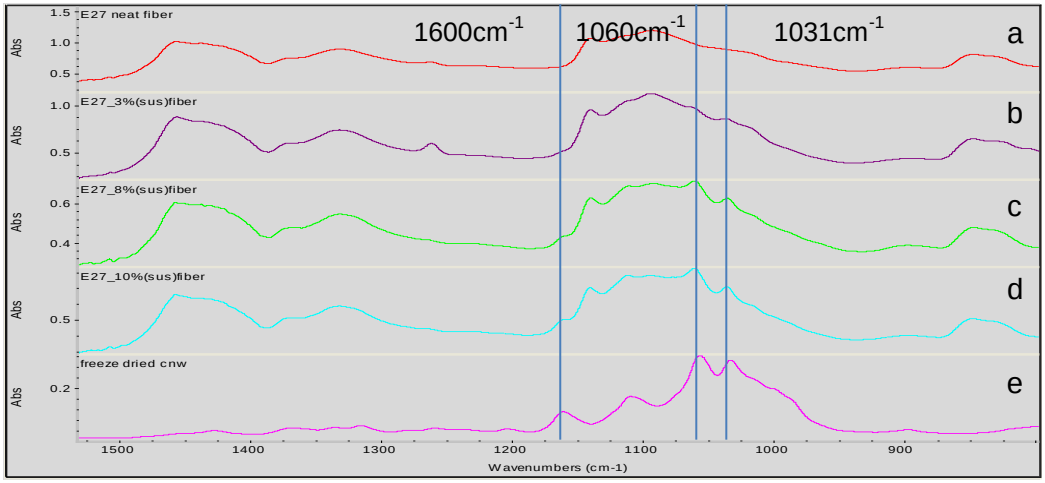

Figure 6.10: FTIR spectra of EVOH27/cnw(sus) fibers containing (a) 0 % cnw, (b) 3 % cnw, (c) 8 % cnw, (d) 10 %cnw and (e) isolated cnw.

Figure 6.12 illustrates the FTIR spectra of EVOH44/chnw nanocomposite fibers. Chitin nanowhiskers were much easier to identify within the EVOH/chnw fibers by way of FTIR characterization due to the prominent amide moiety from the two Amide I bands at 1660 cm^{-1} and 1619 cm^{-1} and the Amide II band[5] at 1556 cm^{-1}. The Amide I and II bands were clearly visible in all the EVOH nanocomposite fiber samples with different chitin nanowhisker loadings as seen in Figure 6.11.

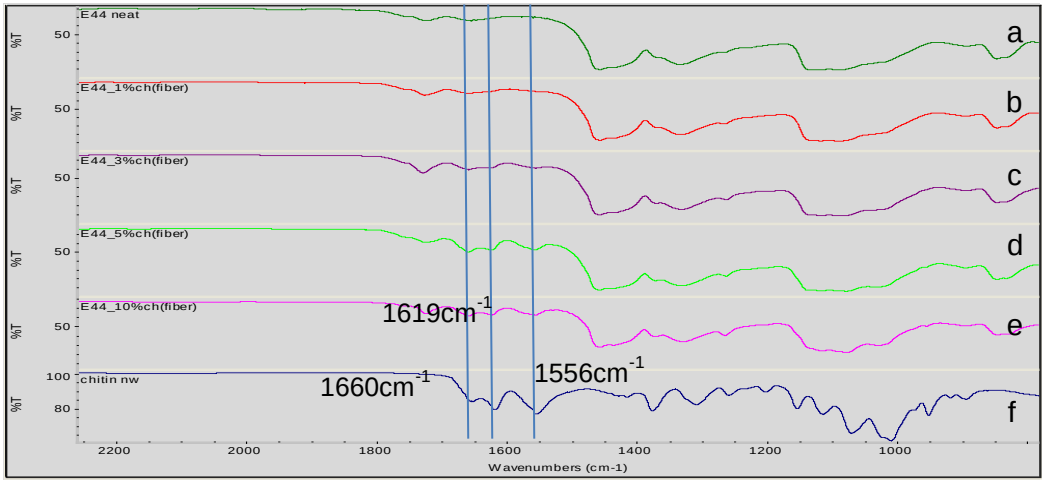

Figure 6.11: FTIR spectra of EVOH27/chnw(fd) fibers containing (a)0 % chnw, (b)1 % chnw, (c) 3 % chnw, (d) 5 %chnw, (e) 10 wt% chnw and (f) isolated chnw.

6.5 Thermogravimetric analysis (TGA)

The thermal stability of EVOH nanocomposite fibers were investigated due to the fact that thermal stability is an important parameter during any further processing of these materials for other applications.

According to the results discussed in Section 5.3.1 the presence of acid traces on the surface of the nanowhiskers inside an EVOH matrix clearly made a contribution towards the increase in degradation temperature for solution cast samples and therefore similar studies were done on the electrospun nanocomposites fibers. Figure 6.12 displays the TGA results of EVOH27 nanocomposite fibers containing 1% cnw and 3% cnw without NaOH treatment (untreated). These curves were compared with that for neat EVOH27 fibers as well as EVOH27/cnw fibers containing 5% and 8% cnw treated with NaOH (base treated). The addition of NaOH was done in an attempt to neutralize any remaining acid in the isolated cnw. The appearance of a small peak in the lower temperature region (250-320 °C) for the EVOH27/cnw nanocomposite fibers (untreated cnw) is visible as well as a large increase in thermal degradation for the main peak (450-510 °C) when compared to the thermal stability of neat EVOH27 fibers.

The EVOH27/cnw nanocomposite fibers (base treated cnw) showed no signs of a peak appearing in the lower temperature region region and the main peaks have a maximum peak degradation temperature of 335-440 °C. A larger increase was therefore seen for the EVOH27/cnw nanocomposite fibers (untreated cnw) than what was observed for the EVOH27/cnw nanocomposite fibers (base treated cnw).

The attempt in neutralizing the nanowhiskers before incorporation into the EVOH matrix during electrospinning therefore seems to lower the thermal stability of the higher temperature degradation peak and cnw seem to be much better protected by the EVOH molecules in the matrix. The appearance of the peak in the lower region may be ascribed to dehydration of alcohol groups within EVOH and depolymerization of cellulose. The degradation processes are catalyzed by sulphuric acid present in the cellulose nanowhiskers[6,7]. This observation can be related to DSC results of EVOH/cnw nanocomposites containing cnw that was not exposed to treatment with a base as already discussed in Section 5.4.2.

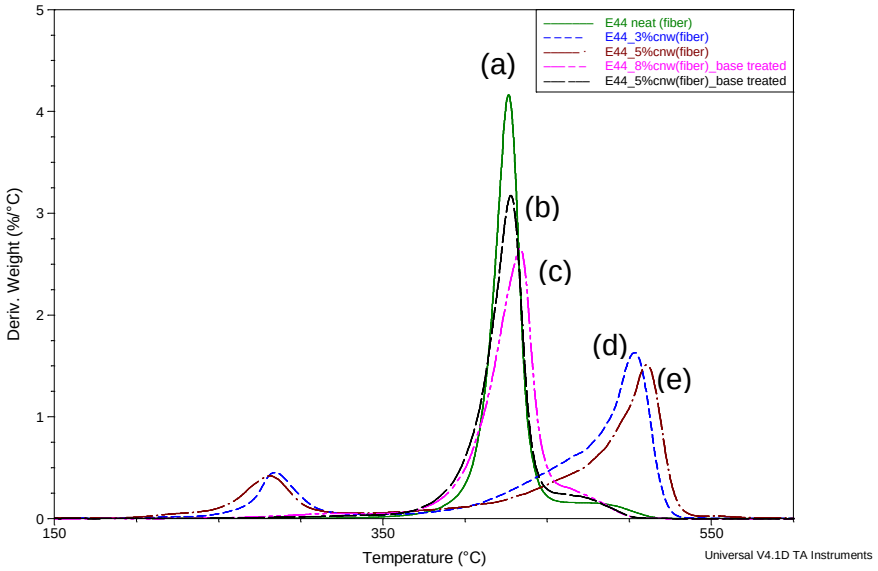

Figure 6.12: Derivative weight loss curves of (a) neat EVOH27 fibers, EVOH27/cnw fibers containing (b) 5% and (c) 8 % neutralized cnw and EVOH27/cnw containing (d) 3% and (e) 5% cnw which were not neutralized with NaOH.

6.5.1 EVOH27/cnw nanocomposite fibers

Table 6.2 displays information about the maximum peak degradation temperatures of EVOH27/cnw nanocomposite fibers containing different loadings of cnw. The table is followed by Figure 6.13 (a) and (b) which show the derivative TGA curves and therefore providing a visual representation of the onset in degradation temperatures of the samples.

Table 6.2: Maximum peak degradation temperatures (°C) of EVOH27/cnw nanocomposite fibers.

wt% cnw	EVOH27(fd)	EVOH27(sus)
0	417.10	417.10
1	429.95	431.04
3	426.68	432.12
5	428.86	435.39
8	423.41	438.66
10	422.74	439.58

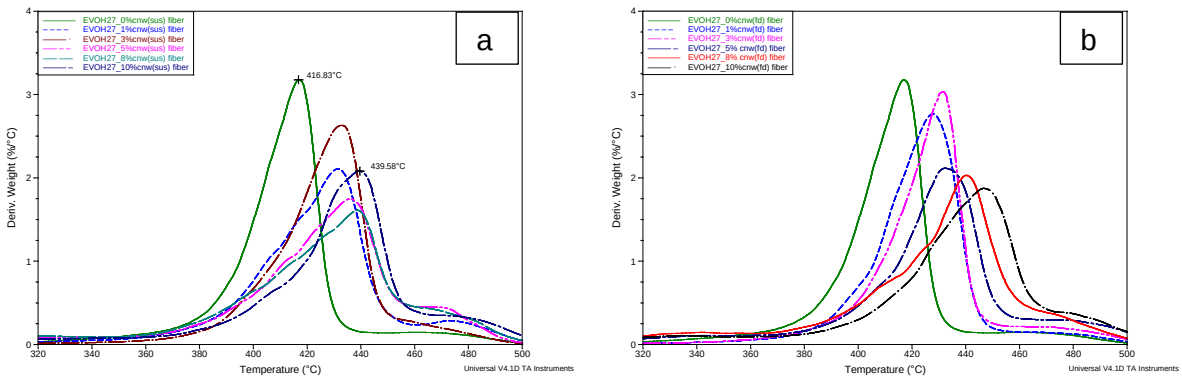

Figure 6.13: Derivative weight loss curves of (a) EVOH27/cnw(sus) nanocomposite fibers and (b) EVOH/cnw(fd) nanocomposite fibers.

The maximum peak degradation temperature is somewhat higher for EVOH27/cnw(sus) fibers than for EVOH/cnw(fd) fibers and displays an increase of 22 °C after addition of 10 wt% cnw. Higher onset in degradation temperatures are observed for all the EVOH27/cnw nanocomposite fibers when compared to that for neat EVOH27 indicating an increase in thermal stability with the addition of cnw. The lower thermal stability of the EVOH27/cnw(fd) nanocomposite fibers when compared to the thermal stability of the EVOH27/cnw(sus) nanocomposite fibers may be attributed to ester sulphate groups being destroyed during the freeze drying process and therefore resulting in less chemical modification of EVOH and that leads to earlier degradation. Agglomeration of cnw during redispersion causing poorer dispersion within the matrix, may also contribute to the lower thermal stability.

6.5.2 EVOH44/cnw nanocomposites fibers

Table 6.3 displays information about the maximum peak degradation temperatures of EVOH44/cnw nanocomposite fibers containing different loadings of cnw. The table is followed by Figure 6.14 (a) and (b) which illustrate the derivative weight loss curves and therefore providing a visual representation of the onset in degradation temperatures.

Table 6.3: Maximum peak degradation temperatures (°C) of EVOH44/cnw nanocomposite fibers.

wt% cnw	EVOH44(fd)	EVOH44(sus)
0	426.58	426.58
1	427.63	433.21
3	431.17	432.94
5	432.81	435.39
8	440.16	433.21
10	446.8	--------

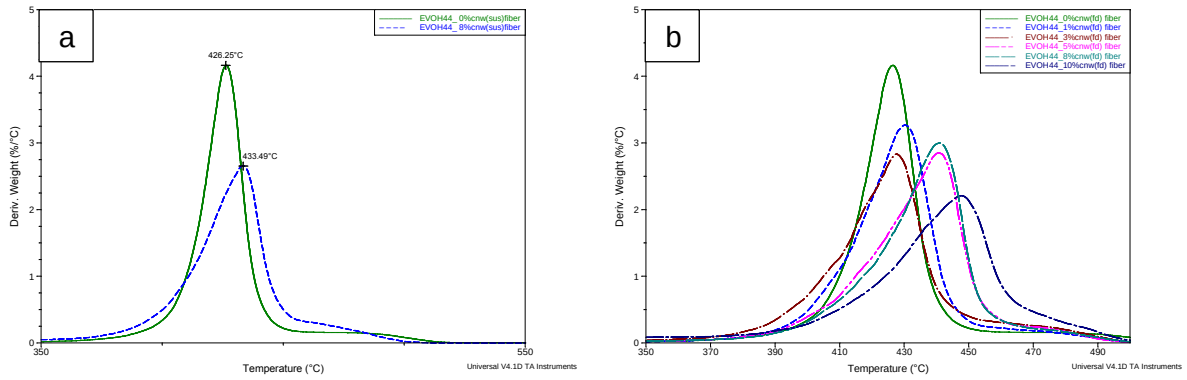

Figure 6.14: Derivative weight loss curves of (a) EVOH44/cnw(fd) nanocomposite fibers and (b) EVOH44/cnw(fd) nanocomposites fibers.

Figure 6.15 shows that only EVOH27/cnw(fd) nanocomposite fibers containing 8 and 10 wt% cnw have degradation onset temperatures higher than that of neat EVOH27. The maximum peak degradation temperature is significantly higher specifically for the EVOH44/cnw(fd) nanocomposite fibers though, which indicates an increase in the thermal stability at higher temperatures. The lower degradation onset temperature for most of the EVOH44/cnw fibers may be due to the presence of sulphate groups present in the nanocomposites which are decreasing the thermal stability. Cellulose nanowhisker agglomerates starting degradation at lower temperatures than the onset of EVOH44 degradation may be another explanation to the low onset in degradation temperature observed. There was not as large difference in thermal stability between EVOH44/cnw(sus) and EVOH44/cnw(fd) fibers as in the case of the EVOH27/cnw fibers.

6.5.3 EVOH27/chnw nanocomposite fibers

Table 6.4 displays information about the maximum peak degradation temperatures of EVOH44/chnw nanocomposite fibers containing different loadings of chnw. The table is followed by Figure 6.15 (a) and (b) which display the derivative weight loss curves and therefore giving a visual representation of the onset in degradation temperatures for EVOH44/chnw fibers.

Table 6.4: Maximum peak degradation temperatures (°C) of EVOH27/chnw nanocomposite fibers.

wt% chnw	EVOH27(fd)	EVOH27 (sus)
0	417.10	417.10
1	413.81	424.37
3	412.94	427.85
5	419.31	426.69
8	417.28	440.58
10	418.31	--------

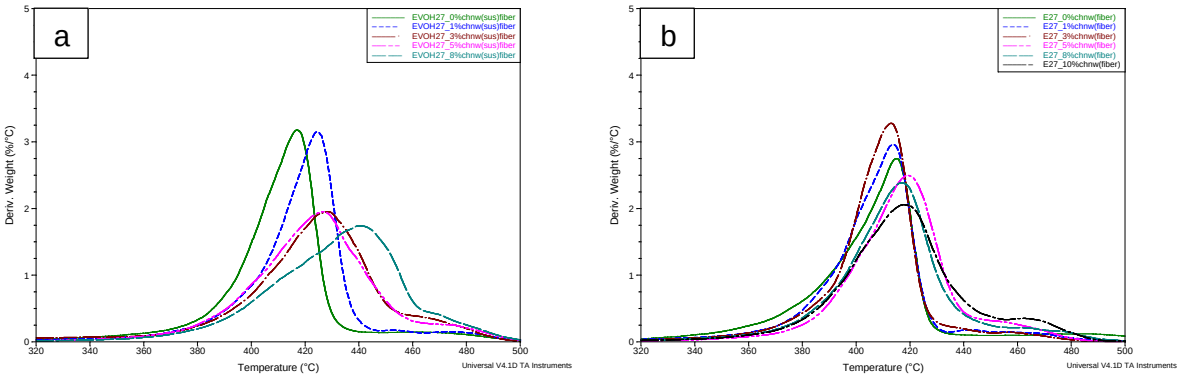

Figure 6.15: Derivative weight loss curves of (a) EVOH27/chnw(sus) nanocomposite fibers and (b) EVOH27/chnw(fd) nanocomposite fibers.

Positive shifts in the maximum peak temperatures are observed in Figure 6.16 which implies an increased thermal stability for all EVOH27/chnw nanocomposite fibers. The EVOH44/chnw(fd) fibers containing 1 and 3 wt% chnw were the only samples showing a decrease in thermal stability. The highest thermal stability was seen for the EVOH27/chnw(sus) nanocomposite fibers. The EVOH27/chnw(fd) fibers do not show a large increase in thermal stability with an increase in the

nanowhisker content. Even the EVOH27/10%chnw(fd) fibers do not show a significant increase in thermal stability. Therefore, the nanowhiskers incorporated as a suspension may be dispersing better within the matrix creating strong hydrogen bonds between chitin and EVOH27 molecules. Chitin nanowhiskers are more hydrophobic than cellulose nanowhiskers and have stronger hydrogen bonding between the molecules due to the amide moiety. It is therefore almost expected that freeze dried nanowhiskers would not result in a well dispersed suspension when redispersed in water and this was also proven by TEM and POL analysis of redispersed chnw (Sections 4.1 and 4.3).

6.5.4 EVOH44/chnw nanocomposite fibers

Table 6.5 displays information about the maximum peak degradation temperatures of EVOH44/chnw nanocomposite fibers containing different loadings of chnw. Incorporation of chnw into EVOH44 increases the thermal stability of EVOH44 rather significantly, especially in the case of the EVOH44/8%chnw nanocomposite fibers. No trend was observed which may be attributed to the electrospun fiber formation process and the possibility that during electrospinning not all the chnw are incorporated into the EVOH44. Chnw form extremely strong hydrogen bonds between molecules, which may result in agglomeration inside the syringe and a possible explanation why these results do not show a clear trend.

Table 6.5: Maximum peak degradation temperatures (°C) of EVOH44/chnw nanocomposite fibers.

wt% chnw	EVOH44(fd)
0	426.58
1	433.09
3	439.69
5	434.14
8	463.66
10	425.11

6.6 Differential scanning calorimetry (DSC) analysis

6.6.1 EVOH/cnw nanocomposite fibers

The DSC results of all EVOH/cnw nanocomposite fibers were compared to that of neat EVOH fiber samples in order to investigate the change in thermal behaviour as a function of cellulose nanowhisker content. Table 6.6 displays the melting points and Table 6.7 the percentage crystallization of the EVOH/cnw nanocomposite fibers. The results displayed in the tables are corrected for the cnw content, assuming a representative sample with regards to the wt% cnw

Table 6.6: Melting points (°C) of EVOH27/cnw nanocomposite fibers and EVOH44/cnw nanocomposite fibers.

wt% cnw	EVOH27(sus)	EVOH27(fd)	EVOH44(sus)	EVOH44(fd)
0	187	187	164	164
1	188	187	164	164
3	187	187	164	164
5	186.	187	164	164
8	186	187	164	163
10	186	187	--	163

Table 6.7: Percentage crystallization of EVOH27/cellulose nanocomposite fibers and EVOH44/cnw nanocomposite fibers.

wt% cnw	EVOH27(sus)	EVOH27(fd)	EVOH44(sus)	EVOH44(fd)
0	68	68	71.	71
1	71	70	72.	74
3	66	66	72	72
5	69	69	724	74
8	67	67	76	75
10	67	67	--	71

Both the EVOH27/cnw(sus) and EVOH27/cnw(fd) nanocomposite fibers show extremely close results in terms of thermal behaviour. No significant changes in terms of % crystallization are observed for any of the EVOH27/chnw samples except for the samples containing 1 wt% chnw where an increase is seen. The melting point stays relatively constant for the EVOH27/cnw(fd) nanocomposite fibers with incorporation of nanowhiskers but decreases slightly in the case of the EVOH27/cnw(sus) fibers when increasing the cnw loading. Even though the amount of crystallization is the same for EVOH27/cnw(sus) and EVOH27/cnw(fd), the crystal structures may differ significantly.

According to the results in Tables 6.6 and 6.7, all the EVOH44/cnw fibers showed an increase in percentage crystallization with melting temperatures being mostly unaffected.

Agglomeration inside the syringe may cause some of the nanowhiskers to remain in the syringe after electrospinning and therefore leads to less whisker incorporation into the electrospun fibers than expected. Crystallization of EVOH44 molecules is therefore less hindered than EVOH27 and may therefore lead to higher percentage crystallization than expected.

6.6.2 EVOH/chnw nanocomposite fibers

Table 6.8 displays the melting points and Table 6.9 the percentage crystallization of the EVOH/chnw nanocomposite fibers. EVOH/chnw nanocomposites fibers were all compared to neat EVOH fibers. The results displayed in the tables are corrected for the chnw content, assuming a representative sample with regards the wt% chnw

Table 6.8: Melting points (°C) of EVOH27/chnw nanocomposite fibers and EVOH44/chnw nanocomposite fibers.

wt% chnw	EVOH27(sus)	EVOH27(fd)	EVOH44(fd)
0	187	187	164
1	188	188	163
3	189	188	164
5	187	188	164
8	186	188	164
10	186	188	165

Table 6.9: Percentage crystallization of EVOH27/chnw nanocomposite fibers and EVOH44/chnw nanocomposite fibers.

wt% chnw	EVOH27(sus)	EVOH27(fd)	EVOH44(fd)
0	68	68.24	71
1	64	70	67
3	66	69	73
5	68	70	76
8	69	67	76
10	59	70	74

The addition of 1 wt% chnw decreases the percentage crystallization in the case of EVOH27/cnw(sus) after which the percentage crystallization starts to increase again up to a chnw loading of 8 wt%. EVOH27/chnw(fd) fibers do not seem to affect the amount of crystallization as much as in the case of the EVOH27/chnw(sus) fibers. The dispersion of chnw therefore seems to cause a greater crystallization hindrance when incorporated as suspension especially the EVOH27/10%chnw(sus) fiber. The melting point also seems to be slightly more affected by the addition of chnw as a nanowhisker suspension.

No clear trend was visible for both percentage crystallization and melting temperature when the chnw content of the EVOH44 nanocomposite fibers was increased. Both variables stay relatively constant except for a large drop in the EVOH44/1%chnw fiber sample as well as the EVOH44/10%chnw fiber sample. The reason for the mentioned crystallization behaviour for EVOH44/cnw fibers may also be due to extremely strong hydrogen bonding between chitin molecules.

6.7 Fluorescence microscopy analysis

EVOH44/cnw nanocomposite fibers and EVOH27/cnw nanocomposite fibers were subjected to fluorescence microscopy analysis in order to investigate whether this technique may be useful in studying the dispersion of nanowhiskers within the polymer matrix. Figure 6.16 to Figure 6.18 display fluorescence images of EVOH27/cnw and EVOH44/cnw nanocomposite fibers containing 8 wt% and 10 wt% cnw.

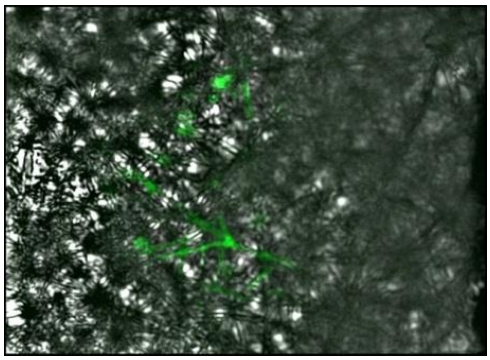

Figure 6.16: An overlay of an optical image and fluorescence image of EVOH27/8%cnw nanocomposite fibers.

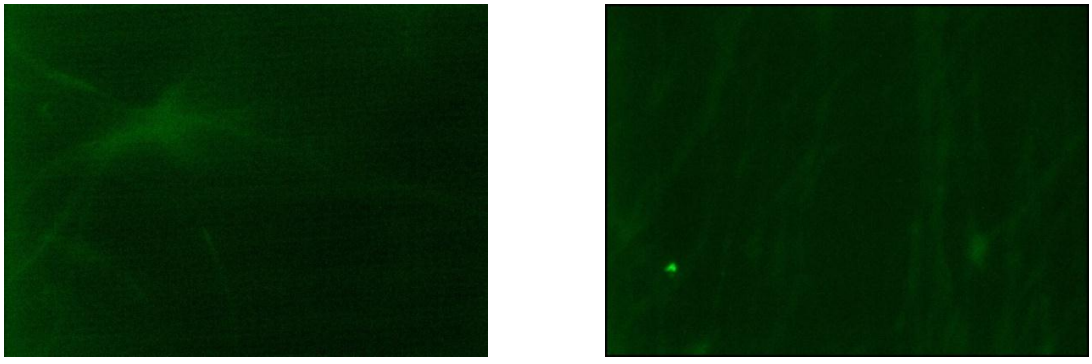

Figure 6.17: Fluorescence images of EVOH27/cnw containing 10 wt% cnw, labelled with FITC.

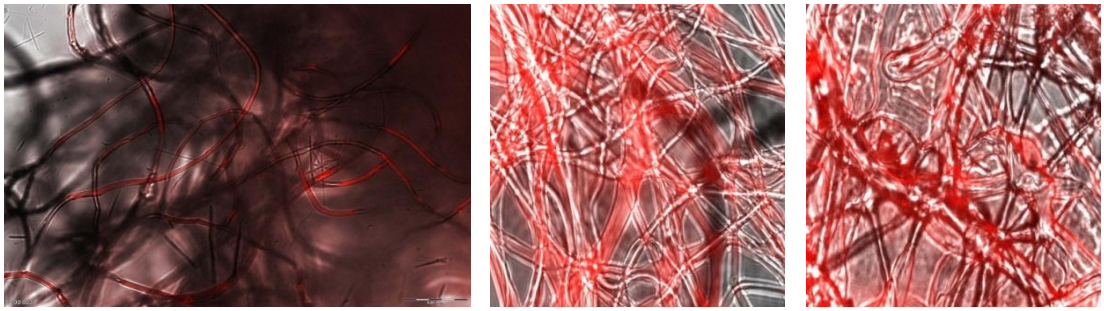

Figure 6.18: Overlays of optical and fluorescence images of EVOH44/cnw fibers containing 10 wt% cnw labelled with Rhodamine B.

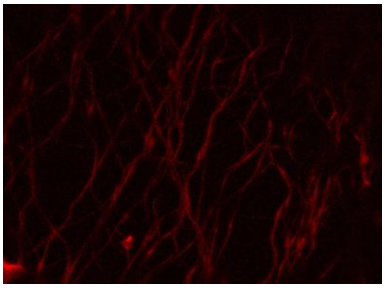

Figure 6.19: Fluorescence image of EVOH27/cnw fibers containing 8 wt% cnw labelled with Rhodamine B.

According to Figure 6.16 to Figure 6.19 no agglomeration or intense fluorescent structures were visible in the images of the electrospun nanocomposite fibers and it was therefore assumed that the nanowhiskers are rather well dispersed within the EVOH fiber.

It is, however, challenging to make any definite conclusions about the dispersion of nanowhiskers within the fibers due to the resolution capabilities of the instrument. The instrument can only observe agglomerated nanowhiskers which produce bigger fluorescent signals. These are then observed as micro structures.

More challenges are provided by the small diameters of the electrospun fibers as well as the sample preparation. The fiber mats are uneven and it is difficult to obtain proper focus of a large enough area (see Figure 6.16). An alternative approach was taken in order to investigate the nanowhisker dispersion. The nanocomposite fiber mats were melted and hot pressed into films in order to compare the fluorescent structures observed to those structures seen in the fluorescent spectroscopy analysis of the nanocomposite solution cast films (Chapter 5.7). Figure 6.20(a) and (b) illustrates a low and high magnification fluorescence image of EVOH44/10%cnw(fd) fibers melt pressed into a thin film. Figure 6.21 (a) and (b) illustrates low and high magnification fluorescence images of a EVOH44/10%cnw(fd) solution cast nanocomposite melt pressed into a film.

Preliminary results seem to display different and smaller agglomerates across the fluorescence image of the EVOH44/10%cnw fiber sample (Figure 6.20 (a)) compared to the EVOH44/10%cnw solution cast nanocomposite (Figure 6.21 (a)) which would suggest that the nanowhiskers seem to be better dispersed in the electrospun fibers than in the case of the solution cast films.

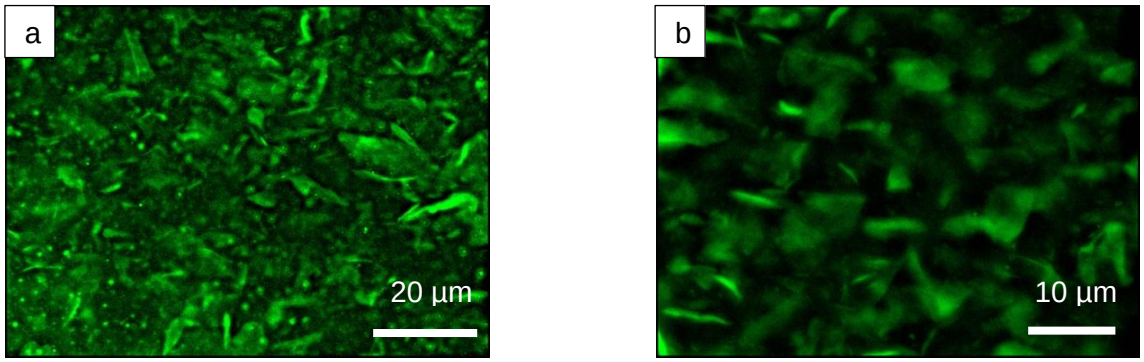

Figure 6.20: Fluorescence images of films melt pressed from EVOH44/10%cnw fibers imaged at a magnification of (a) (x 60) and (b) (x 100).

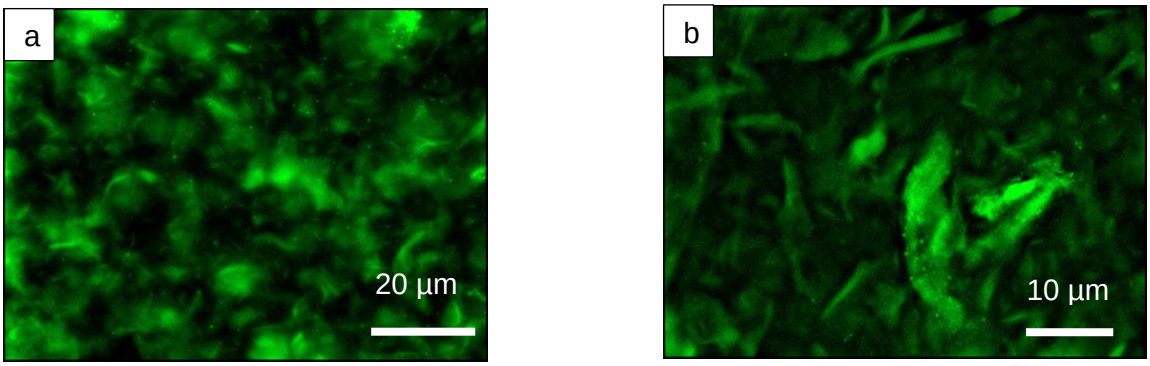

Figure 6.21: Fluorescence images of films melt pressed from EVOH44/10%cnw nanocomposites powders imaged at a magnification of (a) (x 60) and (b) (x 100).

6.8 Conclusions

EVOH27 and EVOH44 nanocomposite fibers containing cellulose and chitin nanowhiskers were successfully electrospun into nanofibers with loadings up to 10 wt% according to SEM analysis. Cellulose and chitin nanowhiskers were also proven to be successfully incorporated into the electrospun EVOH fibers by way of FTIR spectroscopy and TEM imaging. TEM analysis was found to be a more effective technique to use when studying the dispersion of nanowhiskers. Even though FESEM is a possible analysis technique that may be used to prove the incorporation of nanowhiskers by producing cross section images of the electrospun fiber, it is difficult to draw a conclusion about the nanowhisker dispersion. Fluorescence seems to be a good approach in

observing the dispersion of nanowhiskers within a fiber matrix. A fluorescent microscope with higher resolution will especially make a more valuable contribution towards the investigation of nanowhisker dispersion within a polymer matrix. The results obtained are not yet conclusive but can be used as a basis for further investigations.

Thermal data obtained shows that there is a large increase in the thermal stability with addition of cellulose and chitin nanowhiskers which is partly attributed to by chemical modifications in the EVOH matrix and partly to the well dispersed cellulose nanowhiskers. Some thermal behaviour is observed that does not indicate any trend and can probably be ascribed to the extremely small dimensions of cnw and chnw as well as the strong hydrogen interactions between nanowhiskers.

6.9 References

(1) Bhardwaj N, Kundu SC. Electrospinning: A fascinating fiber fabrication technique. *Biotechnology Advances* 2010;28(3):**325-347**.

(2) Martínez-Sanz M, Olsson R, Lopez-Rubio A, Lagaron J. Development of electrospun EVOH fibres reinforced with bacterial cellulose nanowhiskers. Part I: Characterization and method optimization. *Cellulose* 2011;18(2):**335-347**.

(3) Zhou C, Chu R, Wu R, Wu Q. Electrospun Polyethylene Oxide/Cellulose Nanocrystal Composite Nanofibrous Mats with Homogeneous and Heterogeneous Microstructures. *Biomacromolecules* 2011;12(7):**2617-2625**.

(4) Lu P, Hsieh Y. Cellulose nanocrystal-filled poly(acrylic acid) nanocomposite fibrous membranes. *Nanotechnology* 2009;20(41):**415-604**.

(5) Rinaudo M. Chitin and chitosan: Properties and applications. *Progress in Polymer Science* 2006;31(7):**603-632**.

(6) Alexy P, Káchová D, Kršiak M, Bakoš D, Šimková B. Poly(vinyl alcohol) stabilisation in thermoplastic processing. *Polymer Degradation and Stability* 2002;78(3):**413-421**.

(7) Tsuchiya Y, Sumi K. Thermal decomposition products of poly(vinyl alcohol). *Journal of Polymer Science Part A-1: Polymer Chemistry* 1969;7(11):**3151-3158**.

Chapter 7:
Low Density Polyethylene/EVOH (LDPE/EVOH) Composites

7.1 Introduction

Composite materials have become extremely popular in the everyday market. They are used in a variety of applications depending on their enhanced properties. The big challenge is to produce a material with light weight but enhanced properties. Electrospun polymer nanofibers incorporated into another polymer matrix is one possible way of achieving this goal. A previous study have reported on improved mechanical strength, dart impact and sealing properties by dispersing electrospun PET nanofibers into LDPE by way of melt extrusion[1]. It is known that LDPE has excellent barrier properties against water vapour but poor resistance to the permeation of solvents and oxygen. It is for that reason that EVOH, which has high barrier properties against hydrocarbons and oxygen, is sandwiched between LDPE layers forming a multilayer product[2-5]. The present study is investigating the mechanical properties of LDPE containing electrospun neat EVOH27 and neat EVOH44 fibers as reinforcing centre layer. EVOH27 nanocomposites fibers as well as EVOH44 nanocomposite fibers containing cellulose nanowhiskers were also investigated as a reinforcing phase for the LDPE matrix. LDPE containing neat EVOH fibers will be referred to as LDPE/EVOH and LDPE containing EVOH/cnw nanocomposites fibers will be referred to as LDPE/EVOH/cnw.

7.2 Experimental

7.2.1 Preparation of LDPE/PE-g-MA

Polyethylene-graft-(maleic anhydride) (PE-g-MA) was added to LDPE in order to act as a compatibilizer between the incorporated EVOH fibers and the LDPE matrix[2,5,6]. The purpose of a compatibilizer is to aid the compatibility between immiscible polymer blends without changing the crystallization kinetics of the matrix polymer before addition of the incompatible filler.

PE-g-MA was added as 1, 2, 3 and 4 wt% with regard to the weight of LDPE. The mixture was heated and stirred in xylene until everything was dissolved. DSC as well as tensile testing was carried out on the different LDPE/PE-g-MA blends. The purpose was to find a LDPE/PE-g-MA blend which did not alter the properties of neat LDPE. It is very important to ensure that the change in properties of the LDPE/EVOH composites is due to the incorporation of EVOH fibers and not because of the compatibilizer.

7.2.2 Preparation of LDPE/EVOH and LDPE/EVOH/cnw composites

According to DSC and tensile analysis discussed in Section 7.2.1, the 2 wt% PE-g-MA was observed to cause less disruption in the thermal and mechanical properties of LDPE. LDPE containing 2 wt% PE-g-MA was used throughout this study and will be referred to as only LDPE for the remainder of this chapter unless stated otherwise. LDPE without PE-g-MA will be referred to as neat LDPE. LDPE was blended with 2 wt% MA-g-PE as discribed in Section 7.2.1 and transparent films in the range of 0.05-0.06 µm were prepared. This was done using a hydraulic press at a temperature of 120°C and a force of 2 ton.

Electrospun EVOH27 and EVOH44 fibers were placed between two LDPE films and pressed into a composite film at the same conditions as described above. The same procedure was followed using EVOH27/cnw and EVOH44/cnw fibers as the reinforcing phase. The processing method produced transparent LDPE/EVOH as well as LDPE/EVOH/cnw composite films with thicknesses in the range of 0.09-0.1µm. Neat electrospun EVOH27 and EVOH44 samples were used to prepare LDPE/EVOH composites (without any nanowhiskers) in order to develop the technique and compare their properties with that of the LDPE/EVOH/cnw nanocomposites.

Figure 7.1 illustrates a digital image of LDPE, LDPE/EVOH27 before melt pressing and LDPE/EVOH27 after melt pressing. The LDPE/EVOH and the LDPE/EVOH/cnw composite films were transparent even though the EVOH electrospun fibers were not melted in the process. This was proven by SEM analysis which will be discussed in Section 7.6.

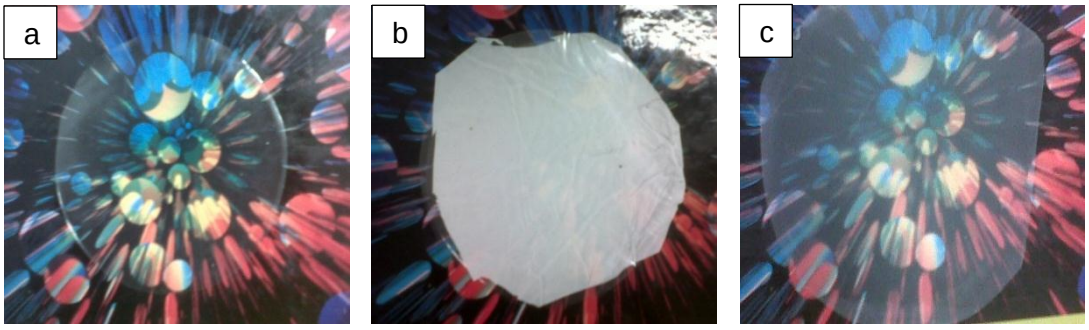

Figure 7.1: Film images of (a) LDPE, (b) a LDPE/EVOH composite sandwich before melt pressing and (c) a LDPE/EVOH composite after melt pressing.

Different concentrations of EVOH solutions produce fibers with different diameters. The diameter will determine the degree of reinforcement within the matrix. Smaller diameters will increase the surface area of the fibers, increasing the interaction and stress transfer between reinforcing phase and

matrix. For the purpose of this investigation, 5 wt% and 7 wt% EVOH27 and EVOH44 solutions were investigated. These LDPE composites will be referred to as LDPE/5EVOH (or LDPE/5EVOH/cnw) and LDPE/7EVOH (or LDPE/7EVOH/cnw) respectively.

All the LDPE/EVOH and LDPE/EVOH/cnw composites were produced in replica. Each replica was used to produce 5 dumbbell shaped films for tensile testing in order to get a good representative average for the stress strain results of each composite.

SEM images were captured for all the fractured tensile samples as well as cryo fractured tensile samples. SEM analysis was carried out in order to observe the morphology and compatibility between the reinforcing phase and the matrix at the cross section.

DSC analysis was carried out on some of the LDPE/EVOH composites in order to proof the incorporation of EVOH and to investigate the influence of EVOH fibers on the crystallization behaviour of neat LDPE.

7.3 Results and discussion

7.3.1 SEM analysis of neat EVOH electrospun nanofibers

The electrosopun fibers from different solution concentrations were investigated using SEM analysis. The average fiber diameters were calculated and plotted. Figure 7.2 displays graphs of the average (a) EVOH27 and average (b) EVOH44 fiber diameter as a function of solution concentration. A definite increase in fiber diameter for both EVOH27 and EVOH44 fibers were observed as the solution concentration is increased.

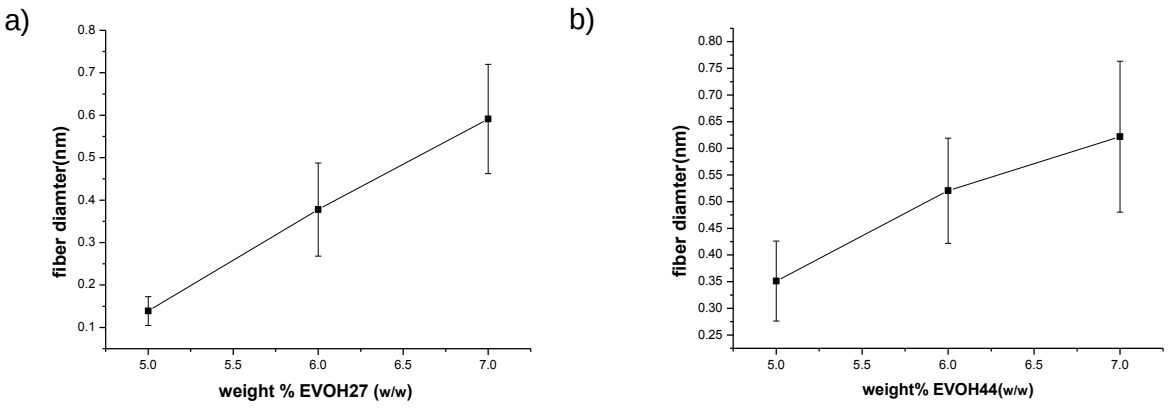

Figure 7.2: The average fiber diameter of (a) EVOH27 and (b) EVOH44 as a function of solution concentration.

Figure 7.3 illustrates SEM images of a 5 wt%, 6 wt% and 7 wt% solution concentration of EVOH27. Figure 7.4 illustrates SEM images of a 5 wt%, 6 wt% and 7 wt% solution concentration of EVOH44. The beading of fibers, especially in the case of EVOH44 fibers, decreased with an increase in the solution concentration which is probably due to an increase in solution viscosity. The increase in solution viscosity allows for better drawing of the polymer.

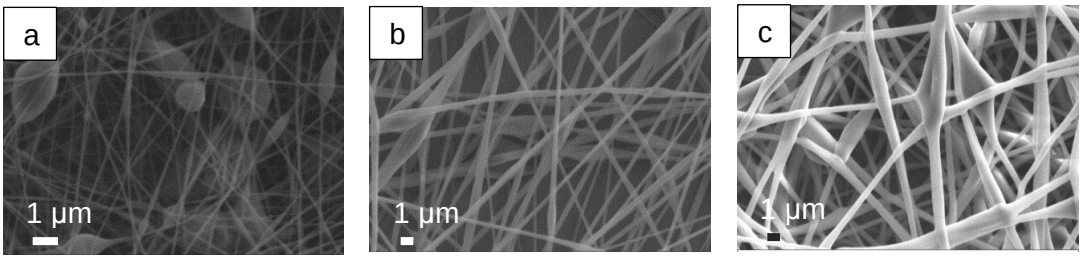

Figure 7.3: SEM images of electrospun EVOH27 from (a) 5 wt%, (b) 6wt% and (d) 7 wt% solutions.

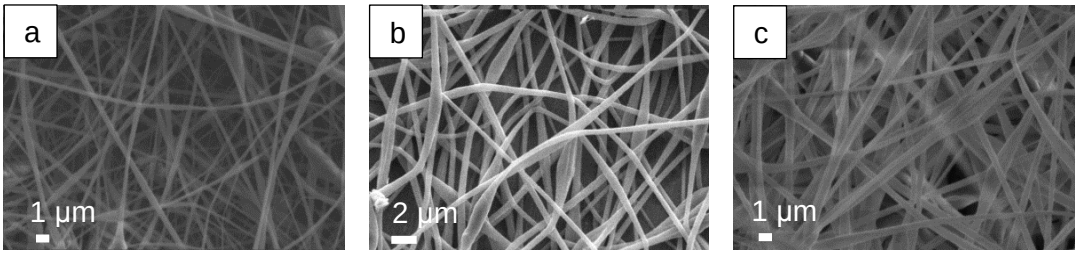

Figure 7.4: SEM images of electrospun EVOH44 from (a) 5 wt%, (b) 6wt% and (d) 7 wt% solutions.

EVOH27 produces fibers much closer to the nanometer range than EVOH44 which may be ascribed to by an increase in PVA content in the copolymer. EVOH27 has higher alcohol content than EVOH44 which causes a much greater disruption of hydrogen bonding between molecules in the presence of water. It may be that this plasticisation effect lowers the viscosity and surface tension compared to the case of EVOH44 solutions.

As already mentioned, EVOH/cnw nanocomposites containing 3 wt%, 8 wt% and 10 wt% cnw were also electrospun in order to incorporate cnw into the LDPE matrix. The average fiber diameters of these EVOH/cnw electrospun fibers were also determined using SEM analysis. The diameters are listed in Table 7.1 in Section 7.1 of this chapter. The EVOH/cnw fibers were electrospun from 5 wt% EVOH solutions.

7.3.2 Tensile testing

Dumbbell films of LDPE/EVOH and LDPE/EVOH/cnw composites were produced which were subjected to tensile testing. This is illustrated by digital images in Figure 7.5. The results of the tensile tests are presented in Table 7.1 and Figure 7.6 displays the stress strain curves of all the LDPE/EVOH and LDPE/ECOH/cnw composites.

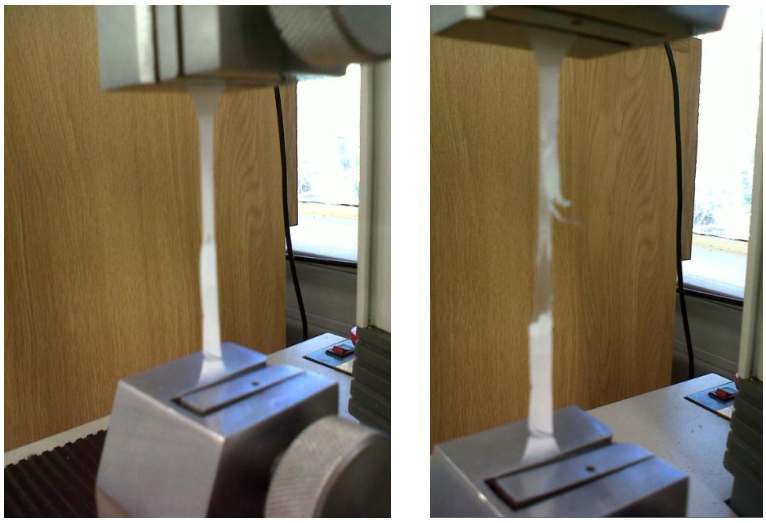

Figure 7.5: Illustration of tensile testing of a LDPE/EVOH composite.

Incorporation of neat EVOH27 and EVOH44 fibers into LDPE resulted in an increase in tensile strength but a decrease in elongation for all samples. Different concentrations of EVOH solutions produced fibers with different diameters. These different electrospun fiber mats displayed slightly different tensile strength and Young's modulus values. It is therefore possible to get a relationship between the fiber diameter and the improvement in composite strength. From Figure 7.2 in Section 7.3.1 it was seen that with an increase in EVOH27 concentration, the average EVOH27 fiber diameter increased to a value of 0.59 µm. The larger fiber diameter resulted in the strongest composite which is discussed further in this section This finding is somewhat contradictive to what one would expect. Smaller diameter fibers are expected to increase the surface area of interactions between filler and matrix and effectively transferring stress to the reinforcing phase. In this particular case, the 5 wt% EVOH27 solution produced fibers with extremely small nanometer diameters but beading was observed extensively throughout the electrospun fiber mat. The beads have dimensions in the micrometer range which definitely decrease the surface area and therefore the adhesion between nanofibers and the polymer matrix.

Table 7.1: Tensile results for different LDPE/EVOH and LDPE/EVOH/cnw composites

Material	Maximum tensile stress (MPa)	Youngs modulus (MPa)	Average fiber diameter(μm)
LDPE	8.8±0.9	0.7±0.15	NA
LDPE/5EVOH27	9.2±1.1	1.7±0.3.	0.14±0.03
LDPE/7EVOH27	11.2 ±0.6	1.7±0.23	0.59±0.10
LDPE/EVOH27/8%cnw	9.5±0.6	1.1±0.2	0.15±0.06
LDPE/EVOH27/10%cnw	9.4±0.7	1.3±0.18	0.12±0.04
LDPE/5EVOH44	9.2±1.1	1.5±0.35	0.35±0.07
LDPE/7EVOH44	9.7±0.5	1.6±0.19	0.62±0.1
LDPE/EVOH44/8%cnw	9.8±1.00	1.05±0.21	0.39±0.15
LDPE/EVOH44/10%cnw	9.2±0.4	1.1±0.14	0.36±0.08
LDPE/EVOH27/10%chnw	10.12±1.1	1.8±0.2	0.51±0.16

LDPE/EVOH/cnw composites containing 8 % cnw and 10 % cnw regarding the weight of EVOH, showed less of an increase in Young's modulus compared to LDPE/EVOH composites. It was reported previously that the fiber diameter changes with the addition of cellulose nanowhiskers due to conductivity and viscosity increases[8]. The change in fiber morphology and average diameter should produce LDPE/EVOH/cnw composites with similar tensile strength results to LDPE/EVOH containing neat EVOH fibers with the same diameter. The incorporation of nanowhiskers into the electrospun fiber mats is also expected to increase the stiffness of the fibers if dispersed uniformly within the electrospun fibers. This increase in stiffness may definitely have an influence on the effectiveness of the eletrospun fiber as the reinforcing phase in LDPE.

LDPE/EVOH44 composites showed a smaller increase in tensile strength than in the case of LDPE/EVOH27 composites. It was also seen from some SEM images of fractured tensile samples discussed in Section 7.3.6 that the LDPE/EVOH44 composites seem to result in more pull outs of

EVOH44 fibers from the matrix compared to observations from LDPE/LDPE27 fractured surfaces. Once again one would expect the EVOH44 to be more compatible with LDPE due to the higher ethylene content in the copolymer. Even though the increase in strength is perhaps lower than what is expected, it is seen that the elongation is in general higher for the LDPE/EVOH44 fiber composites than LDPE/EVOH27 composites.

Values up to 11.2 MPa for the maximum tensile strength were observed for LDPE/EVOH27 composites. Young's modulus almost doubled for most tensile tested LDPE composites with an exception to the LDPE/EVOH44/8%cnw composite. The reason for this observation is unknown. An increase in the number of repeat tensile tests for possible outliers may decrease the error factor and result in much better and representative averages. The EVOH fiber production and method of incorporation makes it difficult to compare different LDPE/EVOH nanocomposites. The number of repeat tests should be enough to keep the error factor to a minimum or the surface to volume ratios of fiber mats should be well known.

The thickness of the fiber mat is one parameter influencing the change in mechanical properties of the LDPE/EVOH and LDPE/EVOH/cnw composites. A comparison tensile test was carried out on two different LDPE/EVOH27 composites. The composites contained EVOH27 fibers with different mat thicknesses. Tensile test results for the LDPE/EVOH27 composite with a much thinner EVOH27 mat showed no change in tensile strength compared to the tensile strength of LDPE but displayed a decrease in elongation. The fiber mat, therefore, does influence the reinforcement and has to be taken into account when interpreting the results. The thickness of the fiber mat is extremely difficult to control precisely. Controlling the thickness after addition of cnw, which influence the fiber diameters, is especially challenging.

The results listed in Table 7.1 therefore gives us a good indication of what can be expected in terms of the mechanical properties of LDPE/EVOH and LDPE/EVOH/cnw composites but it should be taken into account that the surface area and volume of fiber mats may influence results. Proper control or measurement of the volume has to be investigated and included in the calculation of results in future studies.

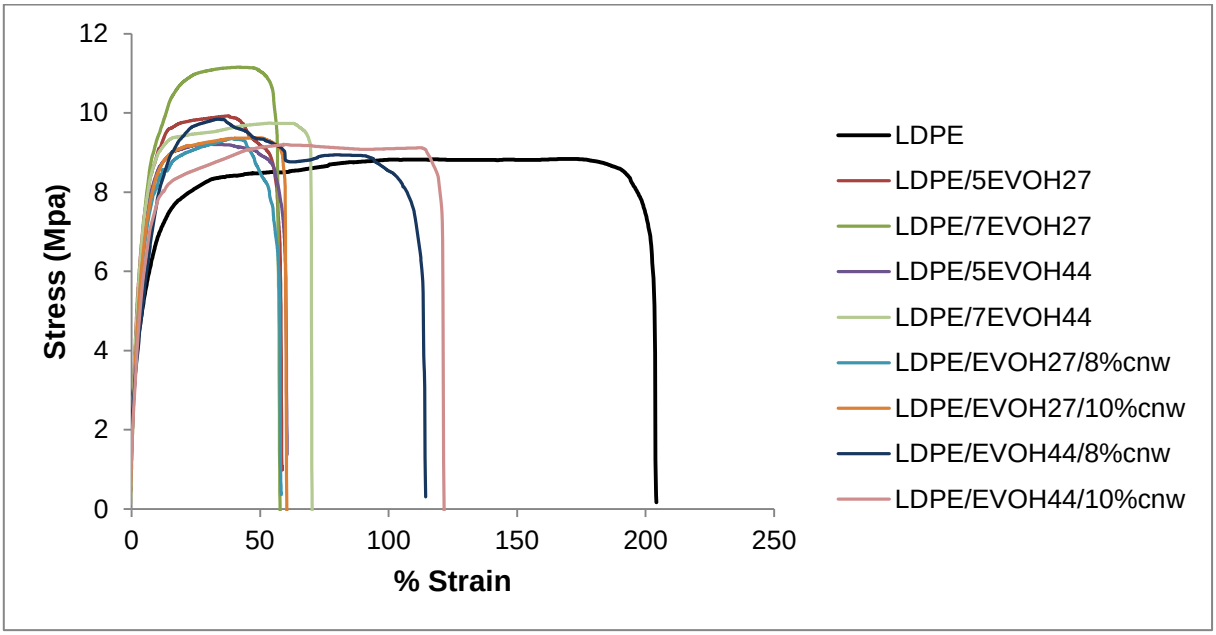

Figure 7.6: Representative stress-strain curves of the different tested specimens shown in the legend of the graph.

Another LDPE composite was produced by incorporating an EVOH/chnw fiber into the LDPE matrix. The EVOH/chnw fiber contained 10 % chitin nanowhiskers regarding the weight of EVOH27 and the LDPE composite will be referred to as LDPE/EVOH27/10%chnw. A very large increase in tensile strength (11.12 MPa) was observed for LDPE/EVOH27/10%chnw. An increase in Young's modulus to a value of 1.8 was observed which is higher than the rest of the LDPE/EVOH/cnw composites (Table 7.1).

Figure 7.7 display the stress strain curves of LDPE/EVOH27/10%chnw and LDPE. The increase in mechanical strength may be attributed to the larger fiber diameters measured for the EVOH27/10%chnw fibers or to the presence of highly crystalline, rigid chitin nanowhiskers which increase the stiffness of the EVOH27 matrix. The increase in EVOH27 stiffness would then be responsible for the increased mechanical strength of the LDPE composite.

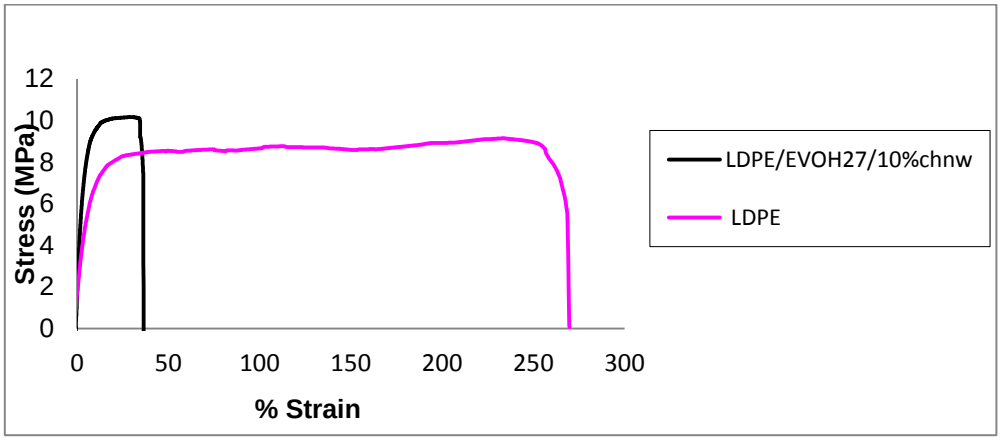

Figure 7.7: Stress -strain curve of LDPE/EVOH27/10%chnw.

7.3.3 SEM images of fractured LDPE/EVOH

SEM analysis was carried out on the fractured surface of the LDPE/EVOH composites after tensile testing and after a cryo fracture process. SEM imaging was proof that the fibers were incorporated into LDPE and still maintain the fiber morphology. Figure 7.8 displays SEM images of fractured tensile bars of LDPE. A smooth surface with no fibers is observed.

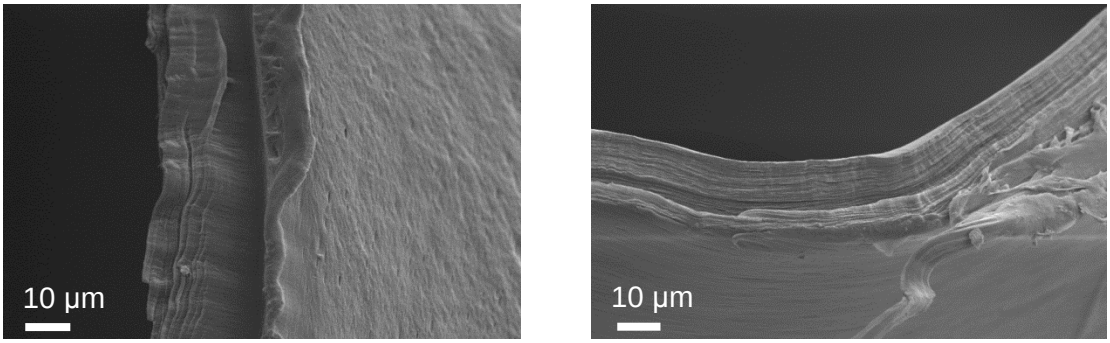

Figure 7.8: SEM image of tensile fractured surfaces of LDPE samples.

Figure 7.9 display SEM images of LDPEM/5EVOH27 and Figure 7.10 LDPE/7EVOH27 composites. Figure 7.11 display images of LDPE/5EVOH44 and Figure 7.12 display images of LDPE/7EVOH44 composites. The fibers are especially well observed in the LDPE/5EVOH27 composite where the beading of fibers is clearly seen at the fractured surface. The LDPE/5EVOH27 specifically showed less of an increase in mechanical properties compared to the other LDPE composites which may be explained from the observations of SEM images. Clear fiber pull outs are seen especially where the beads were imbedded into the matrix.

SEM images of the LDPE/7EVOH27 composite display good compatibility and interfacial adhesion between the reinforcing phase and the LDPE matrix where no clear extensive fiber strains or pull outs are observed.

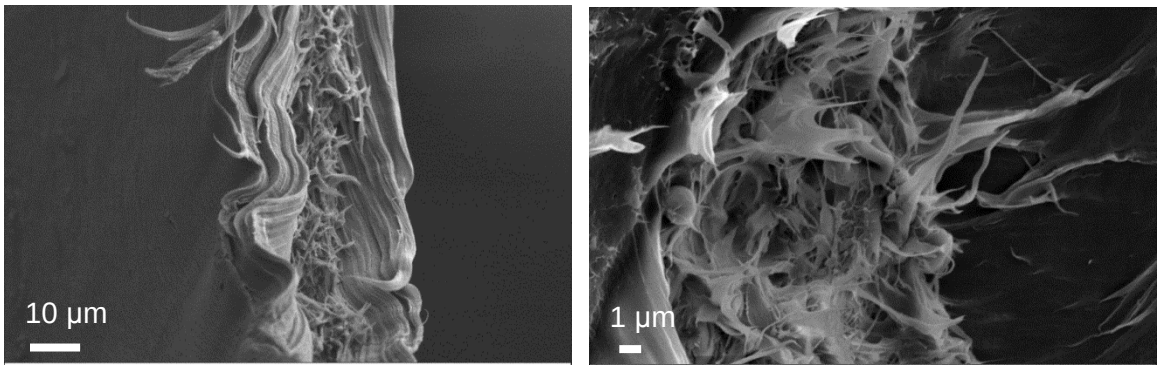

Figure 7.9: SEM images of tensile fractured surfaces of LDPE/5EVOH27.

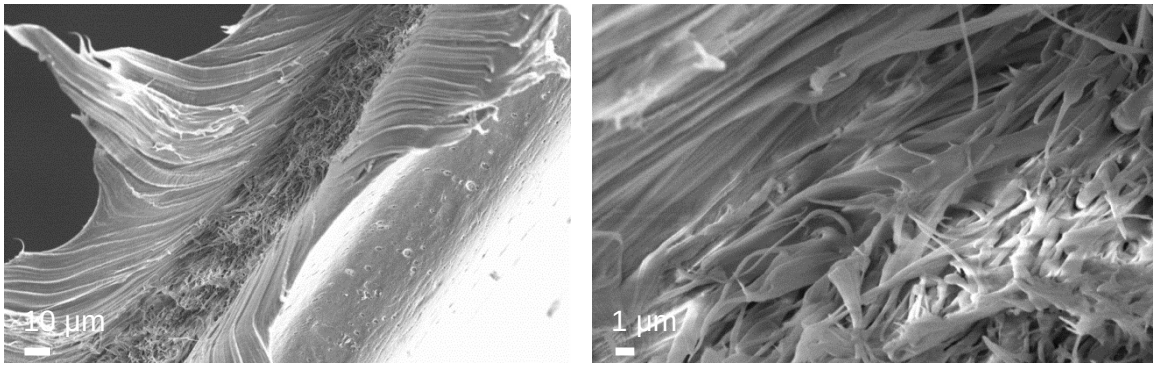

Figure 7.10: SEM images of tensile fractured surfaces of LDPE/7EVOH27.

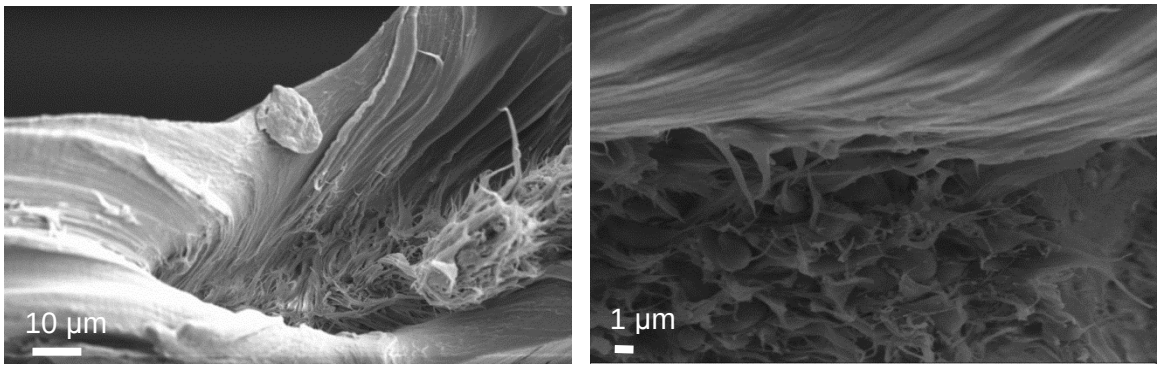

Figure 7.11: SEM images of tensile fractured surfaces of LDPE/5EVOH44.

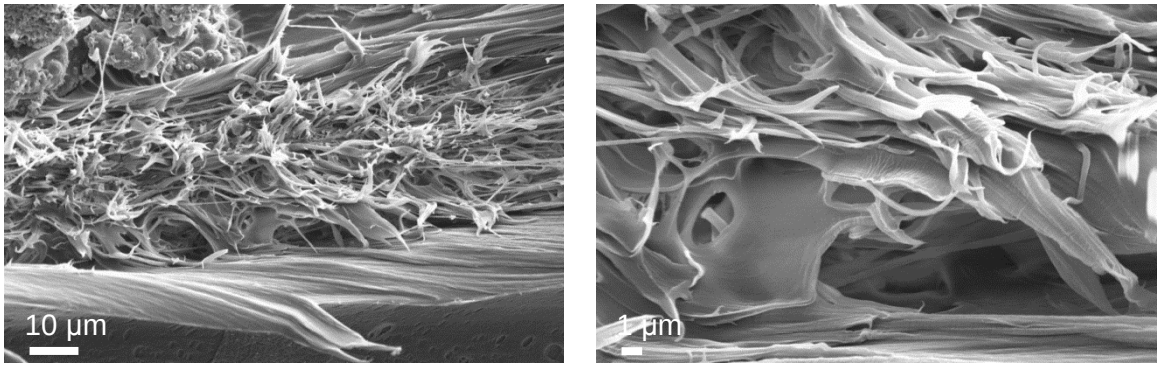

Figure 7.12: SEM images of tensile fractured surfaces of LDPE/7EVOH44.

Figure 7.13 displays cryo fractured surfaces of LDPE/5EVOH44 and LDPE/5EVOH27. Both these LDPE composites displayed pull outs of fibers to some extent. The fiber beads are observed on the fractured surface as well as holes where the fibers with beads were pulled out during the fracture process.

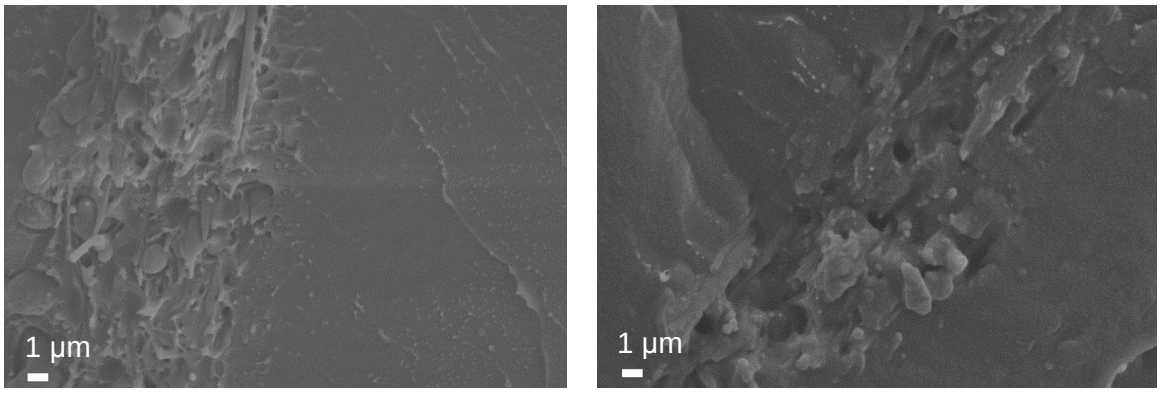

Figure 7.13: SEM images of cryo fractured samples of (a) LDPE/5EVOH44 (b) LDPE/5EVOH27.

Figure 7.14 displays the cryo fractured surface of LDPE/7EVOH27 and Figure 7.15 displays the cryo fractured surfaces of LDPE/7EVOH44

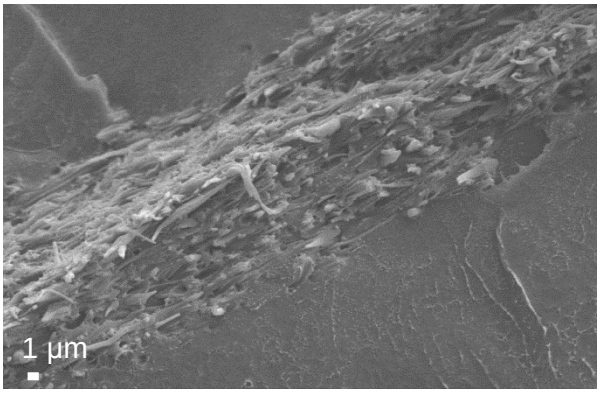

Figure 7.14: SEM images of cryo fractured surfaces of LDPE/7EVOH27.

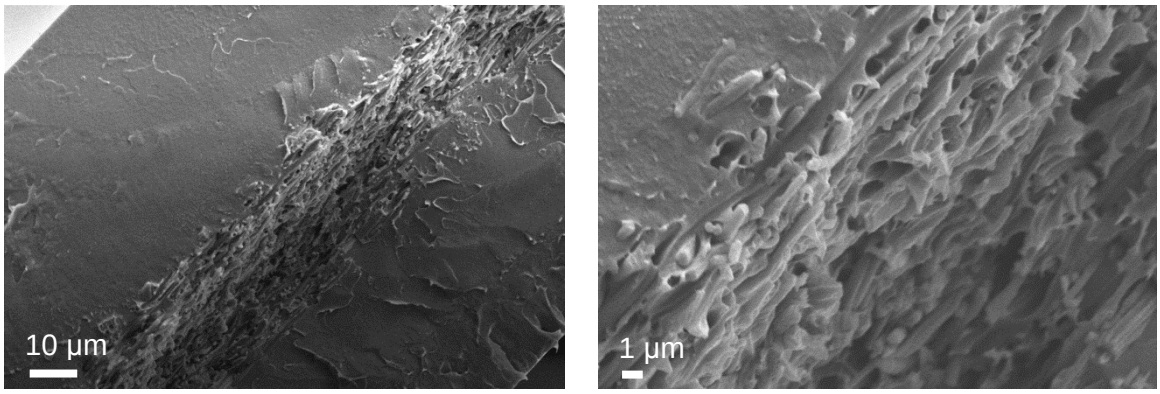

Figure 7.15: SEM images of cryo fractured surfaces LDPE/7EVOH44

Less fiber pull out was observed for the LDPE/7EVOH27 at the fractured surfaces than that observed for the LDPE/7EVOH44 sample. The holes which were formed from the fiber pulled out of the LDPE are definitely larger in diameter for the LDPE/7EVOH44 composites.

In general the compatibility between LDPE and EVOH seems good according to SEM analysis which is verified by the positive increase in Young's modulus and tensile strength.

7.4 Conclusions

Tensile results show a general increase in strength and Young's modulus with a decrease in elongation. The study showed that the best results were seen for the LDPE/7EVOH27 where the SEM images of tensile and cryo fractured surfaces agree well with the stress strain results. The compatibility between EVOH27 and LDPE/MA is clearly seen by less pull outs if any, or loose hanging fiber strains.

The change in mechanical properties for the LDPE composite films is suggested to depend not only on the type of polymer, solution concentration and other influencing parameters but also on the thickness of the fiber mats. The thickness depends on the fiber diameter and the volume of polymer solution to be electrospun. These types of parameters are difficult to control and have to be investigated further in order to properly compare different composites. EVOH27 containing chitin nanowhiskers seems to have a promising effect on the mechanical properties of LDPE

7.5 References

(1) Kulkarni A, Mahanwar P. Effect of dispersion of nanofibers on the properties of LDPE FILMS. *International Journal of Plastics Technology* 2011;15(0):**77-85**.

(2) Kim S, Chun Y. Barrier property by controlled laminar morphology of LLDPE/EVOH blends. *Korean Journal of Chemical Engineering* 1999;16(4):**511-517**.

(3) Cabedo L, Lagarón JM, Cava D, Saura JJ, Giménez E. The effect of ethylene content on the interaction between ethylene-vinyl alcohol copolymers and water—II: Influence of water sorption on the mechanical properties of EVOH copolymers. *Polymer Testing* 2006 10;25(7):**860-867**.

(4) Aucejo S, Catalá R, Gavara R. Interactions between water and EVOH food packaging films. *Food Science and Technology International* 2000;6(2):**159-164**.

(5) Huang C, Wu J, Huang C, Lin L. Morphological, Thermal, Barrier and Mechanical Properties of LDPE/EVOH Blends in Extruded Blown Films. *Journal of Polymer Research* 2004;11(1):**75-83**.

(6) Hotta S, Paul DR. Nanocomposites formed from linear low density polyethylene and organoclays. *Polymer* 2004;45(22):**7639-7654**.

(7) Kenawy E, Layman JM, Watkins JR, Bowlin GL, Matthews JA, Simpson DG, et al. Electrospinning of poly(ethylene-co-vinyl alcohol) fibers. *Biomaterials* 2003;24(6):**907-913**.

(8) Peresin MS, Habibi Y, Zoppe JO, Pawlak JJ, Rojas OJ. Nanofiber Composites of Polyvinyl Alcohol and Cellulose Nanocrystals: Manufacture and Characterization. *Biomacromolecules* 2010;11(3):**674-681**.

8. Conclusions and Future Recommendations

8.1. Conclusions

The preparation of nano-sized cellulose and chitin crystals was successfully carried out by means of acid hydrolysis. TEM and AFM images indicated that the cellulose nanowhiskers produced have dimensions in the range of 50-150 nm (length) and 5-10 nm (width) and chitin nanowhiskers have lengths in the range of 50-200 nm and widths of 5-15 nm. The increase in crystallinity for the obtained cellulose nanowhiskers proved using the absorbance spectrum from FTIR. The ratio that was used to calculate the crystallinity from the FTIR spectra increased from 1.07 for MCC to 1.23 for cnw. TEM, POL and fluorescence microscopy results indicated that freeze dried cellulose and chitin nanowhiskers do not redisperse as well in water as the nanowhiskers which were kept in the water suspension. This observation may be due to strong hydrogen bonding once the whiskers have dried or the loss of ester sulphate groups from the freeze drying process.

Up to 10 wt% cellulose and chitin nanowhiskers were successfully incorporated into an EVOH27 and EVOH44 matrix by way of solution casting and electrospinning. TEM and FTIR analysis results of the produced EVOH/cnw and EVOH/chnw nanocomposites indicated successful incorporation of cellulose and chitin nanowhiskers. TEM images revealed good dispersion of nanowhiskers but agglomeration were definitely present at higher nanowhisker loadings. The electrospun EVOH/cnw and EVOH/chnw fibers were more challenging to analyse with TEM but the nanowhisker dispersion was still easily observed especially for the samples that were sectioned in length. The nanowhiskers were observed to be clearly orientated in the direction of the fiber axis which probably resulted from the electrostatic pull of the EVOH/cnw solution during electrospinning. Embedding the nanocomposites samples in resin and staining the ultra microtomed samples for proper observation under TEM were found to be the most effective method in observing nanowhisker dispersion.

During thermal characterization an increase in thermal stability was observed as well as an increase and decrease in percentage crystallization of EVOH/cnw and EVOH/chnw nanocomposites. The dispersion of nanowhiskers may cause a hindrance for the EVOH molecules to crystallize or even changing the formation of crystallization. It seems that in most cases, the lower nanowhisker loads act as nucleating agents, thus increasing the percentage crystallization in the EVOH nanocomposites. The chitin nanowhiskers seem to behave more unpredictable than the cellulose nanowhiskers due to their more hydrophobic character as well as stronger hydrogen bonding between chitin molecules than in the case of cellulose.

Thermogravimetric analysis results of the nanocomposites showed that the increase in thermal stability at high temperatures could be partly attributed to the presence of acid, causing chemical

modifications. These observations were seen for both solution cast and electrospun EVOH/cnw nanocomposites. Some thermal behaviour is observed that does not indicate any trend and can probably be ascribed to the extremely small dimensions of cnw and chnw as well as the strong hydrogen interactions between nanowhiskers.

Preliminary DMA analyses revealed an increase in the storage modulus for the EVOH44/cnw nanocomposites which indicates that the cellulose nanowhiskers are increasing the stiffness of the matrix by decreasing the mobility of EVOH polymer chains. The mechanical analysis results also showed greater improvement in the storage modulus for the EVOH44/cnw(sus) nanocomposites which may be explained in terms of good dispersion of the nanowhiskers within the matrix.

Agglomeration of the nanowhiskers was observed during fluorescent microscopy but seemed to be evenly distributed in the EVOH/cnw nanocomposites. The results obtained are not yet conclusive but can be used as a basis for further investigations.

The last stage of the project involved the incorporation of electrospun EVOH fibers with and without cellulose nanowhiskers into a LDPE matrix. The aim was to investigate the changes in tensile properties for the LDPE/EVOH and LDPE/EVOH/cnw composites. Tensile results showed a general increase in tensile strength and Young's modulus, especially for LDPE/EVOH27, with a decrease in elongation. The SEM images of tensile fractured surfaces agreed well with the stress strain results. The compatibility between EVOH27 and LDPE was clearly seen by less pull outs if any, or loose hanging fiber strains.

The thickness of the fiber mats seemed to play a significant role in the enhancement of mechanical properties. The thickness of the fiber mats may depend on several parameters including the solution concentration and the type of polymer. The volume and the fiber diameters should therefore be controlled and taken into consideration when the electrospun EVOH and EVOH/cnw fiber mat is incorporated into a LDPE matrix.

8.2 Recommendations for future work

A fluorescent microscope with higher resolution will especially make a more valuable contribution towards the investigation of nanowhisker dispersion within a polymer matrix

The cellulose nanowhiskers were found to contain acid traces on the surface even after extensive washing and treatment with a strong base. Better neutralisation of the cellulose nanowhiskers can be investigated further. Another approach is however to investigate different methods of nanowhisker production in order to avoid degradation during processing at high temperatures.

EVOH is often used in the film packaging industry where it gets sandwiched between hydrophobic polyolefin layers. Studies on water absorption and gas permeability of EVOH/cnw nanocomposites are therefore recommended to investigate.

Further and detailed investigation regarding the incorporation of EVOH/cnw into a LDPE matrix can be carried out incorporating cnw loadings of more than 10 wt% into the EVOH fibers.